

Alma Mater Studiorum – Università di Bologna

DOTTORATO DI RICERCA IN  
GEOFISICA

Ciclo XXI

Settore scientifico-disciplinare di afferenza: GEO/12

TITOLO TESI

Sea Surface Temperature variations and air-sea physics  
parametrizations in the Mediterranean Sea

Presentata da: Daniele Pettenuzzo

Coordinatore Dottorato

Prof. Michele Dragoni

Relatore

Prof. Nadia Pinardi

Co-relatori

Srdjan Dobricic  
William G. Large

Esame finale anno 2010



# Contents

<b>1</b>	<b>Introduction</b>	<b>15</b>
1.1	Physical interactions between ocean and atmosphere . . . . .	15
1.1.1	Physical processes of heat and water fluxes exchange . . . . .	15
1.1.1.1	The radiative part of the heat balance . . . . .	16
1.1.1.2	The turbulent part of the heat balance . . . . .	18
1.1.1.3	The water balance . . . . .	19
1.1.2	Air-Sea Physics parametrizations . . . . .	20
1.2	The Sea Surface Temperature . . . . .	22
1.2.1	The SST measurements . . . . .	23
1.2.2	Definition of Sea Surface Temperature based on the measurement method . . . . .	24
1.2.2.1	The Interface SST ( $SST_{int}$ ) . . . . .	26
1.2.2.2	The Skin SST ( $SST_{skin}$ ) . . . . .	26
1.2.2.3	The subskin SST ( $SST_{subskin}$ ) . . . . .	26
1.2.2.4	The sea temperature at depth ( $SST_{depth}$ ) . . . . .	26
1.2.2.5	The Foundation SST ( $SST_{fnd}$ ) . . . . .	27
1.3	Objectives and structure of this thesis . . . . .	28
<b>2</b>	<b>On the corrections of ERA-40 surface flux products consistent with the Mediterranean heat and water budgets and the connection between basin surface total heat flux and NAO</b>	<b>31</b>

2.1	Introduction . . . . .	32
2.2	Air-Sea interaction physics . . . . .	34
2.3	The ERA-40 Surface Heat Budget . . . . .	36
2.4	Forcing Fields Bias Reduction . . . . .	39
2.4.1	Wind Speed Correction . . . . .	40
2.4.2	SST Correction . . . . .	41
2.4.3	Radiation Correction . . . . .	42
2.4.4	Specific Humidity Correction . . . . .	44
2.4.5	Precipitation Correction . . . . .	45
2.5	Corrected Heat And Freshwater Fluxes . . . . .	46
2.5.1	Interannual Variability . . . . .	48
2.5.2	Climatology . . . . .	50
2.5.3	NAO Changes And The Mediterranean Sea Net Surface Heat Flux	52
2.6	Conclusion . . . . .	55
2.7	Appendix 1: Bulk transfer coefficients . . . . .	57
<b>3</b>	<b>Impact studies of air-sea physics parametrizations in the Mediterranean</b>	
	<b>Forecasting System</b>	<b>61</b>
3.1	Introduction . . . . .	61
3.2	MFS general circulation models . . . . .	63
3.3	Air-sea physics implementation . . . . .	65
3.4	Sensitivity experiments . . . . .	68
3.5	Experiment results . . . . .	69
3.5.1	Comparison with satellite SST . . . . .	69
3.5.2	Comparison with in-situ data . . . . .	72
3.6	Summary and conclusions . . . . .	74
<b>4</b>	<b>Data assimilation of satellite derived Sea Surface Temperatures</b>	<b>77</b>
4.1	Introduction . . . . .	77

## CONTENTS

---

4.2	The Optimal Interpolated SST data set . . . . .	79
4.3	SST assimilation method . . . . .	80
4.4	Experiment design . . . . .	82
4.5	Results . . . . .	85
4.6	Summary and Conclusion . . . . .	88
4.7	Appendix 1: SST nudging and wind-dependent restoring coefficient . .	89
<b>5</b>	<b>Summary and Conclusions</b>	<b>97</b>
	<b>Bibliography</b>	<b>105</b>



# List of Figures

1.1	Heat balance of the Earth [Houghton et al., 1996]. The values reported on the picture have been computed according to the data of Kiehl and Trenberth [1997]. . . . .	17
1.2	Schematic diagram [Stark and Donlon, 2006] showing idealized vertical temperature deviations from $SST_{fnd}$ for deep undisturbed water during daylight warming (left panel) and during night (right panel). The temperature scale is logarithmic. . . . .	25
2.1	Surface downward shortwave radiation data. Each star represents a time average for a given station in the period 1993-2001. Blue, black and red stars are ERA-40 data set, ISCCP-FD and AGIP data respectively. Stations have been ordered by decreasing latitudes, and their position are locate in the map. AGIP data were kindly supplied by ENI-AGIP division, Milan. . . . .	38
2.2	Wind speed correction factor $R_W$ . The ratio is computed for the years 2000 and 2001 according to equation (2.9). The 2 years average QSCAT wind speed is always greater than the ERA-40 one. Values are restricted to being no greater than 1.3, because larger values are mainly due to interpolation problems in coastal areas. . . . .	41

2.3	SST correction term $D_S$ . The difference is computed for the period 1985-2001 according to equation (2.10). The spatial domain is the same of the MFS OGCM, thus the correction for the Black Sea is not possible. . . . .	42
2.4	Surface solar radiation downward correction factor $R_R$ . The ratio is computed following equation (2.11) for the period 1985-2001. The ISCCP-FD radiation is greater than the ECMWF reanalysis one, as demonstrate by comparison with in situ observations, with a north-west south-east gradient. . . . .	44
2.5	Specific humidity correction term $D_H$ in $g/Kg$ . The difference is computed for the period 1980-1993 according to equation (2.12). . . . .	45
2.6	Precipitation correction factor $R_P$ . The ratio has been computed for the period 1979-2001, according to equation (2.13). A north-south pattern is visible in the Mediterranean Basin error field. . . . .	46
2.7	Time series of surface averaged monthly corrected $T_A$ (A), $T_S$ (B), $q_A$ (C), C (D) and $ \vec{V} $ (E) with the bias reductions applied to sea surface temperature, specific humidity and wind speed. The time window is 1958-2001. The mean value (solid line) and $\pm 1$ standard deviation (shaded line) are also indicated. . . . .	47
2.8	Time series of the surface monthly averaged heat fluxes calculated with the final parametrization (equations (2.2), (2.3), (3.2) and (3.3); see column 2 of tab. 2.2) including all the mentioned corrections: $Q_S$ (A), $Q_L$ (B), $Q_E$ (C), $Q_H$ (D) and $Q_T$ (E). The total mean (solid line) and $\pm 1$ standard deviation (shaded line) are also indicated. . . . .	51
2.9	Climatology of $Q_T[W/m^2]$ for the month of July (A), December (B), annual (C) and of $F_T[m/yr]$ annual (D). The pictures are realized using the air sea physics which produces the fluxes of tab. 2.2;column 2 and for the time window 1958->2001. . . . .	53

## LIST OF FIGURES

---

2.10	Panel A: Yearly averaged net surface heat flux, $Q_T$ , (see tab 2.2;column 2) computed with formulas (2.2), (2.3), (3.2) and (3.3) using radiative fields provided by ERA-40 and applying all the correction described in section 2.5. Panel B: 5 years running mean of net surface heat flux (black line; left axes) and Winter (December through March) index of the NAO based on the difference of normalized sea level pressure between Lisbon, Portugal and Stykkisholmur/Reykjavik, Iceland (red line; right axes). . . . .	55
2.11	(a) Kondo [1975] 10 m $C_E$ bulk transfer coefficient as a function of wind speed and for 7 different $T_A - T_S$ values; (b) 10 m $C_E$ bulk transfer coefficient obtained from the Coupled Ocean-Atmosphere Response Experiment (COARE) bulk algorithm (version 3.0) as described in Fairall et al. [2003]. The plot has been obtained for relative humidity equal to 80% and shows $C_E$ as a function of the wind speed for 7 different $T_A - T_S$ values. . . . .	59
3.1	Topography of the entire MFS operational models domain. . . . .	63
3.2	Daily surface averaged SST bias for sim4a (black line) and sim4a_rad (blue line). . . . .	70
3.3	Daily surface averaged SST bias for sim4a (black line) and sim4a_radc (magenta line). . . . .	71
3.4	Daily surface averaged SST bias for sim4a (black line), sim4a_radc (magenta line) and sim4b (green line). . . . .	71
3.5	Daily surface averaged SST bias (Model-OBS) for sim4a (black line), sim3b (cyan line) and sim4b (green line). . . . .	72
3.6	Temperature and salinity RMSE profiles averaged over the year 2005 for sim4a (black line) and sim4b (green line). The respective vertical averaged values are also indicated on the plots. . . . .	73

4.1	Scale decomposition of the SST misfit. Panel (A) shows the SST misfit observed on 2 January 2005 at 12:00. This field is decomposed by means of a mean filter with a spatial radius of about 350 Km in large-scale (panel (B)) and small-scale components (panel (C)). In experiment SST.v2 the only assimilated part is the small scale one, while the large-scale errors are corrected by using an alternative air-sea physics parametrization [Pettenuzzo et al., in press]. . . . .	84
4.2	Daily surface-averaged misfits for the test year 2005. The black line represents the control experiment, without data assimilation, while the blue line includes SST nudging realized using the standard MFS nudging approach with a constant restoring coefficient ( $dQ/dT = -40 W/m^2/^\circ K$ ). The cyan line is relative to experiment SST.v1, where SST has been assimilated using the OceanVar scheme described in Section 4.3. No scale decomposition for SST errors has been applied. . . . .	86
4.3	Daily surface-averaged misfits for the test year 2005. The black line represents the control experiment, without data assimilation, while the blue line include SST nudging realized using the standard MFS nudging approach with a constant restoring coefficient ( $dQ/dT = -40 W/m^2/^\circ K$ ). The green line represents experiment SST.v2, on which the SST misfits have been decomposed into large-scale and small-scale ones. The latter is the only assimilated component, using the OceanVar scheme, while the former errors have been reduced by implementing an alternative air-sea physics parametrization based on the work of Pettenuzzo et al. [in press]. . . . .	87
4.4	Temperature and salinity RMSE profiles averaged over the year 2005 for experiments Sim (black line), MFS (blue line) and SST.v2 (green line). The temperature field is shown on the left panel, while the right one represents the salinity. . . . .	87

## LIST OF FIGURES

---

- 4.5 Plot of the restoring coefficient  $\gamma$  (computed according to equation (4.18)) as a function of 10-metre wind intensity. . . . . 93
- 4.6 Daily surface-averaged misfits for the test year 2005. The black line represents the control experiment, without data assimilation, while blue and red lines include SST nudging realized according to equation (4.5) by using a constant ( $dQ/dT = -40 W/m^2/^{\circ}K$ ) and a wind-dependent ( $\tau_T = c/\gamma$ ; with  $\gamma$  computed as in (4.18)) restoring coefficient respectively. 94
- 4.7 Surface total heat flux maps 10:00 snapshots for the day 30 January 2005: Panel (A) shows the fluxes computed in experiment Sim where no fluxes corrections occur; Panel (B) is relative to the standard setting of MFS (exoperiment MFS) for SST nudging with a constant restoring coefficient  $\partial Q/\partial T = -40 W/m2/^{\circ}K$  corresponding to a restoring time of about 2.5 days; Panel (C) shows the fluxes computed in experiment W-DEP with a correction term wind-dependent calculated starting from equation (4.18). . . . . 95



# List of Tables

1.1	AVHRR/3 spectral characteristics. . . . .	24
2.1	Heat and fresh water total fluxes and components for the period 1985-2001. The first column are the fluxes given in the ERA-40 data set. The other six columns indicate the surface heat flux components obtained with different corrections that have been cumulatively applied. Columns 2, 3 and 4 show the results when bulk formulas (2.2, 2.3, 3.2 and 3.3) are applied and $Q_{SD}$ and $Q_{LD}$ are computed according to equations 2.5 and 2.6, respectively, with no corrections in the ERA-40 input fields, corrected winds and corrected wind plus SST. The remaining columns use $Q_{SD}$ and $Q_{LD}$ from ISCCP-FD. Column 6 and 7 also include the humidity correction and the CMAP precipitation is included only in column 7. . . . .	37
2.2	Heat and freshwater budget components for the 44 year period 1958-2001. The first column represents the values given in the original ERA-40 data set. The second column shows those obtained with the "Corrected ERA-40 data set", including $Q_{SD}$ and $Q_{LD}$ , and calculated by means of equations 2.2, 2.3, 3.2 and 3.3. Also included is the correction for ERA-40 precipitation which is obtained as the sum of convective and large scale precipitation. . . . .	49
2.3	Parameters in expressions for neutral bulk transfer coefficients . . . . .	58

2.4	Sensitivity of the total budget to the bulk transfer coefficient parametrization. Column 1 and 2 show total heat and freshwater fluxes and their components obtained with the "Corrected ERA-40 data set", including $Q_{SD}$ and $Q_{LD}$ , and calculated by means of equations 2.2, 2.3, 3.2 and 3.3, using Kondo [1975] and NASEC bulk transfer coefficients, respectively.	59
3.1	Major differences between the two versions (sim3: OPA 8.1 and sim4: OPA 9.0) of the Mediterranean Forecasting System (MFS) operational models considered in this study. . . . .	65
3.2	Bulk formulae for the computation of the radiative part of the heat balance in MFS standard setting (MFS standard) and with the new formulation. In MFS standard, the shortwave radiation is computed according to Reed [1977] and Rosati and Miyakoda [1988] with $Q_{TOT}$ the total clear sky solar radiation reaching the ocean surface, $C$ the fractional cloud cover, $\beta$ the noon solar altitude in degrees and $\alpha$ the space-dependent albedo [Payne, 1972]. For the longwave flux calculation, MFS uses Bignami et al. [1995], with $\varepsilon$ the ocean emissivity, $\sigma$ the Stefan-Boltzmann constant, $T_S$ the sea surface temperature, $T_A$ the air temperature and $e_A$ the atmospheric vapour pressure. . . . .	67
3.3	Numerical experiments set. Integrations have been carried out for the test year 2005. . . . .	69
3.4	Averaged bias for the year in consideration 2005 relative to the 5 different numerical experiments carried out. The first 4 experiments are realized with NEMO (sim4), while the last one represents the new physics implemented in OPA (sim3). . . . .	72

## LIST OF TABLES

---

4.1	Averaged bias for the year in consideration 2005, relative to the 4 different numerical experiments carried out. Experiment Sim does not assimilate any observation, while experiments MFS and SST.v1 insert the satellite derived sea surface temperature [Marullo et al., 2007] using the MFS standard setting SST nudging and the OceanVar scheme respectively. Experiment SST.v2 also includes the scale decomposition approach for the observed SST error field. The 2005 test year mean biases relative to each experiment are also presented in column 3. . . . .	83
-----	--	----



# Chapter 1

## Introduction

### 1.1 Physical interactions between ocean and atmosphere

#### 1.1.1 Physical processes of heat and water fluxes exchange

The ocean and the atmosphere share a common boundary: the air-sea interface. Direct physical contact enables the two fluids to exchange energy mass and momentum in a wide variety of forms.

Winds are produced in the atmosphere in response to radiative forcing, and transfer momentum to the ocean due to the air-sea density difference. The ocean is not a solid surface, but its velocities are still very much less than those in the atmosphere (typically 3% of the velocity at 10 m), hence a velocity gradient or shear exist at the interface. The force of the atmosphere to the ocean surface may be exerted in two different ways. One is the force applied on irregularities in the surface (waves) associated with pressure differences across them, while the second is by viscous stresses. Those two components form the so-called surface stress or wind stress.

However, in this thesis we will concentrate on the heat and water fluxes at the air-sea interface. The ocean is provided with energy by solar radiation passing through the atmosphere. Infrared radiation from within the atmosphere enters the ocean; it also leaves the ocean to warm the atmosphere. There are also other mechanisms for heat exchange:

the flux of heat from the ocean's surface to the atmosphere through conduction and convection that is not associated with phase changes of water. This energy is known as sensible heat. There will also be an exchange of the molecules themselves, generally resulting in net evaporation, and therefore transfer of latent heat, from the water surface to the atmosphere. Conversely, freshwater is added to the ocean by means of precipitations.

The components of the heat balance (divided in radiative and turbulent parts), which are schematically represented in Figure 1.1, are discussed in detail below along with those related to the water balance.

### **1.1.1.1 The radiative part of the heat balance**

The radiative part of the heat balance is composed of solar shortwave radiation and longwave radiation.

In Figure 1.1 it is shown that about 50% of incident solar radiation reaches the Earth's surface and, on average, about 15% of this is reflected back into space. Over the ocean most of the incident solar radiation is absorbed into the water, although the albedo (defined as the percentage of incoming radiation over outgoing) depends strongly on the angle at which the Sun's radiation hits the surface. There are several complications to this apparently simple picture. Solar radiation suffers significant scattering by air molecules on its passage through the atmosphere. The degree of scatter is inversely proportional to the fourth power of the wavelength, so lower, or blue, wavelengths are preferentially scattered. In this sense, the amount of radiation reaching the sea surface will be further divided into direct and diffuse (scattered). A further complication arises when the sea surface is not calm. The creation of waves means that the sea surface can present a full range of angles to the incident radiation, and this can deeply modify the amount of radiant energy that enters the ocean, and is then absorbed within the sea, converting electromagnetic energy into heat. Most of this absorption is carried out by water molecules. Dissolved salts absorb weakly the ultra-violet, while suspended sediment and plankton absorb variable amounts of solar radiation, depending on their type

## 1.1 Physical interactions between ocean and atmosphere

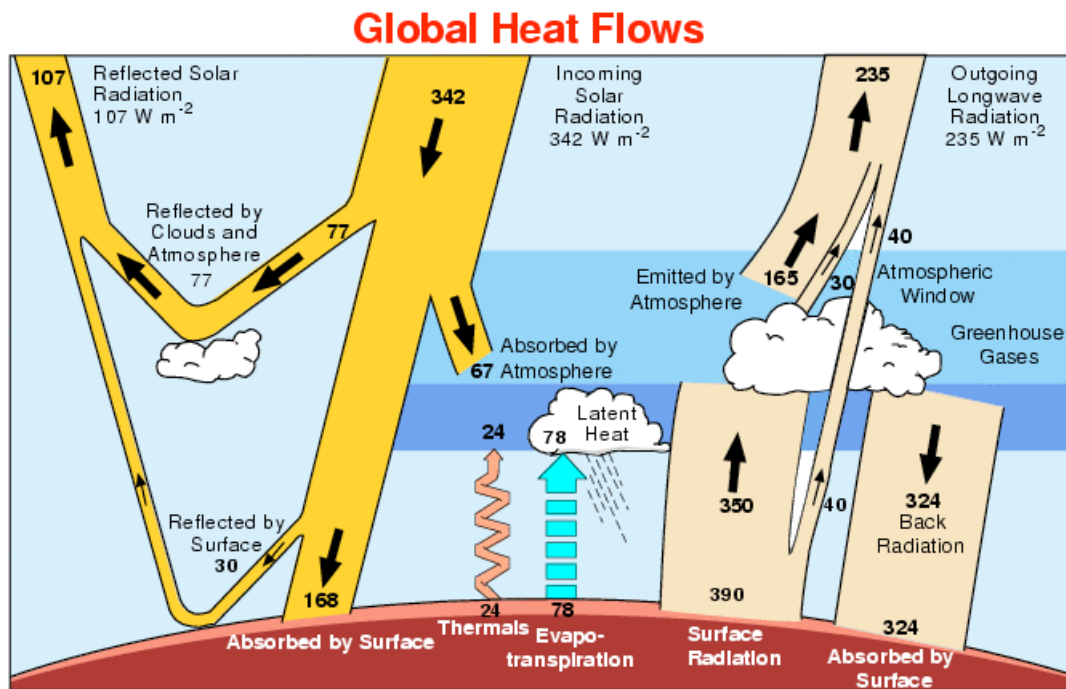


Figure 1.1: Heat balance of the Earth [Houghton et al., 1996]. The values reported on the picture have been computed according to the data of Kiehl and Trenberth [1997].

and concentration. Water is a powerful absorber of the longer, red, wavelengths, and this means that a few metres below the sea surface the blue-green region of the visible portion of the spectrum becomes dominant. Furthermore, less than 50 metres below the surface the light intensity is reduced to a quarter, and direct heating of the ocean from solar radiation is thus confined to a few tens of metres at most, helping to explain the thinness of the summer ocean mixed layer.

The shortwave radiation which is absorbed by atmospheric gases and vapor is emitted again as longwave radiation. Some of this radiation may be absorbed and re-emitted many times, after which it either exits the space or is incident on the sea surface. The latter itself radiates longwave radiation and the determining factor of this amount is the sea surface temperature. To the atmosphere, the ocean appears as a body at a given temperature, radiating according to the Stefan-Boltzmann Law.

The balance between the incident solar radiation energy mostly in the visible range and the energy lost through outgoing infrared radiation determines the radiative budget

of the sea surface.

### 1.1.1.2 The turbulent part of the heat balance

Radiation dominates the exchange of heat between the atmosphere and the ocean; however, other physical mechanisms contribute to the net heat flux: the latent heat of evaporation and the sensible heat.

The former is the dominant of these two components, especially in the Mediterranean Area. When water is evaporated from the ocean surface, energy is supplied to the molecules to free them from the strong inter-molecular bonds within liquid water.

When the water molecules condense to form water droplets, usually in clouds, this energy that was subtracted from the ocean is released to heat the surrounding air. Latent heat transfer is therefore an important means of exchanging energy through the ocean-atmosphere system and also extremely variable both in time and space. It can be near zero in still, foggy conditions or comparable with the radiation term in dry, warm, windy, weather. In the Mediterranean, the latent heat of evaporation may become dominant due to the instabilities that are created in the areas of interest of the main continental winds (Mistral, Bora and Ethesians) that usually occur during severe winter wind regimes.

The smallest component of the heat balance is due to physical contact of the atmosphere and the ocean, which enables energy to be exchanged between them by conduction. Such energy exchange is known as sensible heat. This occurs due to collisions between the molecules of the two fluids at the interface, with energy being transferred to the cooler, and therefore slower, molecules. Sensible heat transfer therefore depends on the temperature difference between the near-surface air and the sea surface.

Both turbulent fluxes are difficult to measure, and are often parametrized within ocean general circulation model by means of empirical formulae.

The sum of the radiative and turbulent parts of the heat balance gives the total heat flux at the surface,  $Q_T$ , according to the following expression:

## 1.1 Physical interactions between ocean and atmosphere

---

$$Q_T = Q_S + Q_L + Q_H + Q_E$$

where  $Q_S$  is the shortwave radiation,  $Q_L$  is the longwave radiation,  $Q_H$  is the sensible heat flux and  $Q_E$  is the latent heat of evaporation.

### 1.1.1.3 The water balance

If water vapour could only be transported by molecular diffusion, it would presumably diffuse upward until the whole atmosphere was saturated. The atmosphere is not saturated, however, because of the motion produced by radiation effects. Air is continually moving upward and downward because of the convection (caused by radiation tending to heat the bottom of the atmosphere more than the top) and because of the horizontal gradients due to more radiation being received in the tropics more than in the polar regions. The upward moving air is carried to levels where the temperature is lower and therefore less moisture can be held. If the air is carried high enough, it becomes saturated, condenses out, and may then fall to the surface as precipitation. The air left behind has less moisture content, so that when it is brought downward again it will be unsaturated. When it get low enough, some of this relatively dry air will get caught up in the shear-driven eddies and be brought down close to the surface itself. Contact of dry air with the surface leads to evaporation, which moisten the air, and so the cycle continues.

Evaporation and precipitation also help to drive the ocean circulation by creating horizontal density gradients. Evaporation, by removing water and concentrating the dissolved salts, increases salinity, and hence density. Precipitation, conversely, by adding freshwater, reduce the salinity, and therefore density. Density gradients produced in this way are the key to understanding the circulation of some specific areas. The Mediterranean, for instance, is a concentration basin (evaporation exceeds precipitation) and the mass equilibrium is maintained by means of the Atlantic water that flows into the basin through the Strait of Gibraltar. These relatively fresher waters are ultimately responsible and govern the thermoaline circulation of the entire basin.

Knowledge of all the components of the heat and water budgets at the air-sea interface are key points in Mediterranean ocean modelling. Unfortunately, given the complexity of the processes involved, they must necessarily be parametrized.

Several techniques have been historically applied and are widely described in the literature, providing different results depending on their approximations and accuracy. This aspect will be the argument of Section 1.1.2.

### 1.1.2 Air-Sea Physics parametrizations

Numerical models of the general circulation of the ocean are increasingly important tools for ocean forecasting. They can be described by well-established sets of mathematical equations valid at every point of the fluid considered. However, except in very special situations not encountered in the real world, exact solution of these equations cannot be found, so an approximation is made by solving for the essential variables of velocity, temperature and salinity at discrete points of a grid space at discrete moments in time. In this picture, the physical processes between ocean and atmosphere treated in Section 1.1 are considered as boundary conditions. Unfortunately, most of these mechanisms occur on fundamentally smaller spatial scales than are likely to be fully resolved within models for the foreseeable future, and often they are not totally understood. Aspects of air-sea interaction must therefore be simplified in order to be represented in ocean general circulation models (OGCM), and this behaviour is known as air-sea physics parametrization.

Until the pioneering joint work of Manabe and Bryan [1969], numerical studies treated the atmospheric and ocean circulation separately, with the energy input either parametrized or specified. In ocean circulation models, the general procedure [Bryan and Cox, 1967] was to prescribe the ocean surface temperature and then calculate the downward heat flux,  $Q_T$ , according to the formula:

$$\frac{Q_T}{\rho_0 C_P} = k \frac{\partial T}{\partial z} = \frac{k}{\Delta z} (T_s - T_1) \quad (1.1)$$

## 1.1 Physical interactions between ocean and atmosphere

---

where  $T_S$  represents the sea surface temperature,  $T_1$  is the temperature at the first level below the surface,  $\rho_0$  and  $C_P$  are the density and the specific heat capacity of the sea water and  $k$  the same vertical eddy diffusion coefficient for heat used in the ocean depths. However, this approach suffered from a major weakness relating to insufficient knowledge of the appropriate value of  $k$  to be used in the surface layer.

This problem was solved by Haney [1971], who was able to formulate a boundary condition for ocean surface temperature which gives the heat flux into the ocean independently from  $k$  by effectuating a Taylor's expansion of the total heat flux formula around an atmospheric equilibrium state assumed to be constant in time. This work represented a milestone in the framework of thermal boundary condition studies and gave birth to a methodology that was later widely applied in ocean modelling and known as the restoring boundary condition technique. The two most important pieces of work following Haney are probably Pierce [1996] and Killworth et al. [2000], who in their work applied the restoring boundary condition as a convenient proxy for reliable surface fluxes, relaxing, however, the surface temperature toward observations, which Haney definitely did not address, thus imposing a time lag in the model's surface tracer fields and systematically underrepresenting the model's surface variability.

Nevertheless, this approach, which helps in avoiding tracer drift in the model simulations, has been adopted in a wide variety of variances and with many improved features. An important example is represented by the work of Artale et al. [2002], which proposes a wind-dependent restoring coefficient which, coupling winds and SST, is able to take into account the different adjustments occurring in the atmospheric boundary layer over the ocean for low- and high-wind regimes.

In the nineties and last ten years, heat fluxes started to be parametrized with empirical (bulk) formulae forced by atmospheric data sets. The seminal work of Rosati and Miyakoda [1988] described the first OGCM application of this methodology. At present, this approach is the most often used, since it is more correct from a physical point of view, although it involves high accuracy in both the bulk formulation and the

forcing fields. Both of these requirements, however, are far from being met (Gilman and Garrett [1994]; Bignami et al. [1995]; Castellari et al. [1998]; Pettenuzzo et al. [in press]).

This last statement assumes a particular relevance in the Mediterranean Sea, which is the area where this study has been focused. The Mediterranean Basin, in fact, due to its semi-enclosed nature and the existence of the narrow Strait of Gibraltar, is one of the few regions in the world ocean where the mass, heat and salt transport are known with enough accuracy to allow for testing and comparison with different implementation of air-sea interaction parametrization and atmospheric data sets in ocean models. Whatever flux parametrization is used when a full heat budget, rather than just the heat exchange, for a particular location is computed, then the additional heat supplied (or lost) due to advection needs to be considered. Several of those studies can be found in literature, but of particular interest is that of Castellari et al. [1998], which was the first to define and introduce the Mediterranean Heat Budget Closure Problem. It states that the heat flux gained through the Gibraltar Strait by advection (considering the Black Sea contribution negligible [Tolmazin, 1985]) must be compensated, over a long enough period of time, by a net heat loss at the surface of the same amount while keeping the water budget of the basin reasonable. This topic will be discussed in Chapter 2 of this thesis.

## **1.2 The Sea Surface Temperature**

Sea surface temperature (SST) is an important indicator of the state of the ocean and of the earth's climate system. Thus, accurate knowledge of SST is essential for climate and ocean monitoring, research, and prediction. SSTs are also used as a surface boundary condition for numerical weather prediction and for other atmospheric model simulations.

Sea Surface Temperature is the water temperature close to the surface. In practical terms, the exact meaning of 'surface' varies according to the measurement method used.

## 1.2 The Sea Surface Temperature

---

### 1.2.1 The SST measurements

There are two main sources of SST data: in-situ and satellite. The in-situ SST data are determined from observations from ships and buoys (both moored and drifting). Most ship observations were made from insulated buckets, hull contact sensors, and engine intakes at depths of one to several meters. Although selected SST observations can be very accurate (see Kent et al. [1993]), typical RMS errors of individual observations from ships are larger than  $1^{\circ}\text{C}$  and may have daytime biases of a few tenths of a degree Celsius. SST observations from drifting and moored buoys were first used in the late 1970s. These observations are typically made by thermistor or hull contact sensor and usually relayed in real time by satellites. Although the accuracy of the buoy SST observations varies, the random error is usually smaller than  $0.5^{\circ}\text{C}$  and, thus, is better than ship error. In addition, typical depths of the measurements are roughly 0.5 m rather than the 1 m and deeper measurements from ships.

In late 1981, Advanced Very High Resolution Radiometer (AVHRR) satellite retrievals improved the data coverage over that of in-situ observations alone. Because the AVHRR cannot see the surface in cloud-covered regions, the biggest challenge in retrieving SST is to eliminate cloud contamination. The cloud-clearing algorithms are different during the day and the night because the AVHRR visible channels are useful in detecting clouds but can only be used during the day. Once clouds have been eliminated, the SST retrieval algorithm is designed to minimize the effects of atmospheric water vapor. The algorithms are ‘tuned’ by regression against quality-controlled buoy data. This procedure converts the retrieval of the temperature of the ‘skin’ (roughly a micron in depth) to a ‘bulk’ (roughly 0.5 m in depth) SST. The tuning is redone when a new satellite becomes operational or when comparison with the buoy data shows increasing errors. The first AVHRR was a 4-channel radiometer, first carried on TIROS-N (launched October 1978). This was subsequently improved to a 5-channel instrument (AVHRR/2) that was initially carried on NOAA-7 (launched June 1981). The latest instrument version is AVHRR/3, with 6 channels, first carried on NOAA-15 launched in

AVHRR/3 Channel	Spectral range [ $\mu m$ ]
Ch. 1	0.58-0.68
Ch. 2	0.725-1.0
Ch. 3A	1.58-1.64
Ch. 3B	3.55-3.93
Ch. 4	10.3-11.3
Ch. 5	11.5-12.5

Table 1.1: AVHRR/3 spectral characteristics.

May 1998 and its spectral characteristics are summarized in Table 1.1.

If the satellite SST retrievals are partially contaminated by clouds, they have a negative bias because cloud temperatures are colder than the SSTs. Negative biases can also be caused by atmospheric aerosols, especially stratospheric aerosols from large volcanic eruptions for example. Although these negative biases are the most frequent, biases of either sign can also occur due to instrument problems (e.g., due to errors in the on-board black-body calibration). Because some biases remain in satellite SST data, in situ data are critical not only for satellite calibration and validation but also for any final bias corrections needed at the time of the analysis. Nevertheless, satellite-measured SST provides both a synoptic view of the ocean and a high frequency of repeat views, allowing the examination of basin-wide upper ocean dynamics not possible with ships or buoys. For example, a ship travelling at 10 knots (20 km/h) would require 10 years to cover the same area a satellite covers in two minutes.

### 1.2.2 Definition of Sea Surface Temperature based on the measurement method

Such a definition of SST provides a necessary theoretical framework that can be used to understand the information content and relationships between measurements of SST made by different satellite and in-situ instruments.

The definitions reported in what follows are given according to the consensus reached at the second [Donlon, 2002b] and third [Donlon, 2003] GODAE High Resolution SST

## 1.2 The Sea Surface Temperature

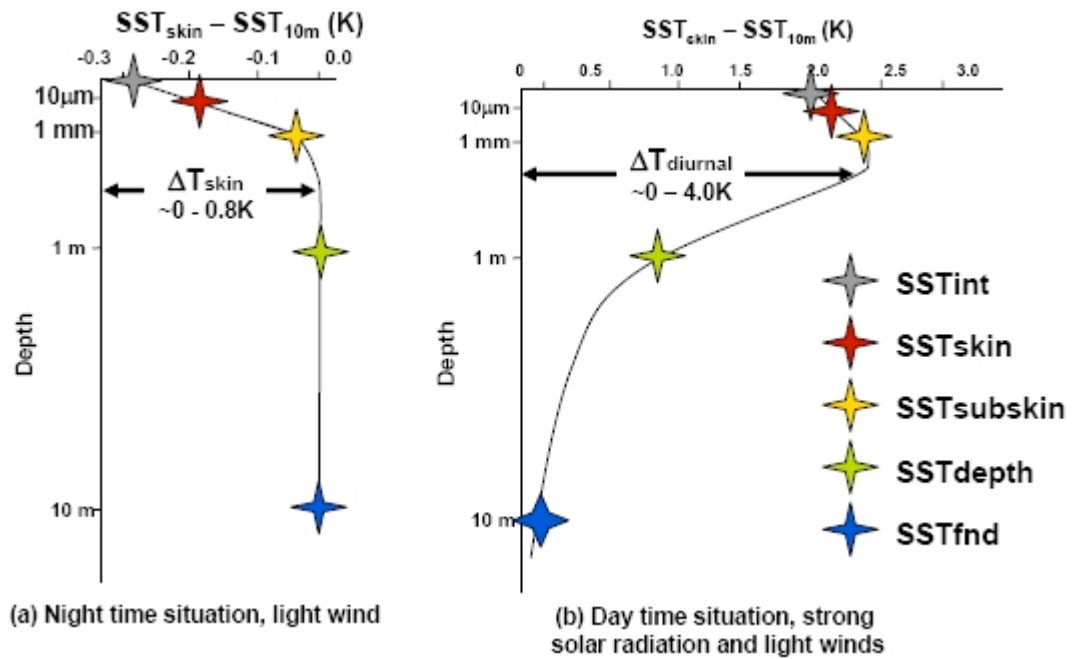


Figure 1.2: Schematic diagram [Stark and Donlon, 2006] showing idealized vertical temperature deviations from  $SST_{fnd}$  for deep undisturbed water during daylight warming (left panel) and during night (right panel). The temperature scale is logarithmic.

Pilot Project (GHRSSST-PP) workshops and have been carefully considered by the GHRSSST-PP Science Team in order to achieve the closest possible coincidence between what is defined and what can be measured operationally, bearing in mind current scientific knowledge and understanding of how the near-surface thermal structure of the ocean behaves in nature.

Figure 1.2 presents a schematic diagram that summarizes the definition of SST in the upper 10m of the ocean and provides estimates for the differences between complementary SST measurements. It encapsulates the effects of dominant heat transport processes and time scales of variability associated with distinct vertical and volume regimes of the upper ocean water column (horizontal and temporal variability is implicitly assumed).

All the definitions of the figure are explained in the following sub-sections.

### 1.2.2.1 The Interface SST ( $SST_{int}$ )

$SST_{int}$  is a theoretical temperature at the precise air-sea interface. It represents the hypothetical temperature of the topmost layer of the ocean water and could be thought of as an even mix of water and air molecules.  $SST_{int}$  is of no practical use because it cannot be measured using current technology.

### 1.2.2.2 The Skin SST ( $SST_{skin}$ )

$SST_{skin}$  is defined as the radiometric skin temperature measured by an infrared radiometer operating in the  $10 - 12 \mu m$  spectral waveband. As such, it represents the actual temperature of the water at a depth of approximately  $10 - 20 \mu m$ . This definition is chosen for consistency with the majority of infrared satellite and ship mounted radiometer measurements.  $SST_{skin}$  measurements are subject to a large potential diurnal cycle including cool skin layer effects (especially at night under clear skies and low wind speed conditions) and warm layer effects in the daytime (see Figure 1.2).

### 1.2.2.3 The subskin SST ( $SST_{subskin}$ )

$SST_{subskin}$  represents the temperature at the base of the thermal skin layer. The difference between  $SST_{int}$  and  $SST_{subskin}$  is related to the net flux of heat through the thermal skin of surface temperature by a microwave radiometer operating in the  $6 - 11 GHz$  frequency range, but the relationship is neither direct nor invariant to changing physical conditions or to the specific geometry of the microwave measurements.

### 1.2.2.4 The sea temperature at depth ( $SST_{depth}$ )

All measurements of water temperature beneath the  $SST_{subskin}$  are obtained from a wide variety of sensors such as: drifting buoys having single temperature sensors attached to their hull; moored buoys that sometimes include deep thermistor chains at depths ranging from a few metres to a few thousand metres; thermosalinograph (TSG) systems

## 1.2 The Sea Surface Temperature

---

aboard ships recording at a fixed depth while the vessel is underway; Conductivity Temperature and Depth (CTD) systems providing detailed vertical profiles of the thermoaline structure used during hydrographic surveys and to considerable depths of several thousand metres; and various expendable bathythermograph systems (XBT). In all cases, these temperature observations are distinct from those obtained using remote sensing techniques, and measurements at a given depth arguably should be referred to as ‘sea temperature’ (ST) qualified by a depth in metres rather than sea ‘surface’ temperatures. The situation is complicated further when one considers ocean model outputs for which the SST may be the mean SST over a layer of the ocean several tens of metres thick.

### 1.2.2.5 The Foundation SST ( $SST_{fnd}$ )

The foundation SST,  $SST_{fnd}$ , is defined as the temperature of the water column free of diurnal temperature variability, or equal to the  $SST_{subskin}$  in the absence of any diurnal signal. It is named to indicate that it is the foundation temperature from which the growth of the diurnal thermocline develops each day.  $SST_{fnd}$  provides a connection with historical ‘bulk’ SST measurements typically used as representative of the oceanic mixed layer temperature. This definition was adopted by GHRSSST-PP to provide a more precise, well-defined, quantity than previous, loosely defined, ‘bulk’ temperature quantities and consequently, a better representation of the mixed layer temperature. The  $SST_{fnd}$  product provides an SST that is free of any diurnal variations (daytime warming or nocturnal cooling). In general,  $SST_{fnd}$  will be similar to a night time minimum or pre-dawn value at depths of 1 – 5 m, but some differences may exist. Only in-situ contact thermometers are able to measure  $SST_{fnd}$ . It cannot be directly measured using either microwave or infrared satellite instruments. Analysis procedures must be used to estimate the  $SST_{fnd}$  from radiometric measurements of  $SST_{skin}$  and  $SST_{subskin}$ .

### 1.3 Objectives and structure of this thesis

This thesis aims at understanding and modelling the Sea Surface Temperature signals in the Mediterranean Sea at synoptic monthly and yearly time scales.

There are two factors that affect the quality of the SST modelling in ocean general circulation models: the inaccuracy to parameterize the net heat and water fluxes at the air-sea interface and the ocean model approximations which do not allow to correctly capture a large variety of dynamical processes associated to the ocean circulation. Furthermore, these sources of errors are characterized by different temporal and (more importantly) spatial scales and thus should be treated differently, especially in relation to the correlation that they have with the dynamics of the subsurface portion of the water column.

In this work, the large-scale error connected to the surface flux computation is reduced by the development and implementation of a novel air-sea physics parametrization which has been validated by means of heat and water budgets considerations in the Mediterranean Sea. The small-scale component, instead, is corrected by assimilating satellite-derived SST observations using a specifically adapted 3-dimensional variational scheme.

The thesis is organized as follows: in Chapter 2 the development of the new air-sea physics is presented. This boundary condition is tested and validated using the ECMWF ERA-40 reanalyses [Uppala et al., 2005], which have been also corrected in order to produce a reference high-frequency data set suitable for forcing OGCMs. Some further analyses have also been carried out in order to associate the obtained interannual heat flux variability with the Mediterranean wind regimes and to explore their teleconnection with the North Atlantic Oscillation (NAO). The formulation and the methodology resulting from the study have been then applied to the MFS ocean general circulation model, and the impact is presented and discussed in Chapter 3. Chapter 4 concerns the last aspect relative to the assimilation of SST. A novel data assimilation scheme OceanVar [Dobricic and Pinardi, 2008] is applied to MFS and ultimately, the impact of the com-

### **1.3 Objectives and structure of this thesis**

---

combined approach method (novel air-sea physics parametrization plus SST assimilation) is evaluated. A summary and some conclusions are contained in Chapter 5.



## Chapter 2

# **On the corrections of ERA-40 surface flux products consistent with the Mediterranean heat and water budgets and the connection between basin surface total heat flux and NAO**

The study described in this chapter has already been published to the Journal of Geophysical Research (*doi:10.1029/2009JC005631*) with the title:

*Pettenuzzo, D., W. G. Large, and N. Pinardi, On the corrections of ERA-40 surface flux products consistent with the Mediterranean heat and water budgets and the connection between basin surface total heat flux and NAO, J. Geophys. Res., doi:10.1029/2009JC005631, in press.*

## 2.1 Introduction

The semi-enclosed nature of the Mediterranean basin plus ocean observations of the long term changes in Mediterranean heat storage and salt content offer the opportunity of calibrating and developing air-sea physics parametrizations so that an overall balance is attained between fluxes at the air-sea interface and lateral fluxes at Gibraltar. The so called “Mediterranean heat budget closure problem” [Castellari et al., 1998] states that the heat flux gained through the Gibraltar Strait by advection (considering the Black Sea contribution negligible [Tolmazin, 1985]) must be compensated, over a long enough period of time, by a net heat loss at the surface of the same amount while keeping the water budget of the basin reasonable. The heat inflow at Gibraltar has been estimated as [Bethoux, 1979] and more recently as [Macdonald et al., 1994]. The net surface water loss due to evaporation,  $E$ , and precipitation,  $P$ , over the basin has been estimated to be  $-1$  m/yr [Bethoux and Gentili, 1994] while Gilman and Garrett [1994] indicate  $-0.71 \pm 0.07$  m/yr. Boukthir and Barnier [2000] determined a deficit of about  $0.6$  m/yr based on the ERA-15 reanalysis, and the range  $-0.5$  to  $-0.7$  m/yr is instead proposed by Mariotti and Struglia [2002]. Therefore, if the multiyear average surface heat and water fluxes from ERA-40 could be found to remain respectively within and between about  $-0.5$  and  $-1.0$  m/yr, we argue that they could be considered to satisfy the “Mediterranean heat budget closure problem”. In order to evaluate the surface heat balance, oceanographers have used empirical bulk formulas together with atmospheric observations, sea surface temperatures and lately numerical weather prediction (NWP) surface fields. These attempts have failed to close the budget, giving positive values for the surface heat balance. Thus, rather ad hoc adjustments for biases have been applied. Garrett et al. [1992] estimated the surface heat balance using the COADS data set [Woodruff et al., 1987] from 1946 to 1988. To reduce the value obtained of they suggested a possible reduction of the solar radiation by a constant factor of 18%, or 33% more cooling by the latent and sensible heat fluxes. Later, Gilman and Garrett [1994] proposed a modified set of formulae based on Garrett et al. [1992], which reduced the solar radiation by

## 2.1 Introduction

---

approximately 9% by taking into account the attenuation of incoming solar radiation due to atmospheric aerosol and increased the net cooling by long wave radiation by about 15% based on preliminary measurements over the Tyrrhenian Sea. These changes produced a surface heat balance of , and so still did not close the Mediterranean heat budget. In another attempt, Castellari et al. [1998] intercompared different air-sea flux formulae using the atmospheric NWP analyses and found the most appropriate ones in order to obtain a negative surface heat balance for the Mediterranean Sea while maintaining an acceptable water balance. They estimated a 1979-1988 mean value of for the surface heat balance, and so again the Mediterranean heat budget was not closed. More recently Tragou [2003] demonstrated, using ground truth observations at several coastal meteorological stations, that the incoming solar radiation is systematically overestimated by for the 30 years period which they considered (1964-1994), by the adopted empirical formulation.

Many other techniques used to correct flux fields in different regions of the global ocean can be found in literature, and a detailed review is included in the introduction of Large and Yeager [2008]. They include assimilation of ocean observations [Stammer et al., 2004], inverse procedures [Isemer et al., 1989], linear inverse analysis [Grist and Josey, 2003] and variational objective analysis [Yu and Weller, 2007].

In this work we use an alternative approach based on the work of Large and Yeager [2008], where spatially dependent correction factors are applied to the basic atmospheric fields required as input to air-sea bulk formulae, including radiation. These correction factors are obtained by comparison of the European Center for Medium Range Weather Forecast (ECMWF) Re-Analysis fields (ERA-40, [Uppala et al., 2005]) to satellite observations and in situ data sets available for the period 1985-2001. The ERA-40 computed heat fluxes themselves do not solve the “Mediterranean heat budget closure problem” in this period, but specific corrections to the surface winds, sea surface temperature, radiative components and relative humidity values do produce a satisfactory solution. The paper will then analyse the resulting time series in order to explain how the surface

heat balance is maintained and is correlated with the North Atlantic Oscillation (NAO) index. We first introduce the air-sea physics notation and parametrizations used in this study (section 2.2). In section 2.3 we will briefly describe the ECMWF ERA-40 fields and discuss their implied surface heat and water balances. Section 2.4 describes the benchmark data sets used for the bias reductions and the correction method. The resulting corrected fluxes time series and climatology are presented in section 2.5, along with correlations with the NAO index. A conclusion and discussion may be found in section 2.6.

## 2.2 Air-Sea interaction physics

The surface heat balance gives the net heat flux at the air-sea interface,  $Q_T$ , as the sum of four dominant terms:

$$Q_T = Q_S + Q_L + Q_E + Q_H \quad (2.1)$$

where  $Q_S$  is the net shortwave radiation flux,  $Q_L$  is the net longwave radiation flux,  $Q_E$  is the latent heat flux of evaporation and  $Q_H$  is the sensible heat flux. All fluxes have been taken positive for water or ocean energy gain. Both components of the radiative part of the heat balance are formed by the upward (negative) and downward (positive) fluxes, which are hereafter, denoted by the subscripts U and D respectively:

$$Q_S = Q_{SD} + Q_{SU} = Q_{SD}(1 - \alpha) \quad (2.2)$$

$$Q_L = Q_{LU} + Q_{LD} = -\varepsilon\sigma T_S^4 + Q_{LD}, \quad (2.3)$$

where  $T_S$  is the sea surface temperature, the ocean emissivity  $\varepsilon$  is taken to be 1 and  $\sigma$  is the Stefan-Boltzmann constant. When needed, a space-dependent albedo,  $\alpha$ , following Payne [1972] is used.

## 2.2 Air-Sea interaction physics

---

The steady state Mediterranean water budget requires that the freshwater entering the basin through the Gibraltar Strait and from the Black Sea plus direct coastal runoff is lost through the surface.

The surface freshwater flux,  $F_T$ , is given by:

$$F_T = E + P \quad (2.4)$$

where evaporation,  $E$ , is usually negative and precipitation,  $P$ , is positive definite.

The starting point of this work is the standard practice used by the Mediterranean Forecasting System (MFS) operational model (Pinardi et al. [2003], Tonani et al. [2008]).

The downward shortwave radiation is computed according to Reed [1977], and to Rosati and Miyakoda [1988].

$$Q_{SD}^{MFS} = Q_{TOT}(1 - 0.62C + 0.0019\beta) \quad \text{if } C \geq 0.3 \quad (2.5)$$

$$Q_{SD}^{MFS} = Q_{TOT} \quad \text{if } C < 0.3$$

where  $Q_{TOT}$  is the total clear sky solar radiation reaching the ocean surface,  $C$  is fractional cloud cover,  $\beta$  is the noon solar altitude in degrees.

For the longwave downward flux calculation, MFS uses the Bignami et al. [1995] formulation:

$$Q_{LD}^{MFS} = [\sigma T_A^4(0.653 + 0.00535e_A)](1 + 0.1762C^2) \quad (2.6)$$

where  $T_A$  is the air temperature,  $e_A$  is the atmospheric vapor pressure [Lowe, 1977].

The turbulent fluxes ( $Q_H$ , sensible, and  $Q_E$ , latent) are:

$$Q_H^{MFS} = -\rho_A C_P C_H \|\vec{V}\| (T_S - T_A) \quad (2.7)$$

$$Q_E^{MFS} = -\rho_A L_E C_E \|\vec{V}\| (q_S - q_A) = L_E E \quad (2.8)$$

where  $\vec{V}$  is the wind speed,  $\rho_A$  is the density of the moist air,  $C_P$  is the specific heat capacity,  $C_E$  and  $C_H$  are turbulent exchange coefficients for temperature and humidity,  $L_E$  is the latent heat of vaporization,  $q_A$  is the specific humidity of air and  $q_S$  is the specific humidity saturated at temperature  $T_S$ . In the MFS configuration, the exchange coefficients for a reference height of 10 m,  $C_E$  and  $C_H$ , are taken constant and equal to  $1.5 \cdot 10^{-3}$  and  $1.3 \cdot 10^{-3}$  respectively. These values have been obtained from the wind speed dependent curves proposed by Kondo [1975]. In this paper we use instead the approximated formula, suggested by the same author, which better captures the wind speed dependent factors. The Kondo parametrization and its choice are described and discussed in Appendix 1 (section 2.7).

## 2.3 The ERA-40 Surface Heat Budget

The ERA-40 data set covers the 45-year period from September 1957 to August 2002 with a time resolution of 6 hours. It is produced with a spectral atmospheric model based on a triangular truncation at wave number 156, which corresponds to a Gaussian grid of  $1.125^\circ$  (about 125 km). In the vertical, the ERA-40 atmospheric model has 60 hybrid levels with the highest at 0.1 hPa.

The assimilation scheme used in ERA-40 is the three-dimensional variational (3D-Var) technique. It allows direct assimilation of raw radiances from TIROS Operational Vertical Sounder (TOVS) instruments. ERA-40 also uses SSM/I passive microwave data to analyze the total column water vapor and 10 m wind speed. Sea Surface Temperature (SST) and ice cover are taken from 2D-Var National Center for Environmental Predictions (NCEP) system and the Hadley Center respectively. Cloud motion winds are taken from geostationary satellites.

The parametrization of turbulent fluxes in the atmospheric model is based on the

### 2.3 The ERA-40 Surface Heat Budget

	ERA-40	No Corr.	+Wind	+SST	+Radiation	+Humidity	+CMAP
$Q_S[W/m^2]$	162	202	202	202	183	183	183
$Q_L[W/m^2]$	-79	-87	-87	-88	-80	-80	-80
$Q_E[W/m^2]$	-86	-80	-99	-100	-100	-91	-91
$Q_H[W/m^2]$	-10	-12	-14	-16	-16	-16	-16
$Q_T[W/m^2]$	<b>-13</b>	<b>24</b>	<b>2</b>	<b>-2</b>	<b>-13</b>	<b>-4</b>	<b>-4</b>
$E[m/yr]$	-1.08	-1.02	-1.27	-1.28	-1.28	-1.17	-1.17
$P[m/yr]$	0.39	0.39	0.39	0.39	0.39	0.39	0.47
$F_T[m/yr]$	<b>-0.69</b>	<b>-0.64</b>	<b>-0.89</b>	<b>-0.90</b>	<b>-0.90</b>	<b>-0.79</b>	<b>-0.70</b>

Table 2.1: Heat and fresh water total fluxes and components for the period 1985-2001. The first column are the fluxes given in the ERA-40 data set. The other six columns indicate the surface heat flux components obtained with different corrections that have been cumulatively applied. Columns 2, 3 and 4 show the results when bulk formulas (2.2, 2.3, 3.2 and 3.3) are applied and  $Q_{SD}$  and  $Q_{LD}$  are computed according to equations 2.5 and 2.6, respectively, with no corrections in the ERA-40 input fields, corrected winds and corrected wind plus SST. The remaining columns use  $Q_{SD}$  and  $Q_{LD}$  from ISCCP-FD. Column 6 and 7 also include the humidity correction and the CMAP precipitation is included only in column 7.

Monin-Obukhov similarity theory. The transfer coefficients depend on stability functions and differ from those used in the MFS system (Appendix 1 (section 2.7)). The roughness lengths for momentum, heat and moisture also include a free convection velocity scale, which represent the near surface wind induced by eddies in the free-convection regime. Further information can be found on Uppala et al. [2005].

For our purposes, all fields have been interpolated with a bi-linear algorithm to a regular 1/16 degree resolution grid. In such a process, the problem due to the influence of the land points on the ocean point values of the final grid has been taken into account. The original sea points have been extended over the land through a process called "sea over land" which iteratively assigns to the first land value the average of the neighbouring sea points, before the interpolation is carried out. This methodology allows the production of a reference high-resolution corrected data set of surface fluxes in the Mediterranean basin assuming that sea-ward ERA-40 field values can be used to extrapolate in the near coastal areas. The interpolation does not add topographic effects that are missing in the original ERA-40 data set but eliminates over-smoothing of the fields, which will occur by simply interpolating across the coastal domain.

In this work we show that the simple usage of the surface flux components given directly by the ERA-40 data set gives a lower than measured estimate of the net surface heat flux. The reason for that is the underestimation of the shortwave radiation flux by about 12%, which is only partially compensated by a less negative latent heat flux (see column 1; tab. 2.1). The ERA-40 solar radiation underestimation is evidenced by comparison with station surface radiation data located in the Adriatic Sea (see figure 2.1) and the Sicily Strait. Figure 2.1 also compares the downward shortwave flux from the International Satellite Cloud Climatology Project global radiative flux data set (ISCCP-FD; Zhang et al. [2004]). The comparison supports the quality of the surface radiation stations and the finding that ERA-40 is too low, by about in the shortwave downward flux.

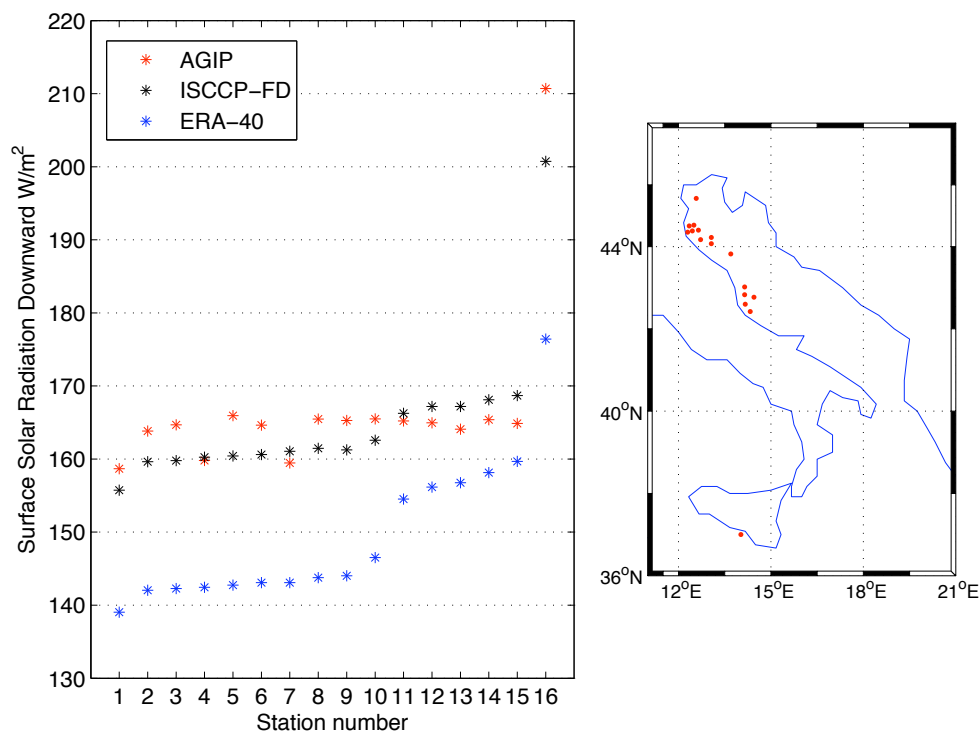


Figure 2.1: Surface downward shortwave radiation data. Each star represents a time average for a given station in the period 1993-2001. Blue, black and red stars are ERA-40 data set, ISCCP-FD and AGIP data respectively. Stations have been ordered by decreasing latitudes, and their position are locate in the map. AGIP data were kindly supplied by ENI-AGIP division, Milan.

These results demonstrate that direct usage of ERA-40 fluxes to force an ocean general circulation model for the Mediterranean Sea would be problematic [Griffies et al.,

## 2.4 Forcing Fields Bias Reduction

---

2008]. The standard practice in ocean forecasting [Pinardi et al., 2003] is to calculate the surface fluxes with the interactive bulk formulas (2.5), (2.6), (3.2) and (3.3) but this gives a very positive surface heat balance ( $24 W/m^2$ ) (see column2; tab. 2.1). We need then to find a correction method to recompute the heat fluxes from ERA-40 fields and close the Mediterranean heat budget.

## 2.4 Forcing Fields Bias Reduction

In order to find a solution to the Mediterranean heat budget closure problem we use an approach based on the work of Large and Yeager [2008]: we correct the atmospheric fields and avoid using formulae for the computation of the radiative components of the surface flux. ERA-40 air temperature is not corrected because of the small impact that this correction would cause to the final heat budget value. The bias correction related to this field is estimated to be less than  $1\text{ }^\circ\text{K}$  and it would produce a total heat balance change smaller than  $1 W/m^2$ .

The correction of the atmospheric fields is possible because of new observational data sets. However, some cover only a limited period of time with respect to ERA-40. For this reason we build up our correction methodology based on three steps:

- Step1: Observational data sets from various periods between 1985 and 2001 are used to determine objective corrections to ERA-40 products (see detailed descriptions on the following sections). These data sets are the QuickScat scatterometer (QSCAT) satellite wind fields [Chin et al., 1998], the satellite SST specifically analysed for the Mediterranean Sea [Marullo et al., 2007], the shortwave and longwave downward radiation (ISCCP-FD), the specific humidity from NOC climatology [Josey et al., 1998] and the CPC Merged Analysis of Precipitation (CMAP) [Xie and Arkin, 1996].

- Step2: We show that best estimates of the surface heat and freshwater fluxes do solve the Mediterranean heat budget closure problem, over the years 1985 through 2001. Since the QSCAT data are limited in time and NOC is a climatology, we only use them

to correct ERA-40 winds and specific humidity, which with uncorrected ERA-40 air temperature, analysed SST, ISCCP-FD radiation and CMAP precipitation give the satisfying values of  $-4 W/m^2$  for the net surface total heat flux, and a deficit  $E + P$  of  $-0.70 m/yr$  (see column 7; tab. 2.1). The adjustments computed in step 1 are then applied to the ECMWF reanalysis for the period 1985-2001, in order to verify that the resulting heat and freshwater fluxes computed with what we will hereafter refer to as the “Corrected ERA-40 Data-set” still satisfy the “Mediterranean heat budget closure problem” constraint.

- Step3: Finally, we assume that the bias reduction corrections, obtained in the previous steps, are constant in time. Thus, they can be applied over the entire ERA-40 period (1958-2001) in order to produce a longer, consistent reference data set.

Some of the computed bias reduction terms are factors (denoted by the letter R: wind, shortwave radiation and precipitation), while others are differences (denote by the letter D: sea surface temperature and specific humidity). The corrections were computed using a linear regression between observed and ECMWF fields which evaluated slope (R) and offset (D) values. For the cases where the slopes were not significantly different from 1, only the additive parts were used, and conversely, only the ratios have been considered for the cases with a resulting offset value close to 0.

### 2.4.1 Wind Speed Correction

The advent of satellite wind products makes the ERA-40 wind speed validation possible. We utilize QSCAT (QuickScat Scatterometer) zonal,  $U_Q$ , and meridional,  $V_Q$ , wind components. These have been constructed 6-hourly on a half degree latitude-longitude grid, following Chin et al. [1998]. The ERA-40 wind speed is corrected by multiplying both its zonal,  $U_{ERA}$ , and meridional  $V_{ERA}$ , components by a spatially-dependent factor  $R_W$ . This correction factor is computed as:

$$R_W = \left\langle (U_Q^2 + V_Q^2)^{\frac{1}{2}} \right\rangle / \left\langle (U_{ERA}^2 + V_{ERA}^2)^{\frac{1}{2}} \right\rangle, \quad (2.9)$$

## 2.4 Forcing Fields Bias Reduction

where  $\langle \rangle$  denotes the average over the two years 2000 and 2001. In order to avoid problems with interpolations in coastal areas, the corrections have been applied only for values of  $R_W$  less than 1.3. There is no attempt to correct wind direction.

Figure 2.2 shows the spatial distribution of the ratio  $R_W$ . A low bias is evident in the ERA-40 wind, with  $R_W > 1$  everywhere, but smallest in the south. The highest values are located in outflow regions of the major continental winds: Mistral (Gulf of Lions), Bora (Adriatic Sea) and Ethesian (Aegean Sea). The overall effects of the corrections are more cooling by the turbulent heat fluxes by about  $22 W/m^2$  and about  $0.25 m/yr$  more evaporation. These are the largest single improvements made to the biases of Table 2.1.

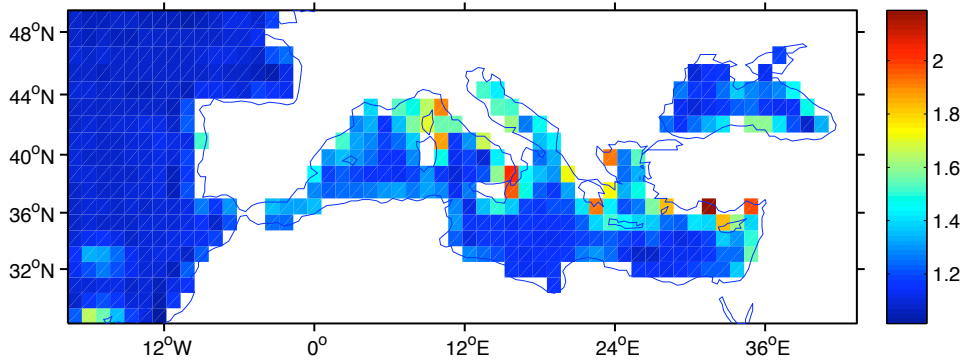


Figure 2.2: Wind speed correction factor  $R_W$ . The ratio is computed for the years 2000 and 2001 according to equation (2.9). The 2 years average QSCAT wind speed is always greater than the ERA-40 one. Values are restricted to being no greater than 1.3, because larger values are mainly due to interpolation problems in coastal areas.

### 2.4.2 SST Correction

In order to reduce the SST bias, we use the OISST (Optimal Interpolated Sea Surface Temperature) data set [Marullo et al., 2007]. Its resolution is daily on a  $1/16$  degree latitude-longitude grid that matches the MFS OGCM grid for the Mediterranean basin. Unfortunately this domain is smaller than the one of our basic forcing fields, so no SST corrections could be computed for the Black Sea. The data set has been developed starting from satellite infrared AVHRR images from 1985 to 2005, and has been validated with in situ measurements in order to exclude any possibility of spurious trends due to

instrumental calibration errors/shifts or algorithms malfunctioning related to local geophysical factors. The validation showed that satellite OISST is able to reproduce in situ measurements with a mean bias of less than  $0.1 K$  and RMS of about  $0.5 K$  and that errors do not drift with time or with the percent interpolation error.

We compute the correction term for the period 1985-2001 as:

$$D_S = \langle OISST \rangle - \langle T_S^{ERA} \rangle, \quad (2.10)$$

where  $\langle \rangle$  denotes the average over the 17 years, and the resulting space dependent correction (figure 2.3) is added to the 6-hourly SST of ERA-40,  $T_S^{ERA}$ . The resulting time series is showed in figure 2.7B. The sea surface temperature correction affects the longwave radiation  $Q_L$ , the latent heat of evaporation  $Q_E$  and the sensible heat flux  $Q_H$  for a total contribution in the net surface heat flux  $Q_T$  of  $-4 W/m^2$ .

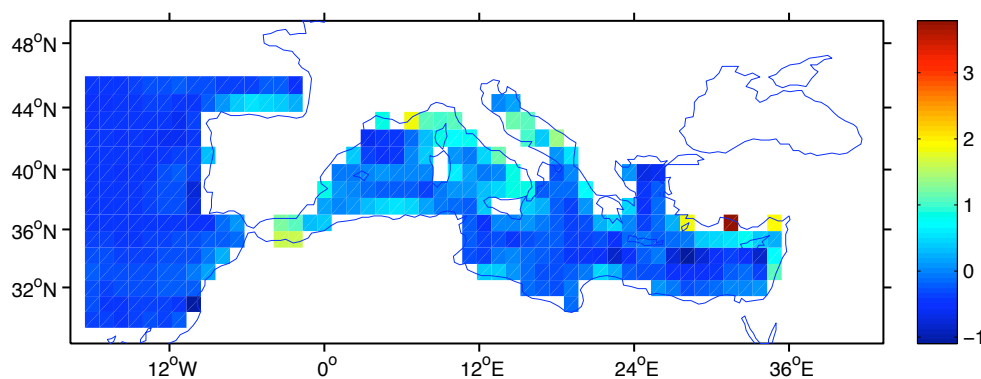


Figure 2.3: SST correction term  $D_S$ . The difference is computed for the period 1985-2001 according to equation (2.10). The spatial domain is the same of the MFS OGCM, thus the correction for the Black Sea is not possible.

### 2.4.3 Radiation Correction

Recent ISCCP (International Satellite Cloud Climatology Project) global radiative flux data products have been created by integrating the NASA Goddard Institute for Space Studies climate GCM radiative transfer model with a collection of global atmospheric data sets, including ISCCP clouds and surface properties [Zhang et al., 2004]. Most

## 2.4 Forcing Fields Bias Reduction

---

importantly, this ISCCP-FD data set provides fields of downwelling shortwave,  $Q_{SD}^{ISCCP}$ , and longwave,  $Q_{LD}^{ISCCP}$ , radiation as in equations 2.2 and 2.3. Moreover, since  $Q_{SD}^{ISCCP}$  and  $Q_{LD}^{ISCCP}$  have been derived in concert from the same input, they should derive full advantage of any cancellation of cloud errors. The data resolution is 3-hourly on a 2.5 degree longitude-latitude grid, but it is difficult to properly remap the diurnal cycle. Therefore, for our purposes, the data have been integrated to daily values and interpolated to the ERA-40 grid.

Using these fields, we are now able to compute the ISCCP-FD net radiation from equations 2.2 and 2.3 which produces the values of columns 5, 6 and 7 in table 2.1.

The solar heating is lowered by  $19 W/m^2$  compared to equation 2.5, but there is a partial compensation of about  $8 W/m^2$  from the longwave compared to equation 2.6. Note, the net short wave radiation flux of from ISCCP-FD agrees with the proposal of Gilman and Garrett [1994], without making additional corrections for dust.

As described on step 2 of our correction methodology, in order to eliminate the bias that we could demonstrate exists on the ERA-40 radiation products, we have computed the ratio  $R_R$  as:

$$R_R = \langle Q_{SD}^{ISCCP} \rangle / \langle Q_{SD}^{ERA} \rangle \quad (2.11)$$

where the two fields have been averaged for the period 1985-2001.

The resulting correction factor is shown in figure 2.4. The ISCCP-FD shortwave radiation is bigger than the ERA-40 one over the entire Mediterranean Basin with a strong North-West to South-East gradient and the largest errors occurring in the Levantine Sea.

The corrected net shortwave radiation time series, obtained by monthly averaging the ECMWF radiation multiplied to the factor is represented in figure 2.8A.

Regarding the long wave radiation component, the difference between  $Q_{LD}^{ISCCP}$  and  $Q_{LD}^{ERA}$  is less than 2% so an adjustment is not justified.

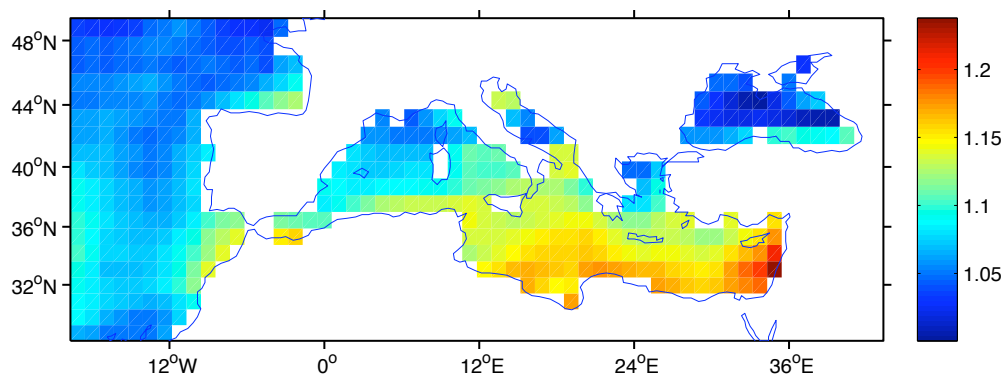


Figure 2.4: Surface solar radiation downward correction factor  $R_R$ . The ratio is computed following equation (2.11) for the period 1985-2001. The ISCCP-FD radiation is greater than the ECMWF reanalysis one, as demonstrate by comparison with in situ observations, with a north-west south-east gradient.

#### 2.4.4 Specific Humidity Correction

The reference data set for this bias reduction is the NOC1.1 flux climatology, which is the renamed version of the Original SOC flux climatology [Josey et al., 1998]. The flux fields have been determined from in situ meteorological reports in the COADS 1a (Comprehensive Ocean Atmosphere Dataset 1a) covering the period 1980-93. A major innovation in the production of the climatology was the correction of the meteorological reports for various observational biases using additional measurement procedure information from the WMO47 list of ships.

In the MFS model implementation, the specific humidity is computed by the empirical formula:

$$q_A(T_d) = 0.98\rho^{-1}640.38 \cdot e^{(-5107.4/T_d^{ERA})}$$

where  $T_D$  is the ERA-40 dew point temperature given in °K and the 0.98 factor only applies over sea water. More accurate formulations are available, but not necessary, due to the uncertainty of the 0.98 factor and of the transfer coefficient,  $C_E$ , of equation (3.3), for instance.

However, the ERA-40 reanalysis atmosphere is drier than NOC, leading to the correction term shown in figure 2.5. It is the difference:

## 2.4 Forcing Fields Bias Reduction

$$D_H = \langle q_A^{NOC} \rangle - \langle q_A^{ERA} \rangle \quad (2.12)$$

where the two averages have been computed for the period 1980-1993.

After correction, ERA-40 reanalysis becomes wetter, and the latent heat and evaporation are less negative by  $9 \text{ W/m}^2$  and  $0.11 \text{ m/yr}$ , respectively. Again, in order to avoid errors as mentioned in section 2.4.1 we have limited the corrections to be no greater than  $1.5 \text{ g/m}^3$ . The monthly mean surface averaged resulting specific humidity is shown in figure 2.7C.

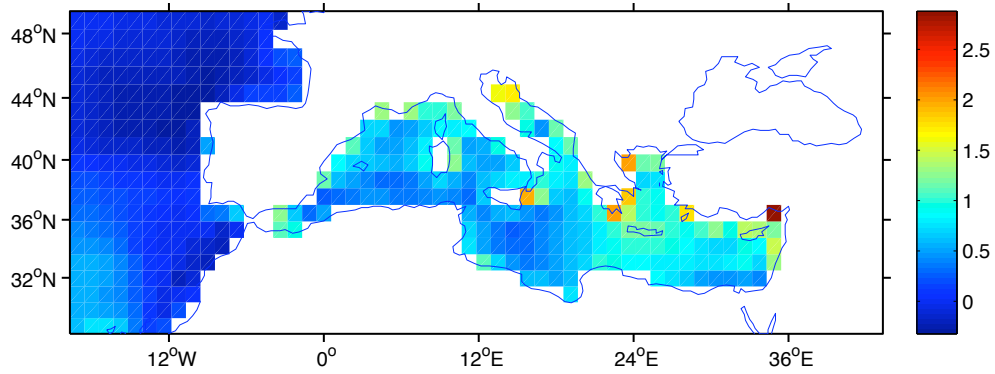


Figure 2.5: Specific humidity correction term  $D_H$  in  $\text{g/Kg}$ . The difference is computed for the period 1980-1993 according to equation (2.12).

### 2.4.5 Precipitation Correction

With the above corrections and the uncorrected ERA-40 rainfall (given by the sum of Large scale and Convective precipitation) we obtain a deficit  $E + P$  of about  $-0.79 \text{ m/yr}$  (see column 6; tab. 2.1). We decided to apply a further correction to the ECMWF reanalysis based on the CMAP data set [Xie and Arkin, 1996]. These are gridded fields of monthly precipitation obtained by merging estimates from five sources of information with different characteristics: gauge-based monthly analysis from the Global Precipitation Climatology Centre, three types of satellite estimates [the infrared-based GOES Precipitation Index, the microwave (MW) scattering-based Grody, and the MW emission-based Chang estimates], and predictions produced by the operational forecast model of

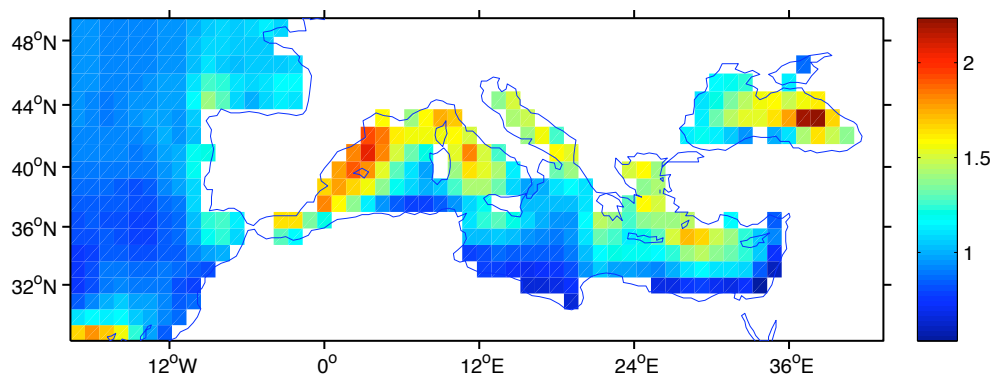


Figure 2.6: Precipitation correction factor  $R_P$ . The ratio has been computed for the period 1979-2001, according to equation (2.13). A north-south pattern is visible in the Mediterranean Basin error field.

the European Centre for Medium-Range Weather Forecasts (ECMWF).

Figure 2.6 shows the ratio:

$$R_P = \frac{\langle P^{CMAP} \rangle}{\langle P^{ERA} \rangle} \quad (2.13)$$

where the averages have been computed for the period 1979-2001. The ECMWF reanalysis precipitation is less over the northern Mediterranean basin, but more over the southern.

This last correction leads to a deficit  $E + P$  of  $-0.70 \text{ m/yr}$  for the period 1985-2001, which is comparable to that obtained by Gilman and Garrett [1994] (even though their larger evaporation is compensated by more precipitation) and consistent with the results of Mariotti and Struglia [2002] who proposed  $-0.5$  to  $-0.7 \text{ m/yr}$  as the range for the excess of evaporation over precipitation.

## 2.5 Corrected Heat And Freshwater Fluxes

In the previous section we have determined the field corrections, which produce the best estimates for heat and freshwater fluxes in the considered time window 1985-2001 (see column 7; tab. 2.1). At this point we assume that the space-dependent correction factors are constant in time and apply them over the entire ERA-40 reanalysis period

## 2.5 Corrected Heat And Freshwater Fluxes

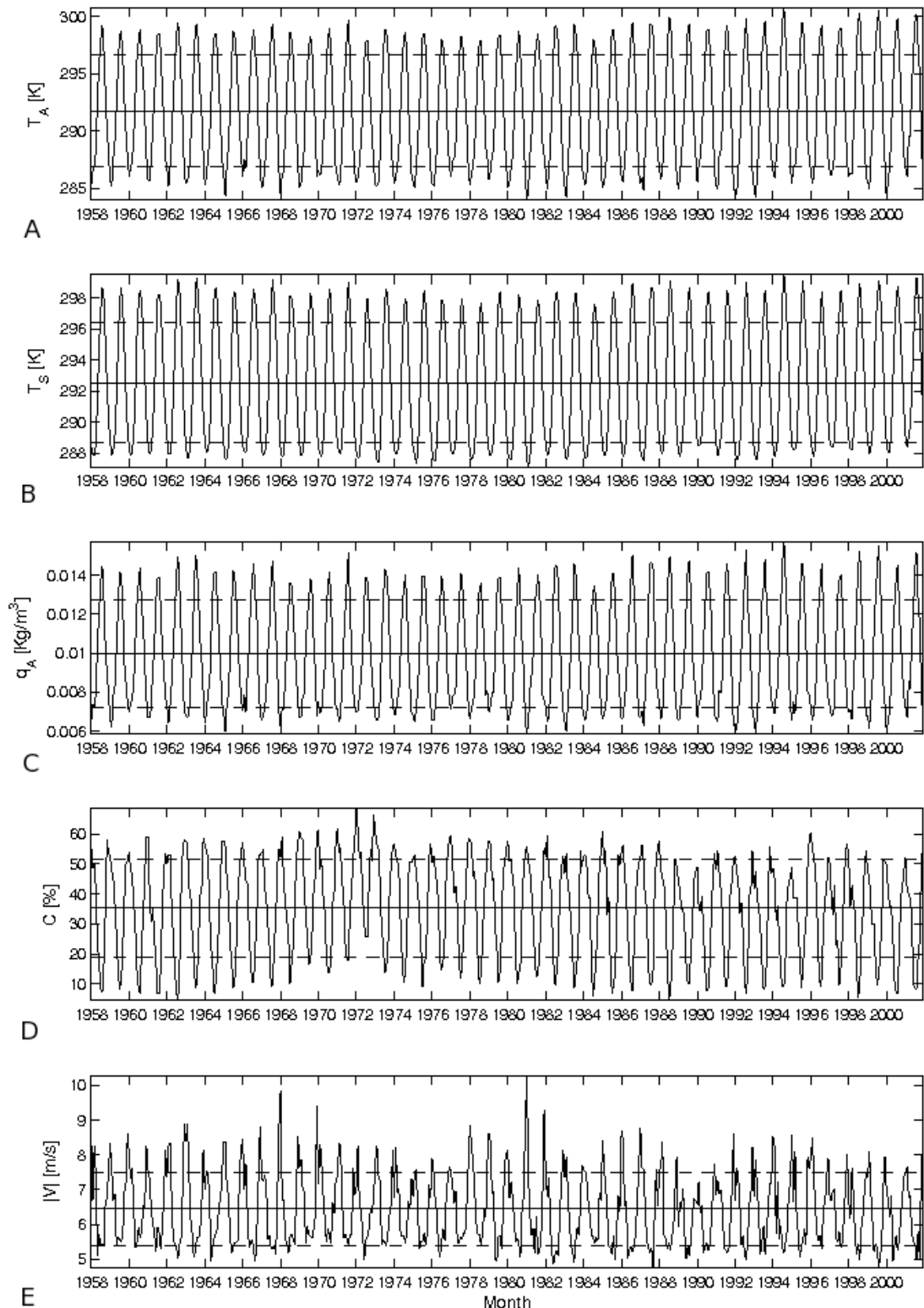


Figure 2.7: Time series of surface averaged monthly corrected  $T_A$  (A),  $T_S$  (B),  $q_A$  (C),  $C$  (D) and  $|\vec{V}|$  (E) with the bias reductions applied to sea surface temperature, specific humidity and wind speed. The time window is 1958-2001. The mean value (solid line) and  $\pm 1$  standard deviation (shaded line) are also indicated.

(1958-2001).

The results are shown in table 2.2. In column 1, the flux components given directly in the original ERA-40 data set are presented. In column 2, instead, we show those obtained with the "Corrected ERA-40 data set", calculated applying equations 2.2, 2.3, 3.2 and 3.3 using corrected ERA-40 shortwave radiation and uncorrected longwave radiation. Regarding the freshwater balance, both deficits  $E + P$  satisfy the values found in literature and cited in section 2.1, but also for the 44-year reanalysis period the heat fluxes directly taken from ERA-40 fail to close the budget, according to the measurements of the heat gained through the Strait of Gibraltar ([Bethoux, 1979] and [Macdonald et al., 1994]). In the ECMWF reanalysis, the underestimation of the shortwave radiation flux is only partially compensated by less negative turbulent fluxes, such as the lower evaporation, which is redressed by a too low precipitation over the Mediterranean Basin.

On the other hand, when we apply all the corrections and the new formulation for the radiative fluxes, the budget is recovered and the "Mediterranean heat budget closure problem" is solved.

The budget has been evaluated also using the original resolution ERA-40 fields and the value of  $Q_T$  in Table 2.2 becomes  $-5 W/m^2$ , a value still within the  $6 \pm 3 W/m^2$  uncertainty on the heat budget mean value.

An interesting effect of the corrections is the change in the balance of terms. The  $17 W/m^2$  increase in solar radiation is absorbed over a range of ocean depths, while the increased latent and sensible cooling is only from the surface. This shift in balance could have a profound effect on the seasonal cycle of SST, particularly during the spring heating and restratification season [Denman and Miyake, 1973].

### 2.5.1 Interannual Variability

We now examine the interannual variability of the corrected heat balance components. Daily components have been calculated then monthly averaged over the basin.

## 2.5 Corrected Heat And Freshwater Fluxes

	ERA-40	Corrected
$Q_S [W/m^2]$	161	178
$Q_L [W/m^2]$	-78	-79
$Q_E [W/m^2]$	-86	-92
$Q_H [W/m^2]$	-10	-14
$Q_T [W/m^2]$	<b>-13</b>	<b>-7</b>
$E [m/yr]$	-1.08	-1.18
$P [m/yr]$	0.39	0.53
$F_T [m/yr]$	<b>-0.70</b>	<b>-0.64</b>

Table 2.2: Heat and freshwater budget components for the 44 year period 1958-2001. The first column represents the values given in the original ERA-40 data set. The second column shows those obtained with the "Corrected ERA-40 data set", including  $Q_{SD}$  and  $Q_{LD}$ , and calculated by means of equations 2.2, 2.3, 3.2 and 3.3. Also included is the correction for ERA-40 precipitation which is obtained as the sum of convective and large scale precipitation.

The time series of monthly net shortwave radiation (figure 2.8A), obtained using equation (2.2) and the corrected  $Q_{SD}$  from ERA-40 data set, ranges from a winter minimum of  $53 W/m^2$  to a summer maximum of  $302 W/m^2$ . It is dominated by a strong seasonal cycle with a small interannual signal, mostly due to the cloud coverage. In particular, the time series shows a summer cool anomaly during the years 1970-1973 which is due to an anomalous high cloud coverage during the same period (see figure 2.7D). The same effect is also evident in the net longwave radiation,  $Q_L$ , time series (figure 2.8B) where this term reaches its highest value of  $-60 W/m^2$ . In fact, since clouds have opposing effects on the two radiative components of the heat balance, there is a significant compensation between the two terms but again the effects on the SST will be different.

The sensible heat flux,  $Q_H$ , is the smallest of the four terms (figure 2.8D). It becomes positive during the months of April or May and remains negative for the remaining part of the year. It ranges from a maximum of  $7 W/m^2$  to a minimum value of  $-71 W/m^2$  with strong interannual variability relative to its mean. There are five large minima during the years 1967, 1969, 1980, 1991 and 1999, which are related to strong wind regimes and air temperature anomalies during the same period (see figure 2.7).

The latent heat flux,  $Q_E$ , time series (figure 2.8C) is always negative, ranging from a

summer maximum of  $-30 \text{ W/m}^2$  to a winter minimum of  $-130 \text{ W/m}^2$ .

Finally, the surface total heat flux,  $Q_T$ , time series (figure 2.8E) shows a smooth signal dominated by the net short wave radiation flux and interannually modulated by  $Q_E$  and  $Q_H$ . It ranges from  $-275 \text{ W/m}^2$  to  $181 \text{ W/m}^2$ . However, it's important to notice that while the maxima of the time series, which occur during the months of May and June, show values which differ at most by about  $30 \text{ W/m}^2$ , the December minima can vary by more than  $130 \text{ W/m}^2$ . This peculiarity of the Mediterranean basin plays a significant role in the climatological heat budget. Over the 44 years, replacing the 10 most negative values (the years 1962, 1967, 1968, 1969, 1980, 1986, 1990, 1991, 1995 and 1998) with the interannual average of the minima of the corrected  $Q_T$ , would change the overall mean from  $-7 \text{ W/m}^2$  to about  $-3.5 \text{ W/m}^2$ . Since we pointed out that the surface total heat flux is mainly interannually modulated by the latent heat of evaporation and the sensible heat flux which are strongly affected by the wind regimes in the Mediterranean, this means that the total heat budget is closed by approximately half of its long term value by few strong cooling events due to cold and dry winds blowing over the basin during winter time. This peculiarity proves the importance of choosing a long enough time window when one attempts a budget study for this particular geographical area, since those extreme events have necessarily to be included in the budget computation

### 2.5.2 Climatology

Figure 2.9 shows the pattern of climatological values of corrected  $Q_T$  for the months of July (A), December (B), annual (C) and of annual  $F_T$  (D). These months also represent the maximum heat loss and heat gain respectively. The heat flux annual mean shows minima in the north-western Mediterranean (Gulf of Lion), in the Adriatic Sea and northern Ionian Sea, and in the Aegean Sea, essentially reflecting the pattern of the principal continental winds (Mistral, Bora, Ethesian). The maxima are instead located in the Alboran Sea, in the Channel of Sicily and in the Levantine. Figure 2.9C shows a north-west to south-east pattern. Moreover, in areas of maxima the summer heating

## 2.5 Corrected Heat And Freshwater Fluxes

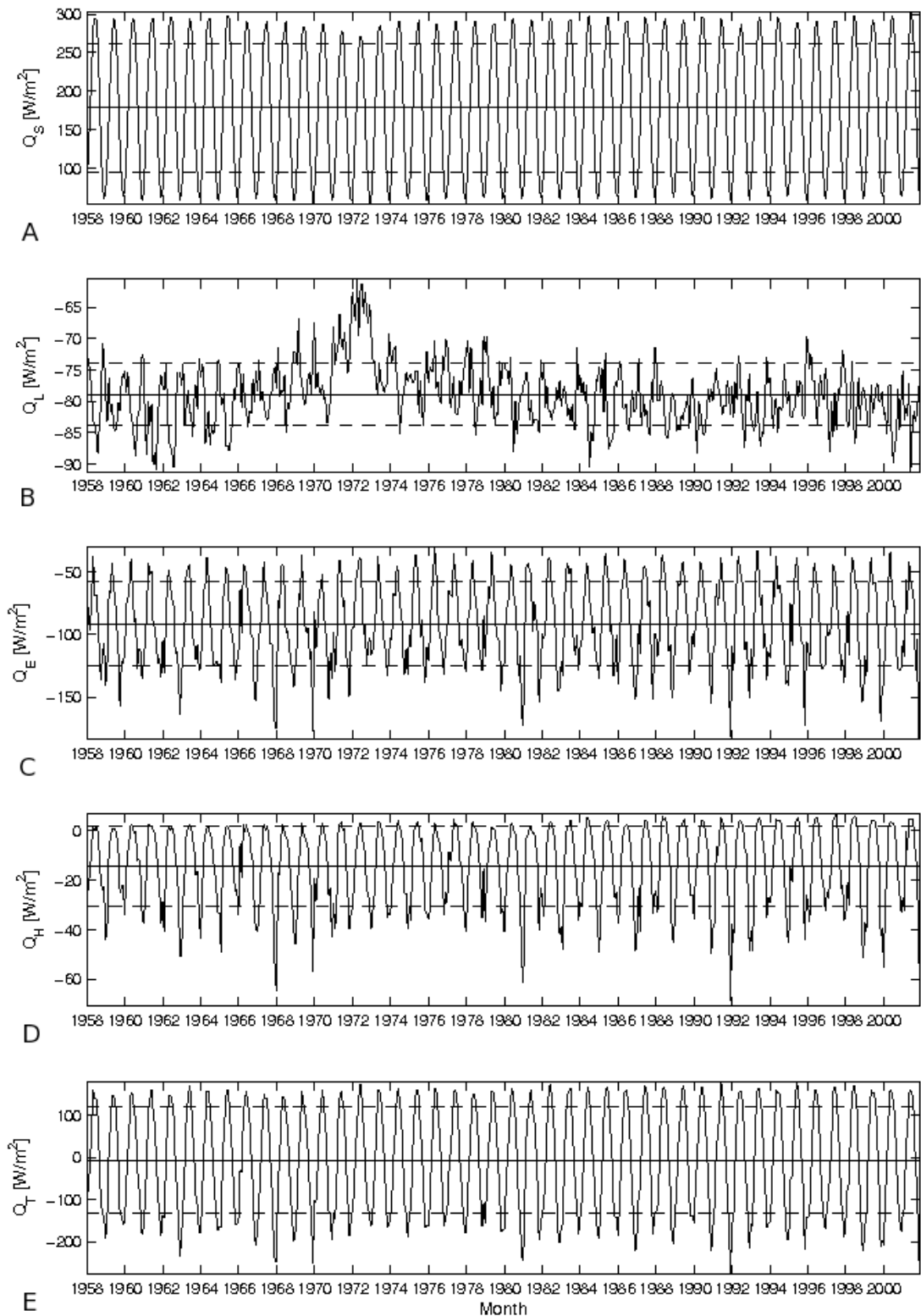


Figure 2.8: Time series of the surface monthly averaged heat fluxes calculated with the final parametrization (equations (2.2), (2.3), (3.2) and (3.3); see column 2 of tab. 2.2) including all the mentioned corrections:  $Q_S$  (A),  $Q_L$  (B),  $Q_E$  (C),  $Q_H$  (D) and  $Q_T$  (E). The total mean (solid line) and  $\pm 1$  standard deviation (shaded line) are also indicated.

(A) is much larger than winter cooling (B), while the opposite behaviour occurs for the minima.

The Southampton Ocean Centre (SOC) climatology [Josey et al., 1998] (not shown) also provides a global estimate of surface heat and freshwater fluxes but over the Mediterranean Sea its average heat flux of  $42 \text{ W/m}^2$  is much larger than the measured heat transport at Gibraltar. Nevertheless, the spatial pattern is similar to the corrected ERA-40  $Q_T$ .

The total freshwater flux (figure 2.9D) shows a strong north-south gradient, with small areas where the precipitation exceeds the evaporation located on the northern coasts of the Mediterranean basin.

### **2.5.3 NAO Changes And The Mediterranean Sea Net Surface Heat Flux**

The North Atlantic Oscillation (NAO) has been described as the indicator of the strength of the zonal flow along the mid and high latitudes of the North Atlantic. The positive and negative phases of the North Atlantic Oscillation are defined by the differences in pressure between the persistent low over Greenland and Iceland and the persistent high off the coast of Portugal. During a positive NAO phase, both systems are stronger than usual, that is, the low has a lower atmospheric pressure and the high has a higher atmospheric pressure. During the negative phase of the NAO, both systems are weaker, lowering the difference in pressure between them. The NAO is one of the major modes of monthly to interdecadal variability in the Northern Hemisphere atmosphere, accounting for about one-third of the wintertime total variance. Interest in the NAO has been recently renewed mainly because of a trend towards the positive phase of the oscillation, particularly in the last two or three decades.

In this section we explore the Mediterranean-NAO teleconnection, which supposedly should be a dominant mode of variability in the Mediterranean [Rixen et al., 2005]. After all, the ocean communicates with the overlying atmosphere through changes in the heat fluxes. Moreover, heat flux is a more physically meaningful parameter than the SST (see

## 2.5 Corrected Heat And Freshwater Fluxes

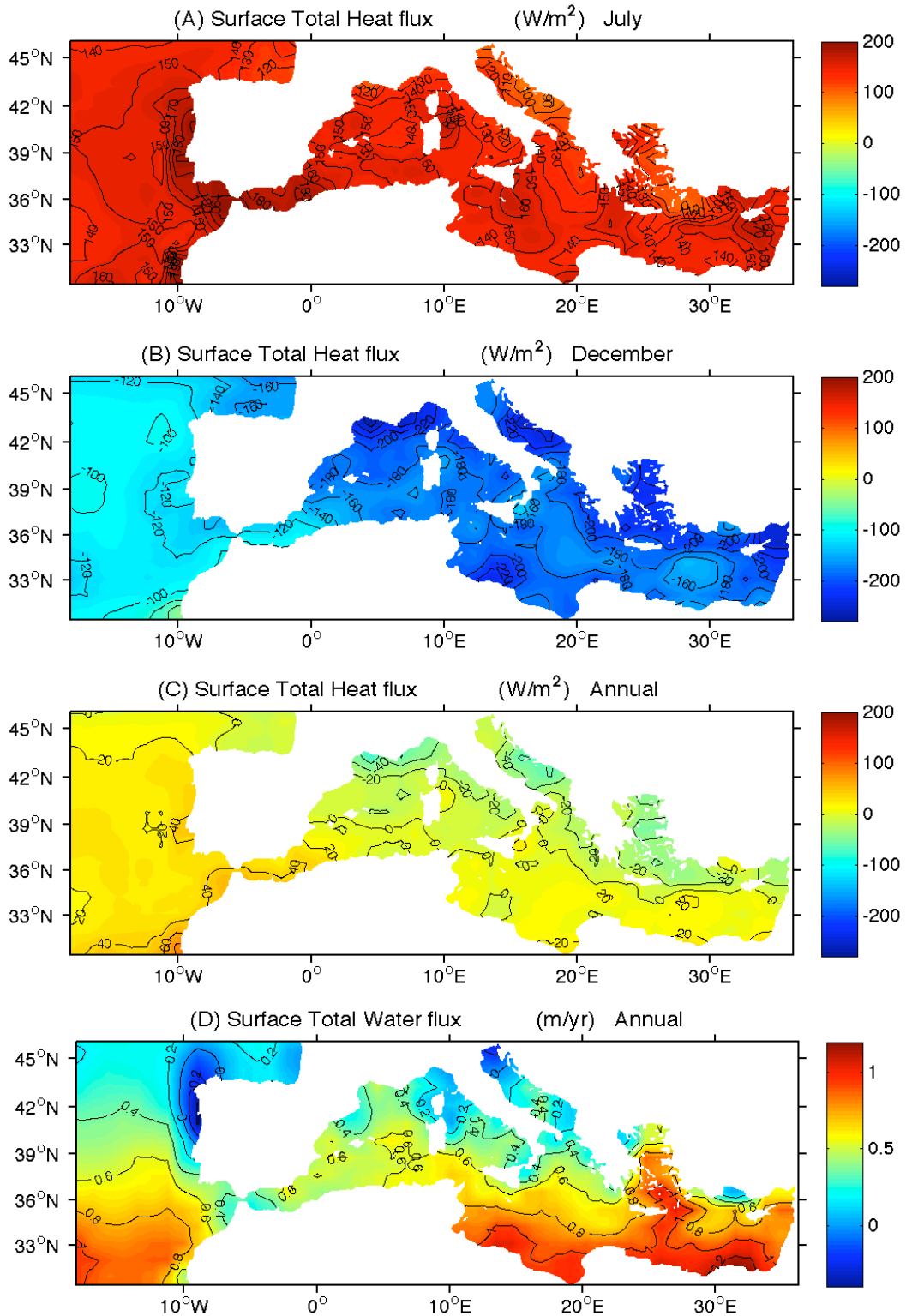


Figure 2.9: Climatology of  $Q_T [W/m^2]$  for the month of July (A), December (B), annual (C) and of  $F_T [m/yr]$  annual (D). The pictures are realized using the air sea physics which produces the fluxes of tab. 2.2; column 2 and for the time window 1958->2001.

figure 2.10A for annual averages of  $Q_T$ ).

For this reason, we compared the Winter (December through March) NAO index based on the difference of normalized sea level pressure between Lisbon, Portugal and Stykkisholmur/Reykjavik, Iceland, with the annual mean  $Q_T$  anomaly time series, computed as the differences of the yearly mean total heat fluxes from the overall mean of  $-7 W/m^2$  given in Table 2.2. The sea level pressure anomalies at each station were normalized by division of each seasonal mean pressure by the long-term mean (1864-1983) standard deviation. Normalization is used to avoid the series being dominated by the greater variability of the northern station. The station data were originally obtained from the World Monthly Surface Station Climatology. Further details can be found in Hurrell et al. [2001].

The correlation coefficient that we obtained between the two yearly time series is 0.37 with a 95% confidence interval of  $0.08 < C < 0.60$ , which is very small, however, a similar oscillation at longer time-scales was noticeable in the two curves (not shown). In order to quantify this information, we computed for both  $Q_T$  anomaly and NAO index a five-year running mean, and we compared the two resulting time series (figure 2.10B). The resulting correlation coefficient has the much more significant value of 0.68 and a 95% confidence interval of  $0.48 < C < 0.81$ , meaning that the two fields have a high positive correlation. We can argue that this relationship is at least partially due to the wind regimes induced by the NAO itself: a positive index implies lower winds over the Mediterranean Basin, which determines lower evaporation and consequentially a lower latent heat flux which is, as we pointed out, the largest modulation factor of the net total surface heat flux. Conversely, a negative NAO index is accompanied by a stronger wind regime over the basin, that implies greater evaporation and as a direct consequence a low  $Q_T$  anomaly. Moreover, the climatological nature of this correlation once again confirms the importance of the choice of a long period for budget studies in the Mediterranean Sea, since the long time scale effects of the NAO must be definitely taken into account because of their direct implication on the air-sea interaction heat exchange processes.

## 2.6 Conclusion

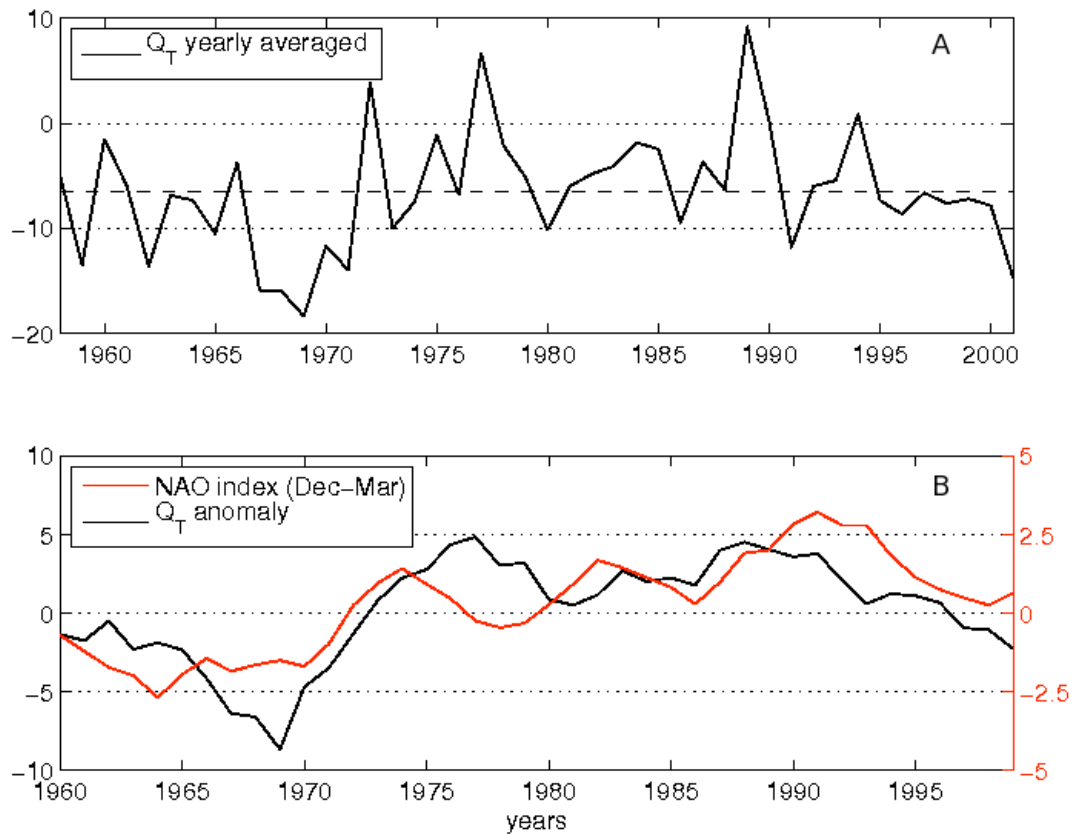


Figure 2.10: Panel A: Yearly averaged net surface heat flux,  $Q_T$ , (see tab 2.2;column 2) computed with formulas (2.2), (2.3), (3.2) and (3.3) using radiative fields provided by ERA-40 and applying all the correction described in section 2.5. Panel B: 5 years running mean of net surface heat flux (black line; left axes) and Winter (December through March) index of the NAO based on the difference of normalized sea level pressure between Lisbon, Portugal and Stykkisholmur/Reykjavik, Iceland (red line; right axes).

## 2.6 Conclusion

In this paper, we show that the Mediterranean Sea places a valuable constraint on the long-term mean basin averaged  $Q_T$ , which should compensate for the measured net heat inflow at Gibraltar. Furthermore, freshwater budget considerations constrain the evaporation, and consequently the latent heat flux. These are aspects of so called "Mediterranean heat budget closure problem", which have been addressed by the data sets of this study.

We demonstrate that ECMWF ERA-40 reanalysis without any corrections to its surface fields does not close the budget. In addition, the individual components of the surface heat balance are incompatible with some in situ local observations (figure 2.1).

For this reason, we adapted a correction method, developed by Large and Yeager [2008] for the global ocean, to the Mediterranean Sea. This method is based on the determination of the best estimate of the heat and freshwater budgets for a reference period chosen to match the availability of important reference data sets. For this period (1985-2001) we have computed different space dependent bias reduction terms which when applied to the ERA-40 reanalysis forcing fields along with the use of a new formulation for radiative fluxes, allow the satisfaction of the Mediterranean closure problem. Averaged over the basin, they increase the shortwave radiation by  $21 W/m^2$ , increase the wind speed by 25%, increase the specific humidity by about  $1 g/Kg$  and increase the sea surface temperature (SST) by less than  $1 ^\circ C$ . Locally the SST correction ranges from more than  $2 ^\circ C$  to about  $-1 ^\circ C$ . The precipitation is increased by about a factor of 2 off some northern coasts and reduced along the southern and eastern margins where there is little rainfall. The correction terms have been then extended to the entire ERA-40 period (1958-2001). In this way, we have realized what we called the "Corrected ERA-40 data set" that is an high frequency (6-hourly) data set suitable for forcing ocean models in the Mediterranean area. Recently the MFS model has been used as a test-bed to check the correction method for the atmospheric fields and air-sea physical parametrizations described in this paper. Preliminary results obtained during a one-year integration experiment show an improvement in the estimation of the SST and a positive impact on the model temperature and salinity profiles if compared with in situ data. The impact of air-sea physical parametrizations on the model simulation quality will be an area of active research in the near future.

Among all the corrections, the one to the wind speed has the largest effect ( $-22 W/m^2$ ) on the final surface heat balance. Furthermore, the interannual modulation of  $Q_T$  is imposed by the latent heat flux,  $Q_E$ , and the sensible heat flux,  $Q_H$ , (see figure 2.8) which are strongly dependent on the wind speed and wind speed events during wintertime.

Shortwave radiation correction is also large for the ERA-40, probably due to the compensating effects in the atmospheric model, which has produced it. Moreover, in

## 2.7 Appendix 1: Bulk transfer coefficients

---

situ and satellite data sets confirm that the annual mean value should be about  $180W/m^2$  as previously found by Gilman and Garrett [1994].

Finally, the net surface heat flux,  $Q_T$ , is related to the winter NAO index. A correlation coefficient of 0.68 has been found after a 5-year running mean filter has been applied to the two time series. This aspect underlines the fact that the correlation is to be considered in a climatological sense. In other words, NAO yearly variations are not directly correlated to annual mean heat flux anomalies over the Mediterranean Sea but only the long time scale modulation can be associated to teleconnections.

Wind anomalies during winter are responsible for half the negative heat budget of the basin. Our study points out the need for longer time series of fluxes to really understand their low frequency variability and to solve the heat budget closure problem.

## 2.7 Appendix 1: Bulk transfer coefficients

The bulk transfer coefficients used in this work for the computation of latent heat of evaporation and sensible heat fluxes (eq. 3.2 and 3.3) are taken according to Kondo [1975], who suggested the following approximate formulas for neutral stability, when the wind speed is expressed in  $m/s$ :

$$10^3 C_H(10m) = a_h + b_h \left\| \vec{V} \right\|^{p_h} + c_h (\left\| \vec{V} \right\| - 8)^2 \quad (2.14)$$

$$10^3 C_E(10m) = a_e + b_e \left\| \vec{V} \right\|^{p_e} + c_e (\left\| \vec{V} \right\| - 8)^2 \quad (2.15)$$

where the numerical constant  $a_{h,e}$ ,  $b_{h,e}$ ,  $c_{h,e}$  and  $p_{h,e}$  vary with a range of wind speed speeds as shown in Table2.3. The coefficients for non-neutral cases are expressed in terms of a practical index of atmospheric stability, which are obtainable from wind speed and the difference of temperatures at the sea surface. Figure 2.11a shows  $C_E$  computed according to equation 2.15 for neutral condition ( $T_A - T_S = 0$ ) and for other 6 non-neutral cases ( $T_A - T_A = 3.0, 2.0, 1.0, -1.0, -2.0, -3.0$ ).

$\ \vec{V}\ $ [m/s]	$a_h$	$a_e$	$b_h$	$b_e$	$c_h$	$c_e$	$p_h$	$p_e$
0.3 to 2.2	0	0	1.185	1.23	0	0	-0.157	-0.16
2.2 to 5	0.927	0.969	0.0546	0.0521	0	0	1	1
5 to 8	1.15	1.18	0.01	0.01	0	0	1	1
8 to 25	1.17	1.196	0.0075	0.008	-0.00045	-0.0004	1	1
25 to 50	1.625	1.68	-0.017	-0.016	0	0	1	1

Table 2.3: Parameters in expressions for neutral bulk transfer coefficients

The formulation is obtained under the condition that no ocean spray exists. In strong wind regimes, it is almost certain that the effect of the ocean spray on the temperature and humidity profiles would be important thus leading to unrealistic coefficient values. This approximation is reasonable in the Mediterranean Basin where the average wind speed is about  $6\text{ m/s}$ , however the previous equations are not used for wind speed greater than  $50\text{ m/s}$ .

This parametrization is used for consistency with the Mediterranean Forecasting System (MFS) standard air-sea physics which was calibrated in a comparison study between different bulk formulas [Castellari et al., 1998].

In order to provide an estimate of the sensitivity of our results on different exchange coefficients, we recomputed the total heat and freshwater budgets using an alternative parametrization.

Figure 2.11b shows the coefficient obtained from the Coupled Ocean-Atmosphere Response Experiment (COARE) bulk algorithm (version 3.0) as described in Fairall et al. [2003] and then expressed as polynomial functions by Kara et al. [2005]. These so-called NRL Air-Sea Exchange Coefficients (NASEC) include stability dependence through air-sea temperature difference, wind speed at 10 m above the sea surface and relative humidity.

Table 2.4 presents the total fluxes and their components computed at the original ERA-40 resolution using Kondo and NASEC parametrizations. The coefficients are about 10% different at low wind speed and this produces a difference of  $8\text{ W/m}^2$  in the latent heat of evaporation and  $1\text{ W/m}^2$  in the sensible heat flux. This result confirms the

## 2.7 Appendix 1: Bulk transfer coefficients

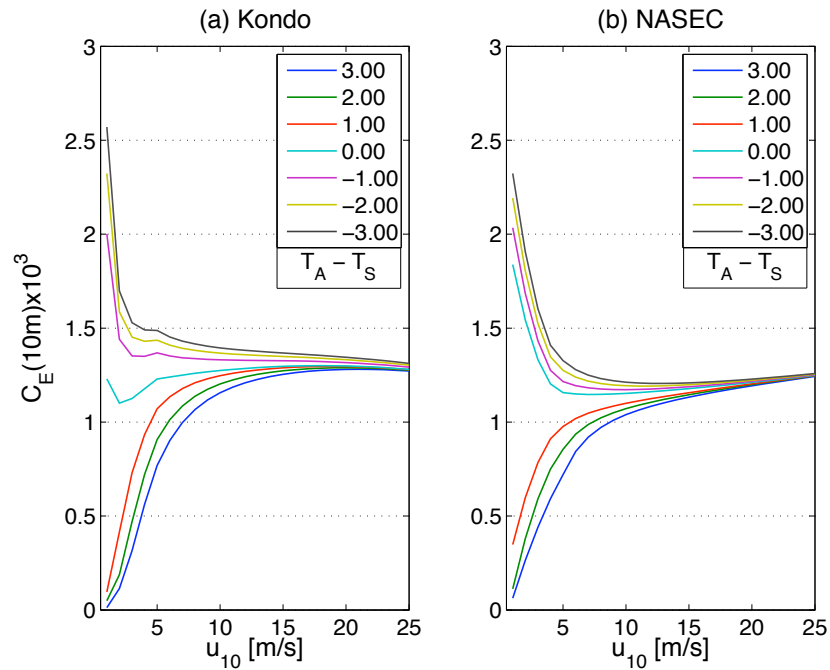


Figure 2.11: (a) Kondo [1975] 10 m  $C_E$  bulk transfer coefficient as a function of wind speed and for 7 different  $T_A - T_S$  values; (b) 10 m  $C_E$  bulk transfer coefficient obtained from the Coupled Ocean-Atmosphere Response Experiment (COARE) bulk algorithm (version 3.0) as described in Fairall et al. [2003]. The plot has been obtained for relative humidity equal to 80% and shows  $C_E$  as a function of the wind speed for 7 different  $T_A - T_S$  values.

	Kondo	NASEC
$Q_S [W/m^2]$	182	182
$Q_L [W/m^2]$	-79	-79
$Q_E [W/m^2]$	-94	-86
$Q_H [W/m^2]$	-14	-13
$Q_T [W/m^2]$	<b>-5</b>	<b>4</b>
$E [m/yr]$	-1.20	-1.10
$P [m/yr]$	0.53	0.53
$F_T [m/yr]$	<b>-0.67</b>	<b>-0.57</b>

Table 2.4: Sensitivity of the total budget to the bulk transfer coefficient parametrization. Column 1 and 2 show total heat and freshwater fluxes and their components obtained with the "Corrected ERA-40 data set", including  $Q_{SD}$  and  $Q_{LD}$ , and calculated by means of equations 2.2, 2.3, 3.2 and 3.3, using Kondo [1975] and NASEC bulk transfer coefficients, respectively.

choice of Kondo [1975] for the Mediterranean Sea, which gives the value of  $94 W/m^2$  as suggested by Gilman and Garrett [1994] with corrected atmospheric fields from ERA-40.

# Chapter 3

## Impact studies of air-sea physics parametrizations in the Mediterranean Forecasting System

### 3.1 Introduction

A main subject of discussion in the ocean modelling community is the parametrization of air-sea exchanges. Feedback between ocean and atmosphere are challenging because of the complexity of physical processes that involve a wide range of space and time scales in the atmospheric and ocean boundary layers , the atmosphere being characterized by shorter timescales and larger space scales than the ocean.

A standard practice in operational oceanography is to perform simulations and forecasts, introducing air-sea interaction fluxes computed by means of empirical (bulk) formulae and available atmospheric data sets (i.e. Rosati and Miyakoda [1988], Castellari et al. [1998]). This approach, even if correct from a physical point of view, involves high accuracy in the formulation of the bulk formulas and in the atmospheric forcing fields, but even today both of these requirements are far from being met (Gilman and Garrett [1994]; Bignami et al. [1995]; Pettenuzzo et al. [in press]).

The Mediterranean Sea is a basin where a wide range of oceanic processes and interactions of global interest occur. The shallow Strait of Gibraltar connects it with the Atlantic Ocean, and the Mediterranean basin can be subdivided in two parts, the Western and Eastern Mediterranean Seas, separated by the shallow and narrow Strait of Sicily. Through Gibraltar, the fresher Atlantic water flows into the basin, replacing both the evaporated water and the denser and saltier Mediterranean water flowing out into the Atlantic. The incoming water layer is about 50-100 m thick and flows eastward, changing progressively its hydrological properties, becoming warmer and saltier because of the air-sea interaction processes and the mixing. Actually, the existence of a narrow strait makes the Mediterranean Sea one of the few region in the World Ocean where the mass, heat and salt transports are known with enough accuracy to allow for testing different air-sea interaction parametrizations in ocean general circulation numerical models.

Since 1999, the Mediterranean Forecasting System (MFS) has been producing analysis and forecasts in the Mediterranean Sea [Pinardi et al., 2003]. The MFS model is forced by momentum, water and heat fluxes interactively computed by bulk formulae using the 6-hourly, 0.5-degree resolution operational analyses and forecasts from the European Center for Medium-Range Weather Forecasts (ECMWF) and models predicted sea surface temperature. The choice of the MFS standard air-sea physics parametrization is based on the work of Castellari et al. [1998], who defined a set of calibrated bulk formulae in the framework of a comparison study including different available data sets and formulations, and were based on heat and water budget considerations.

However, very recently Pettenuzzo et al. [in press] have shown that using the ECMWF ERA-40 reanalysis [Uppala et al., 2005] together with the MFS ‘calibrated set’ of bulk formulae fails to close the Mediterranean budget for a 44-year period ranging from 1958 to 2001. Moreover, they showed that the computed solar radiation is in disagreement and overestimates the locally-observed values by about 10%. For this reason, they proposed an alternative air-sea physics parametrization, which with modified bulk formulae and a set of bias reduction terms for the basic forcing fields is able to accomplish the closure

### 3.2 MFS general circulation models

---

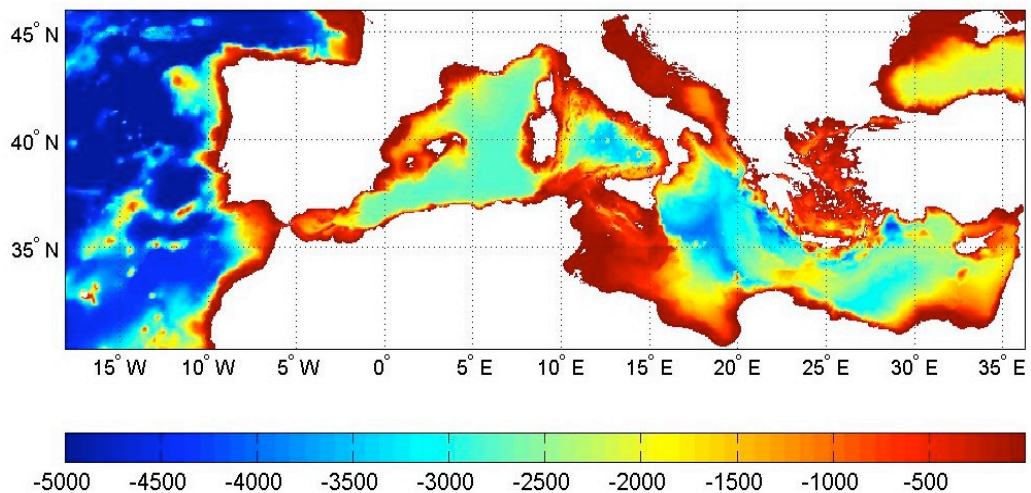


Figure 3.1: Topography of the entire MFS operational models domain.

of the heat and water budgets.

In this paper, we evaluate the impact of the new air-sea physics adapted and implemented in MFS. In Section 3.2, we will describe the numerical models used in this work and their relative differences. Details of the air-sea physics implementation and of the set of experiments are treated in Section 3.3. In Section 3.5, we will present the experiment results and compare them with observed satellite and in-situ data. A summary and conclusion may be found in Section 3.6.

### 3.2 MFS general circulation models

The present Mediterranean Forecasting system (MFS) operational models are two implicit free-surface versions of the Ocean PARallelise code (OPA, Madec et al. [1998]) and (OPA 9.0 Madec [2008]) to which we will refer in this paper as sim3 [Tonani et al., 2008] and sim4 [Oddo et al., 2009], respectively. The MFS domain covers the entire Mediterranean Basin and extends into the Atlantic (see Figure 3.1). Both models have a 1/16-degree horizontal resolution and 72 unevenly spaced vertical z-levels, and the main difference between the two model set up concerns the vertical partial cells approximation used in sim4.

Another important modification is the parametrization of surface water and salt fluxes: in sim3 the rate  $E - P - R$ , with  $E$  being the evaporation,  $P$  the precipitation and  $R$  the river runoff, is estimated by means of a relaxation toward a surface climatological salinity [Tonani et al., 2008], while in sim4,  $E$  is derived directly from the latent heat flux,  $P$  is taken from monthly mean Climate Prediction Center Merged Analysis of Precipitation (CMAP) data [Xie and Arkin, 1996] and  $R$  is composed of monthly mean climatological data. Only seven major rivers have been implemented, that is, the Ebro, Nile and Rhone (Global Runoff Data Center; Fekete et al. [1999]), Po, Vjosa, Seman and Bojana [Raicich, 1996]. In this configuration, the Dardanelles inflow has also been parametrized as a river and its monthly climatological net rates are taken from Kourafalou and Barbopoulos [2003].

The advection scheme for active tracer has also been upgraded from the 2nd order centered used in sim3 to a mixed up-stream/MUSCL (Monotonic Upwind Scheme for Conservation Laws, [Van Leer, 1979], as implemented by Estubier and Lévy [2000]) in sim4. This new scheme has the capability to switch to a simple up-stream scheme in areas where numerical instabilities might occur such as in proximity of the river mouths, in the Strait of Gibraltar and close to the Atlantic lateral boundaries.

However, the major model improvement of sim4, with respect to sim3, concerns the parametrization of the connection between the Mediterranean Sea and the North Atlantic Ocean [Oddo et al., 2009]. In sim3, the Atlantic part of the model consists of three closed boundaries where, in order to keep the solution realistic, the temperature and salinity are relaxed toward monthly climatological values [Levitus, 1998] using a space-dependent relaxation function. In sim4, instead, the Atlantic box is nested within the monthly mean climatological fields computed from the daily output of the MERCATOR 1/4-degree resolution global model [Drevillon et al., 2008], spanning 2001 to 2005. In this way the total volume is allowed to change producing improvements particularly evident in the Mediterranean sea level seasonal variability and in the salinity characteristics of the Modified Atlantic Water.

### 3.3 Air-sea physics implementation

	<b>sim3</b>	<b>sim4</b>
<b>Vertical Discretization</b>	z-levels	z-levels + partial cells
<b>(Evaporation-Precipitation-Runoff)</b>	Relaxation to surface salinity climatology	Interactively computed CMAP Precipitation Clim. Runoff
<b>Tracer Advection</b>	2nd order centered	MUSCL+up-stream
<b>Lateral Boundaries</b>	Closed+relaxation to Levitus Clim	Open - nested with MERCATOR

Table 3.1: Major differences between the two versions (sim3: OPA 8.1 and sim4: OPA 9.0) of the Mediterranean Forecasting System (MFS) operational models considered in this study.

Further details of the differences described above, and summarized in Table 3.1 can be found in Oddo et al. [2009].

### 3.3 Air-sea physics implementation

In this paper we show the impact of the implementation in MFS of a novel air-sea physics parametrization based on the work of Pettenuzzo et al. [in press] for the surface heat flux, which is given by the sum of four dominant terms:

$$Q_T = Q_S + Q_L + Q_E + Q_H \quad (3.1)$$

where  $Q_S$  is the net shortwave radiation flux,  $Q_L$  is the net longwave radiation flux,  $Q_E$  is the latent heat flux of evaporation and  $Q_H$  is the sensible heat flux and all the fluxes have been considered positive down.

In its standard setting, MFS uses empirical (bulk) formulae for the computation of the four components of the heat balance given in (3.1). The shortwave radiation  $Q_S$  is computed by means of the Reed [1977] formula with an incoming radiation  $Q_{TOT}$  modified according to Rosati and Miyakoda [1988], while for the longwave component  $Q_L$ , the Bignami et al. [1995] formulation is applied (see Table 3.2; column 1). The turbulent part of the balance is computed according to the following standard empirical formulae:

$$Q_H^{MFS} = -\rho_A C_P C_H \|\vec{V}\| (T_S - T_A) \quad (3.2)$$

$$Q_E^{MFS} = -\rho_A L_E C_E \|\vec{V}\| (q_S - q_A) = L_E E \quad (3.3)$$

where  $\vec{V}$  is the wind speed,  $\rho_A$  is the density of the moist air,  $C_P$  is the specific heat capacity,  $C_E$  and  $C_H$  are turbulent exchange coefficients for temperature and humidity taken according to Kondo [1975],  $L_E$  is the latent heat of vaporization,  $q_A$  is the specific humidity of air and  $q_S$  is the specific humidity saturated at temperature  $T_S$ .

Pettenuzzo et al. [in press] proposed two main changes: the modification of the bulk formulae for the computation of the radiative part of the heat balance and the reduction of the biases of the basic forcing fields, including radiation, by means of a set of bias reduction terms computed by comparison of the adopted atmospheric data set with more reliable observational data.

In the new formulation, both shortwave and longwave downward components are taken directly from the ECMWF (European Center for Medium Range Weather Forecasts) operational analyses and the net fields are computed using a space dependent albedo  $\alpha$  [Payne, 1972] and with the addition of a black-body-like term, respectively, with  $\epsilon$  being the ocean emissivity,  $\sigma$  the Stefan-Boltzmann constant and  $T_S$  the sea surface temperature (see Table 3.2; column 2). The ECMWF downward radiation components are 3-hourly cumulative fields expressed in  $W/m^2 \cdot s$ , thus the radiation provided to the numerical model is a 3-hourly integral average.

The forcing fields entering the remaining part of the heat balance of (3.1) are also taken from the ECMWF operational analysis at 6-hourly temporal frequency (00:00, 06:00, 12:00, 18:00 UTC) and 0.5° horizontal resolution. The meteorological variables used are: 2 m air temperature, 10 m wind speed zonal and meridional components and 2 m dew point temperature. The latter is used to calculate specific humidity  $q_A$  using the following empirical approximated formula [Large and Yeager, 2008]:

### 3.3 Air-sea physics implementation

MFS standard	New formulation
$Q_S = \begin{cases} Q_{TOT}(1 - 0.62C + 0.0019\beta)(1 - \alpha) & \text{if } C \geq 0.3 \\ Q_{TOT}(1 - \alpha) & \text{if } C < 0.3 \end{cases}$	$Q_S = Q_{SD} + Q_{SU} = Q_{SD}^{ECMWF}(1 - \alpha)$
$Q_L = -\varepsilon\sigma T_S^4 + [\sigma T_A^4(0.653 + 0.00535e_A)](1 + 0.1672C^2)$	$Q_L = Q_{LU} + Q_{LD} = -\varepsilon\sigma T_S^4 + Q_{LD}^{ECMWF}$

Table 3.2: Bulk formulae for the computation of the radiative part of the heat balance in MFS standard setting (MFS standard) and with the new formulation. In MFS standard, the shortwave radiation is computed according to Reed [1977] and Rosati and Miyakoda [1988] with  $Q_{TOT}$  the total clear sky solar radiation reaching the ocean surface,  $C$  the fractional cloud cover,  $\beta$  the noon solar altitude in degrees and  $\alpha$  the space-dependent albedo [Payne, 1972]. For the longwave flux calculation, MFS uses Bignami et al. [1995], with  $\varepsilon$  the ocean emissivity,  $\sigma$  the Stefan-Boltzmann constant,  $T_S$  the sea surface temperature,  $T_A$  the air temperature and  $e_A$  the atmospheric vapour pressure.

$$q_A(T_D) = 0.98\rho^{-1}640.38e^{(-5107.4/T_D)} \quad (3.4)$$

where  $T_D$  is the ECMWF dew point temperature given in °K and the 0.98 factor only applies over seawater.

The choice of the variables to be corrected is slightly different from the methodology proposed in Pettenuzzo et al., [2010]. In particular, the sea surface temperature in this case is a free evolving prognostic variable of the model and it is not corrected. Regarding precipitation, in sim4 we directly use the monthly mean CMAP data while in sim3, since the deficit  $E - P - R$  is obtained by means of a relaxation toward a climatological salinity, it is not used at all, so a correction is also not needed. Thus, the corrected fields are limited to shortwave radiation downward, wind speed and specific humidity using the ISCCP-FD (International Satellite Cloud Climatology Project) radiative products [Zhang et al., 2004], QSCAT (QuickScat Scatterometer) zonal and meridional wind components [Chin et al., 1998] and version 2 of the Coordinated Ocean-ice Reference Experiments (CORE IAF.v2) humidity data [Large and Yeager, 2008], respectively. The three bias reduction terms are computed according to the following formulae:

$$R_R(t) = \left\langle Q_{SD}^{ISCCP} \right\rangle / \left\langle Q_{SD}^{ECMWF} \right\rangle \quad (3.5)$$

$$R_W(t) = \left\langle (U_{QSCAT}^2 + V_{QSCAT}^2)^{\frac{1}{2}} \right\rangle / \left\langle (U_{ECMWF}^2 + V_{ECMWF}^2)^{\frac{1}{2}} \right\rangle \quad (3.6)$$

$$D_H(t) = \left\langle q_A^{CORE} \right\rangle - \left\langle q_A^{ECMWF} \right\rangle \quad (3.7)$$

where  $Q_{SD}$  is the shortwave radiation downward,  $U$  and  $V$  are the zonal and meridional wind components,  $q_A$  is the 10 m specific humidity and the relative corrected fields are obtained according to:

$$Q_{SD}^{corr} = Q_{SD}^{ECMWF} \cdot R_R(t) \quad (3.8)$$

$$U^{corr} = U_{ECMWF} \cdot R_W(t); \quad V^{corr} = V_{ECMWF} \cdot R_W(t) \quad (3.9)$$

$$q_A^{corr} = q_A^{ECMWF} + D_H(t) \quad (3.10)$$

The three correction factors are monthly means evaluated from the data in the time window from 1998 to 2004, and yearly averaged are consistent with those obtained for the ERA-40 reanalysis by Pettenuzzo et al. [in press], showing an underestimation of all of their relative fields.

### 3.4 Sensitivity experiments

Table 3.3 shows the experiments carried out in order to evaluate the impact of the new physics in MFS simulations done with sim4 and sim3 models. Sim4a is the control experiment, and represents the standard setting of MFS air-sea physics parametrization: radiative fluxes are computed using bulk formulae listed in column 1 of Table 3.2 and the forcing fields are taken from the original ECMWF data set, uncorrected. In sim4a.rad, we implemented only the new formulation for both shortwave and longwave radiation

### 3.5 Experiment results

---

<b>Exp Name</b>	<b>Description</b>
sim4a	MFS standard setting air-sea physics (NEMO)
sim4a.rad	New radiation formulation (NEMO)
sim4a.radc	New radiation formulation + SSRD correction (NEMO)
sim4b	New radiation formulation + all corrections (NEMO)
sim3b	New radiation formulation + all corrections (OPA)

Table 3.3: Numerical experiments set. Integrations have been carried out for the test year 2005.

while in sim4a.radc the correction to the downward shortwave radiation computed according to (3.5) is included. Finally, sim4b contains all the corrections computed according to (3.5), (3.6) and (3.7) along with the new formulation for radiative fluxes.

Moreover, the impact of the new physics is evaluated in sim3, in the last experiment, denominated sim3b. The aim is to point out the different results obtained in a twin experiment realized with the implementation of the same new air-sea physics parametrization into the two different MFS numerical models.

Each integration has been carried out for the test year 2005. The experiments are compared in their capability to reproduce the sea surface temperature but further analysis of subsurface fields are required before a comprehensive assessment is obtained.

## 3.5 Experiment results

### 3.5.1 Comparison with satellite SST

In this section, the midnight surface basin-averaged values of simulated sea surface temperatures from each experiment of Table 3.3 are compared with the OISST (Optimal Interpolated Sea Surface Temperature) data set [Marullo et al., 2007]. The OISST is a daily mean series, centred around 00:00 am, of reanalysed SST maps over a  $1/16^\circ$  regular grid that match the MFS OGCM domain and developed for the period 1985-2005 starting from mono-sensor AVHRR (Advanced Very High Resolution Radiometer) satellite images. In Marullo et al. [2007] a complete validation of this product has been performed. They showed that satellite SST is able to reproduce in-situ measurements with

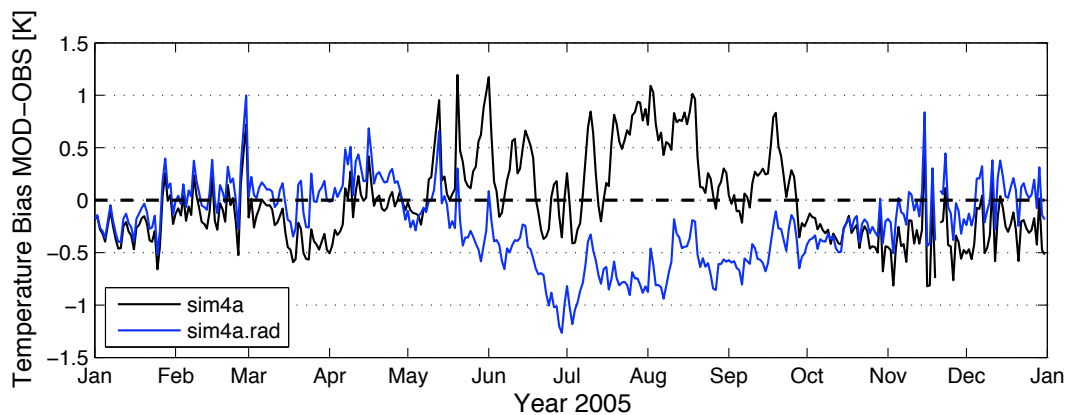


Figure 3.2: Daily surface averaged SST bias for sim4a (black line) and sim4a\_rad (blue line).

a mean bias of less than 0.1 K and a root mean square error of about 0.5 K. The optimal interpolation algorithm is applied to fill the gaps that are present in the original satellite data due to the presence of clouds, however, in order to be sure to avoid unrealistic values, our comparison has been limited to the portion of the Mediterranean basin where actual observations exist by considering only the satellite data with an associated error less than 10%. The set of experiments and the relative results are summarized in Table 3.4.

Figure 3.2 shows the impact of the new formulation for the radiative component of the heat balance. The two experiments (sim4a and sim4a.rad) differ mostly during the warm months of the year (May to September) when the warm bias of the standard MFS air-sea physics becomes a cold one using the new formulation. This result is in agreement with the finding of Pettenuzzo et al. [in press], who demonstrated that the standard MFS air-sea physics overestimated the shortwave radiation  $Q_S$ . However, the yearly averaged bias obtained in experiment sim4a.rad is still greater than that computed for sim4a (see Table 3.4).

The addition of the correction for the shortwave radiation downward, computed according to equation (3.5) yields the magenta curve of Figure 3.3. The effect of the radiation correction is to reduce the cold bias during the warmest months, for a yearly averaged bias of  $0.28^\circ K$  which is now smaller than that obtained with the MFS standard

### 3.5 Experiment results

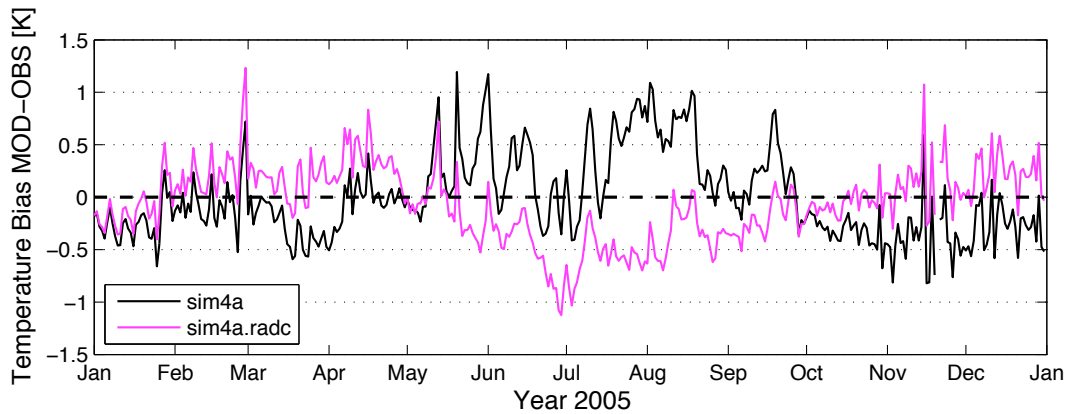


Figure 3.3: Daily surface averaged SST bias for sim4a (black line) and sim4a\_radc (magenta line).

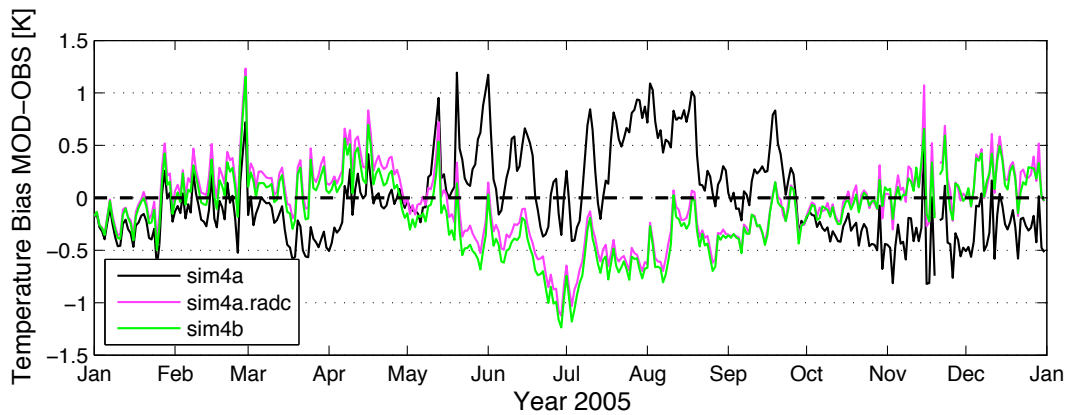


Figure 3.4: Daily surface averaged SST bias for sim4a (black line), sim4a\_radc (magenta line) and sim4b (green line).

formulation ( $0.32^{\circ}K$ ) (see Table 3.4). Furthermore, the green line of Figure 3.4 (sim4b) includes also the correction of the 10 m wind speed and of the 10 m specific humidity as given in (3.9) and (3.10) respectively. The increased winds entail higher turbulent fluxes, and in particular a greater evaporation, only partially compensated by the opposite effects of the wetter atmosphere. The cold bias observed during the summer month slightly increases, but the 2005-averaged value of  $0.29 K$  is still smaller than that relative to the control experiment (sim4a) (see Table 3.4).

Finally, Figure 3.5 compares the two twin experiments (sim4b: green line and sim3b: cyan line) realized implementing the proposed air-sea physics parametrization in both the MFS operational models. The good impact obtained in sim4 is not evident in sim3,

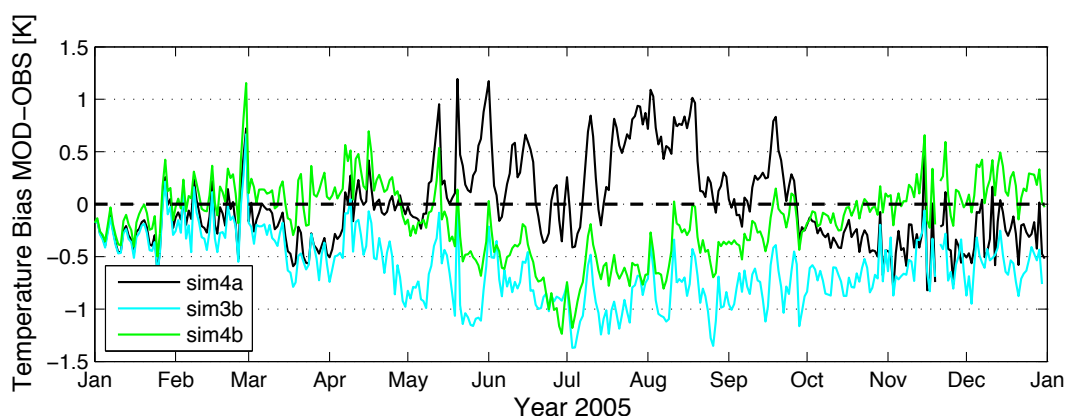


Figure 3.5: Daily surface averaged SST bias (Model-OBS) for sim4a (black line), sim3b (cyan line) and sim4b (green line).

<b>Exp</b>	<b>2005 Average Bias</b>
sim4a	0.32
sim4a.rad	0.35
sim4a.radc	0.28
sim4b	0.29
sim3b	0.61

Table 3.4: Averaged bias for the year in consideration 2005 relative to the 5 different numerical experiments carried out. The first 4 experiments are realized with NEMO (sim4), while the last one represents the new physics implemented in OPA (sim3).

and the high cold bias of sim3b, which is present for the whole of 2005, provides an yearly averaged value of  $0.61 \text{ }^\circ\text{K}$  (see Table 3.4).

### 3.5.2 Comparison with in-situ data

An important issue connected with the implementation of our proposed air-sea physics parametrization is the different effects that its two components, namely the new formulation plus the correction terms, cause to the different portions of the water column. In MFS the solar radiation penetrates the water column according to an the extinction coefficients formulation proposed by Poulson and Simpson [1977]. Moreover, the increased evaporation given by the augmented corrected winds obviously affects the surface salinity. For these reasons, we decided to include in our validation method a direct comparison of model salinity and temperature profiles with those observed by ARGO floats

### 3.5 Experiment results

[Poulain et al., 2007].

Figure 3.6 shows the temperature and salinity root mean square error profiles for the control experiment sim4a (black lines) and the one including the new formulation and all the forcing fields corrections applied to sim4 (sim4b; green lines). Regarding the temperature, both experiments give the same column-averaged value of  $0.65^{\circ}\text{K}$ , but sim4a shows a significant improvement at the surface, confirming the positive impact found in the comparison with satellite-observed SST data. This positive impact is also reflected in the salinity field, where the RMSE of the experiment including the new physics is smaller than that of the control experiment in the first 150 metres of the water column.

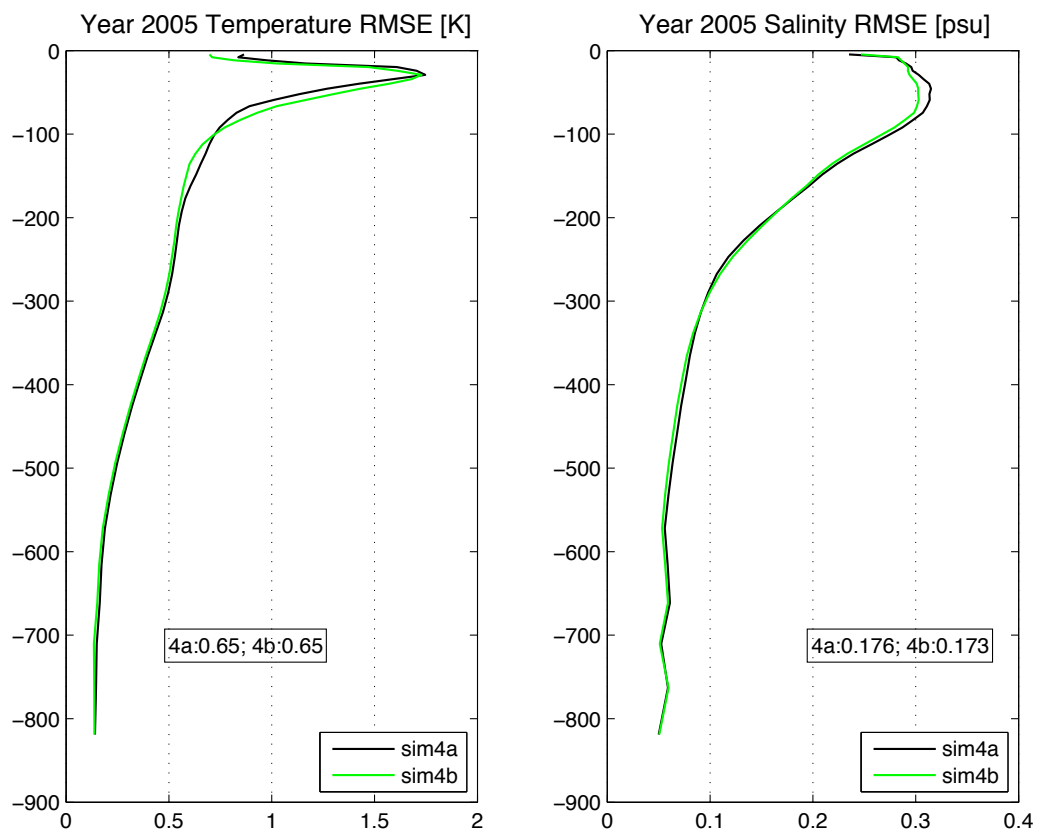


Figure 3.6: Temperature and salinity RMSE profiles averaged over the year 2005 for sim4a (black line) and sim4b (green line). The respective vertical averaged values are also indicated on the plots.

### 3.6 Summary and conclusions

The Mediterranean Basin, because of its semi-enclosed nature, offers the opportunity of calibrating and developing air-sea physics parametrizations that are able to attain a steady state balance between the fluxes at the sea surface and the lateral transport through the Strait of Gibraltar. Bearing in mind those considerations, in 1998 Castellari et al. individuated a ‘calibrated set’ of empirical formulae, which became later the standard setting boundary condition of MFS.

However, Pettenuzzo et al. [in press] have shown recently that the simple use of the ‘calibrated set’ of formulae, forced by the ECMWF ERA-40 reanalysis, fails to close the budget providing a great overestimation of the heat amount exchanged from the atmosphere to the ocean. Moreover, they proposed a novel air-sea physics parametrization, based on a new radiative flux formulation plus a set of bias corrective terms for the atmospheric forcing fields that is able to close the heat and water budgets at the surface.

The proposed alternative formulation for the radiative part of the heat balance, included in the new physics, represents at least three main advantages: firstly, the fact that the downward fluxes are taken directly from an atmospheric model assures the possibility of an easy ocean-atmospheric coupling with a continuous feedback between the two models; secondly, avoiding the use of the Reed [1977] and Bignami et al. [1995] formulae, which are specifically tuned for the Mediterranean Basin, it increases model portability and makes it suitable for different areas in the Global Ocean; and finally, all the physical characteristics of the atmosphere, including for example aerosol, atmospheric dusts and effects of different cloud types, which cannot be correctly parametrized by the standard bulk formulae are now already comprised in the atmospheric model that provides the downward fluxes.

The impact of the new physics in the sim4 operational model has been evaluated for the test year 2005, emphasizing the contribution of each single component. The new formulation for the radiative component of the heat balance transforms an observed warm bias during the summer months into a cold one (Figure 3.2). The addition of the

### 3.6 Summary and conclusions

---

bias reduction term for the downward shortwave radiation is capable to decrease the cold bias, providing an yearly-averaged value of  $0.28\text{ }^{\circ}\text{K}$ , which is smaller than the  $0.32\text{ }^{\circ}\text{K}$  relative to the control experiment realized with the MFS standard setting air-sea physics (Figure 3.3). The effects of the correction to 10 metres wind speed and specific humidity, in term of SST, are relatively small, on the other hand. The increased corrected winds entail greater turbulent fluxes and, as a consequence, more cooling of the sea surface, but this effect is partially compensated by a smaller evaporation, due to the higher specific humidity (Figure 3.4).

Furthermore, the effects of the new physics has been evaluated in terms of temperature and salinity profiles, by comparison with in-situ data. This validation underlines the fact that the positive effects of the new parametrization are not limited to the sea surface, but also extend to the first part of the water column. The root mean square error profiles of Figure 3.6 confirm a slight improvement in the sea surface temperature representation and also show a reduced error in the salinity field limited in the first 150 metres of the water column. This last finding reinforces the correctness of increased evaporation as a direct consequence of the corrected fluxes.

On the other hand, given the nature of the methodology applied for the computation of the bias reduction terms, it is important to notice that in the considered period three major changes were made to the ECMWF operational model: an increase of the spectral resolution (from T213 to T319; April 1998), the implementation of 51 vertical levels to replace the previous existing 31 (March 1999) and another spectral resolution increase in November 2009 (from T319 to T511). For this reason, differences in the correction terms could exist within the time window.

Finally, the comparison of experiments sim4b and sim3b shown in Figure 3.5 provides an estimate of the limits of the proposed approach. The impacts of the boundary condition implemented and evaluated in this study are shown to be actually model dependent. The two experiments have been carried out starting from the same initial conditions and with the same settings including the turbulent closure scheme, but the resulting

model SSTs start to diverge from the month of March onwards, and remain different by about 0.5 °K for the rest of the year. The reason of this divergence is associated to the different parametrizations listed in Table 3.1 but more work is required before a physical explanation of the results can be attained.

# Chapter 4

## Data assimilation of satellite derived Sea Surface Temperatures

### 4.1 Introduction

A very important task in ocean forecasting is to determine the ocean initial condition as accurately as possible and this is achieved by using data assimilation algorithms which correct the initial state of the forecast with the insertion of available observations (see Ghil and Malanotte-Rizzoli [1991] for an extensive review). These methods have been developed mainly for the atmosphere, but oceanographic problems differ from their meteorological counterparts in several respects: poor data coverage, less mature numerical codes, the existence of geometries and boundaries, and in general different requirements.

The availability of data is a core issue in oceanographic data assimilation. The ocean in-situ observations are relatively sparse in both time and space. In this regard, satellites can provide a unique data set at very high resolution. There has been considerable interest in assimilating altimetry data in the Mediterranean Sea (Demirov et al. [2003], Dobricic et al. [2005], Dobricic and Pinardi [2008]), however, relatively little attention has been paid to the assimilation of SST. In this regard, the Mediterranean Forecasting System (MFS; Pinardi et al. [2003]) is not an exception: since 1999, a large effort has

been spent to improve the quality of its analysis of the ocean state through data assimilation of Sea Level Anomaly (SLA) as observed by satellite [Le Traon et al., 2003], temperature and salinity profiles from XBT [Manzella et al., 2007] and ARGO floats [Poulain et al., 2007]. Up to now, however, the observed SST is inserted with a simple correction of the total surface fluxes (Tonani et al. [2008]).

A major reason for that is probably connected to the impression that assimilation of SST data cannot effectively correct the subsurface ocean state, along with the technical difficulties related to the determination of a vertical error correlation matrix and the generation of imbalances between the thermal and dynamical fields during the assimilation process. Moreover, there generally exist large systematic differences in the spatial distribution of variance between the model SST field and the observed one. With the assimilation, the structure of the model SST is quickly forced to resemble its observational counterpart. However, the model adjustment is relatively slow, especially for adjustments of the thermocline that is mainly affected by the wind stress and for which the impact of the SST is of little significance.

These problems could be solved in theory with the implementation of well-defined error covariance matrices for the model and observations. However, the design of the error covariance structures is difficult and not well understood. Recently, an assimilation scheme based on Error Subspace Statistical Estimations (ESSE) was proposed [Lermusiaux and Robinson, 1999], which combines data and dynamics in accord with their dominant uncertainties, but its large computational cost would limit its application on an OGCM. Alternatively, Tang and Kleeman [2002] proposed a strategy which involved the assimilation of two proxy data sets, SST and subsurface thermal data, into the ocean model, so that the observational forcing is not too strong in the regions where the model SST has a significant different variance structure comparable to the observations.

In this work we propose a different approach: a novel scheme for SST data assimilation based on a 3-dimensional variational technique (OceanVar; [Dobricic and Pinardi, 2008]) is applied to the MFS ocean general circulation model and the peculiarity of

## 4.2 The Optimal Interpolated SST data set

---

this scheme lies in the scale decomposition method for the observed SST misfit. The methodology consists in the separation of the large scale component (connected to the errors in the computation of surface fluxes) from the small scale component (related to the dynamical characteristics of the ocean circulation not well resolved by the model, and correlated with the subsurface). In this way, the correction deriving from the assimilation of only the small scale part, can be extended to the water column.

The paper is structured as follows: in Section 4.2 we describe the sea surface temperature observational data set which has been adopted in our study; Section 4.3 contains a general description of the new SST assimilation scheme, while the experiments set and its impact on MFS are shown in Section 4.4 and 4.5. A summary and the conclusions may be found in Section 4.6.

## 4.2 The Optimal Interpolated SST data set

The SST re-analysis data set used in this work is obtained from infrared satellite observation measured by means of an advanced very high-resolution radiometer (AVHRR) sensor [Marullo et al., 2007].

The algorithm applied to estimate SST is the Pathfinder [Evans and Podesta, 1996], based on a nonlinear function of the infrared AVHRR channels statistically regressed against in-situ measurements of SST. In addition, considering that infrared spacecraft radiometers measure the brightness temperature relative to the skin layer, it follows that Pathfinder SSTs are representative of the  $SST_{skin}$  field minus a mean value of the  $SST_{skin} - SST_{bulk}$  temperature difference. This implies that SST estimates taken in conditions that deviate from ‘mean’ can significantly differ from corresponding in-situ bulk measurements, which should be the value actually compared with a first layer OGCM temperature field. This problem should however be minimized by the fact that the data set has been constructed using exclusively satellite night passes (in a time window ranging from 23:00 to 6:00), since temperature at all depths collapse to the same value

overnight.

The optimal interpolation methodology is used in order to fill the gaps due to the presence of clouds and other environmental factors in the original 4 Km-resolution product. Data voids have been interpolated using space and time correlation functions estimated directly from the AVHRR data. Daily objective maps were then produced in a  $1/16^\circ$ -resolution regular grid that matches the MFS domain, using a Gaussian correlation function with an e-folding distance of 160 Km and a decorrelation time of 10 days.

The re-analysis data set, spanning 1985 to 2005, has been subjected to a complete validation using in-situ products, in order to exclude any possibility of spurious trends due to instrumental calibration errors/shifts or algorithm malfunctioning related to local geophysical factors. The validation showed that the satellite SST is able to reproduce in-situ measurements with a mean bias of less than  $0.1^\circ\text{K}$  and an RMSE of about  $0.5^\circ\text{K}$  and that errors do not drift with time or with the percentage of interpolation error.

### 4.3 SST assimilation method

The OceanVar scheme iteratively finds the minimum of the following cost function, which is then linearized around the background state:

$$J = \frac{1}{2}(\bar{x} - \bar{x}_B)^T B^{-1}(\bar{x} - \bar{x}_B) + \frac{1}{2}(H(\bar{x}) - y)^T R^{-1}(H(\bar{x}) - y) \quad (4.1)$$

where  $\bar{x}$  is the analysis state vector,  $\bar{x}_B$  is the background state vector,  $B$  is the background error covariance matrix,  $R$  the observational error covariance matrix,  $H$  is the observational operator and  $d = H(\bar{x}) - y$  is the misfit. The state vector considered in MFS is composed by the following model state variables:

$$\bar{x} = [T, S, \eta, u, v]^T \quad (4.2)$$

with  $T$  being the model temperature,  $S$  the salinity,  $\eta$  the free-surface elevation and

### 4.3 SST assimilation method

---

$u$  e  $v$  the two velocity components.

A specific feature of OceanVar is the decomposition of the background error covariance matrix as  $B = VV^T$ , with  $V$  modelled as a sequence of linear operators:

$$V = V_D V_{uv} V_\eta V_H V_V \quad (4.3)$$

In equation (4.3), the linear operator  $V_V$  contains the vertical covariances that are represented by multivariate EOFs of surface elevation and vertical profiles of temperature and salinity [Dobricic et al., 2005],  $V_H$  contains the horizontal covariances, which are assumed to be Gaussian with a constant correlation radius,  $V_\eta$  is constituted by a barotropic model which calculates the sea surface error derived from temperature and salinity errors,  $V_{uv}$  calculates velocity errors by splitting the velocity field into the barotropic and baroclinic components, and  $V_D$  applies a divergence damping filter to the velocity field near the coastline. All the details of the data assimilation scheme are given in Dobricic and Pinardi [2008].

The assimilation cycle is daily and during each 1-day model forecast, the SST misfits are computed at midnight. For the misfits calculation, only the portion of the Mediterranean Basin for which the satellite-derived SST associated error is less than 10% is considered, in order to avoid possible artifacts derived from the use of the optimal interpolation methodology to fill the gaps due to the presence of clouds or other atmospheric factors in the original satellite images.

The OceanVar calculates then corrections to the background state by solving the minimization of the cost function (4.1).

Moreover, the well-known problem connected to the uncorrelation between surface and sub-surface errors [Tang et al., 2004] has been solved by limiting the 3-dimensional corrections of the background state to the upper portion of the water column during the warm months of the year. In the Mediterranean basin, during late spring-summer, a strong thermocline forms which then it is fully eroded each winter. The corrections due to SST are then calculated only in the portion of the vertical domain for which the

temperature of a given layer differs from the model SST by less than 10 °K.

## 4.4 Experiment design

The data assimilation scheme described in Section 4.3 is applied to the operational version of a general circulation model [Oddo et al., 2009]. The model has a free surface, which is evolved using an implicit temporal scheme (Madec et al. [1997]; Roullet and Madec [2000]). The horizontal resolution is about 7 Km in the latitudinal direction and between 6 Km and 5 Km in the longitudinal direction. The model has 72 levels with a 3 metre deep surface layer. In the Mediterranean Sea, the first baroclinic Rossby radius of deformation is approximately 10 Km Robinson et al. [1987], therefore the horizontal model resolution allows the development of mesoscale eddies, although the smallest ones are barely resolved. The MFS domain, which covers the entire Mediterranean Sea, also includes an Atlantic box, which is nested within the monthly mean climatological fields computed from the daily output of the MERCATOR ¼-degree resolution global model [Drevillon et al., 2008], spanning 2001 to 2005.

The atmospheric fluxes of heat and momentum are calculated using interactive bulk formulas forced by the ECMWF 0.5-degree resolution operational analysis. For the surface water and salt fluxes, the evaporation is derived directly from the latent heat flux, precipitation is taken from monthly mean Climate Prediction Center Merged Analysis of Precipitation (CMAP) Data [Xie and Arkin, 1996] and the runoff discharge (including the Dardanelles inflow, which is parametrized as a river) is taken from monthly mean climatological data (Global Runoff Data Center; Fekete et al. [1999]; Raicich [1996]; Kourafalou and Barbopoulos [2003]).

All the experiments start on 1 January 2005 from the same initial conditions provided by MFS and last for the entire year.

Four different experiments have been carried out and are summarized in Table 4.1. The control experiment, Sim, does not assimilate any observation. In the second ex-

## 4.4 Experiment design

Exp	Description	2005 Average Bias [K]
Sim	Simulation	0.32
MFS	SST nudging with constant factor ( $\partial Q_S / \partial T_S = -40 \text{ W/m}^2 / ^\circ\text{K}$ )	0.44
SST.v1	SST assimilation with OceanVar	0.19
SST.v2	Scale decomposition of SST errors field. New air-sea physics parametrization + OceanVar	0.18

Table 4.1: Averaged bias for the year in consideration 2005, relative to the 4 different numerical experiments carried out. Experiment Sim does not assimilate any observation, while experiments MFS and SST.v1 insert the satellite derived sea surface temperature [Marullo et al., 2007] using the MFS standard setting SST nudging and the OceanVar scheme respectively. Experiment SST.v2 also includes the scale decomposition approach for the observed SST error field. The 2005 test year mean biases relative to each experiment are also presented in column 3.

periment, MFS, the observed SST is introduced into the model using the standard MFS SST nudging (see Appendix 4.7 for further details), while experiment SST.v1 uses the OceanVar scheme with the methodology described in the previous section.

The last experiment, SST.v2, includes a scale decomposition for the observed temperature misfit. The proper representation of the sea surface temperature in a generic ocean general circulation model is mainly affected by two factors at different spatial scales. The large-scale factor is connected to the lack of precision, and the consequent biases, of the air-sea interaction fluxes while the small-scale one is related to the dynamical processes, which are not correctly represented, or sometime totally missed in the OGCM. In panel (A) of Figure 4.1, the SST misfit,  $p$ , of 2 January 2005 at 12:00 is presented as an example. The large scale component,  $p_L$ , is obtained by filtering with a spatial mean filter having a radius of 50 grid points (about 350 Km) and it is then subtracted to the total field in order to obtain the small scale component,  $p_S$ , according to:

$$p_S = p - p_L \quad (4.4)$$

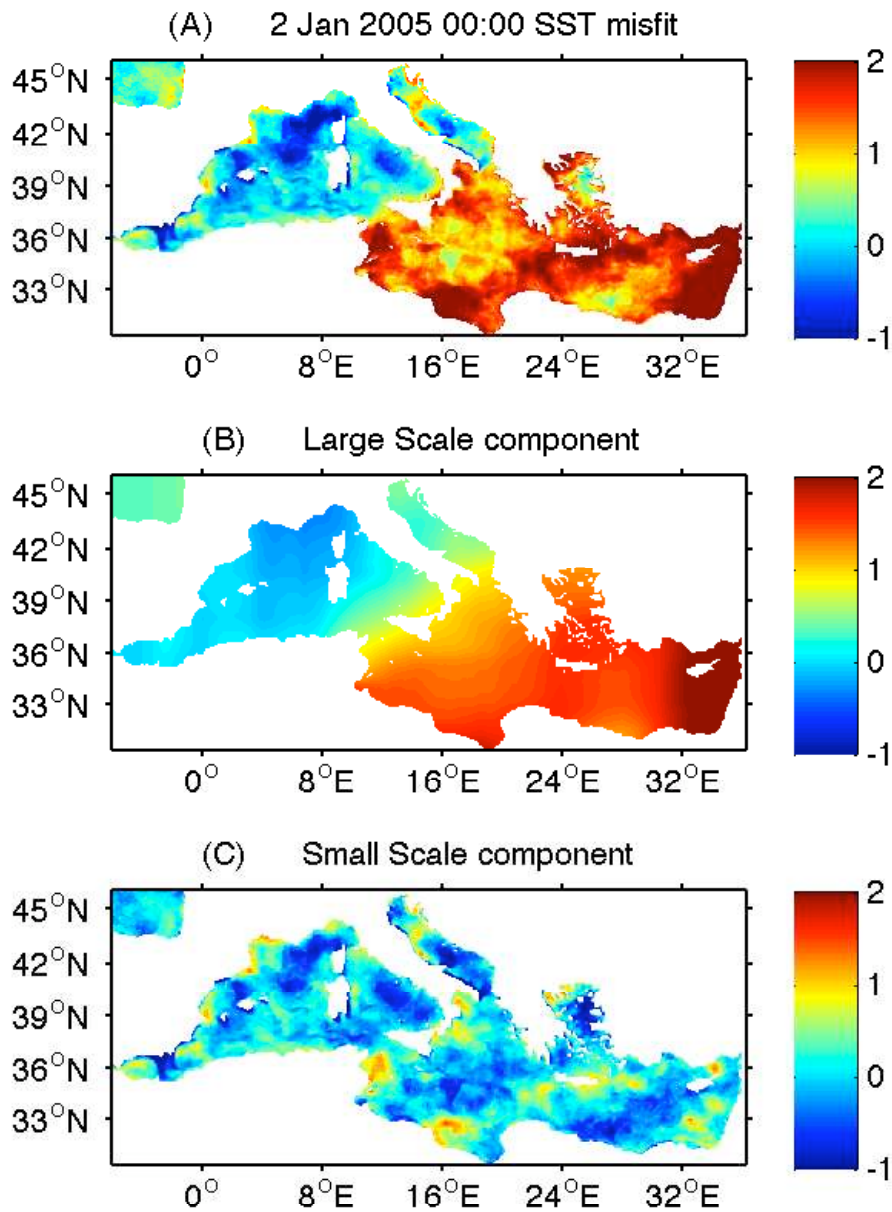


Figure 4.1: Scale decomposition of the SST misfit. Panel (A) shows the SST misfit observed on 2 January 2005 at 12:00. This field is decomposed by means of a mean filter with a spatial radius of about 350 Km in large-scale (panel (B)) and small-scale components (panel (C)). In experiment SST.v2 the only assimilated part is the small scale one, while the large-scale errors are corrected by using an alternative air-sea physics parametrization [Pettenuzzo et al., in press].

## 4.5 Results

---

The latter, which is the only part of the SST error connected to the subsurface, is assimilated in the system using the OceanVar scheme. Moreover, a novel air-sea physics parametrization [Pettenuzzo et al., in press], based on the direct use of the downward radiation components taken directly from the ECMWF operational analysis and on a set of bias reduction terms for shortwave radiation downward, wind speed and specific humidity is adopted. This novel boundary condition parametrization has been validated with heat and water budget considerations in the Mediterranean using the ECMWF ERA-40 reanalysis [Uppala et al., 2005] and it is considered as being capable of providing the more correct surface heat and water fluxes necessary to reduce the large-scale observed SST model error.

## 4.5 Results

The evaluation of the novel sea surface temperature assimilation scheme has been mainly performed by comparing misfits with satellite-derived observations of SST that have also been assimilated. However, it is important to note that all these misfits are calculated before the assimilation has taken place. In this way, the comparison can be referred to as semi-independent. Another estimate of the errors has been computed by calculating yearly averaged Root Mean Square Errors (RMSEs) of salinity and temperature analysis with their corresponding in-situ observations. In this way we have been able to assess the impact of surface data assimilation in the subsurface dynamics.

Figure 4.2 shows the daily surface-averaged misfits for the three experiments Sim, MFS and SST.v1 relative to the test year 2005. The first remarkable result coming out of this is that for the period considered the standard SST nudging technique adopted in MFS does not provide an improvement in terms of SST representation with respect to the simple simulation. The experiment MFS (blue line) has a higher warm bias during the summer months compared to the control experiment Sim (black line). Conversely, the use of the novel OceanVar SST assimilation method (exp. SST-v1; cyan line) entails

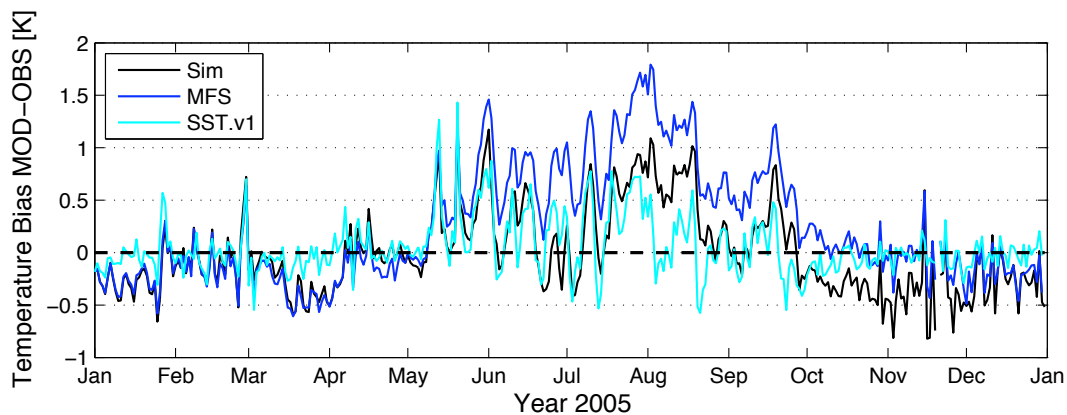


Figure 4.2: Daily surface-averaged misfits for the test year 2005. The black line represents the control experiment, without data assimilation, while the blue line includes SST nudging realized using the standard MFS nudging approach with a constant restoring coefficient ( $dQ/dT = -40 W/m^2/^\circ K$ ). The cyan line is relative to experiment SST.v1, where SST has been assimilated using the OceanVar scheme described in Section 4.3. No scale decomposition for SST errors has been applied.

a significant improvement during the entire considered period. The yearly averaged bias for the three experiments are listed in Table 4.1 showing the improvements.

Finally, in Figure 4.3 the impact of the scale decomposition of SST errors included in experiment SST.v2 is presented. The daily bias corresponding to the green line has been further reduced with respect to experiment SST.v1 and its error seasonal signal has also been removed (see Figure 4.2). The biases observed during summer time, the most difficult period for simulating the Sea Surface Temperature in the Mediterranean due to the complex stratification processes which take place at this time of the year, is greatly reduced despite a small increment during the last few months of the time window considered. This behaviour can be associated to the different impact on the thermocline formation and erosion, respectively. The yearly averaged bias also slightly decreases with respect to experiment SST.v1 (see Table 4.1).

The good impact of the combined approach (new physics parametrization plus small-scale SST errors assimilation) applied in experiment SST.v2 is also confirmed by the independent comparison with in-situ profiles shown in Figure 4.4. At the surface, the temperature RMS errors of the three experiments (Sim, MFS and SST.v2) show that SST.v2 has a positive impact down to 400 metres, while the MFS standard nudging

## 4.5 Results

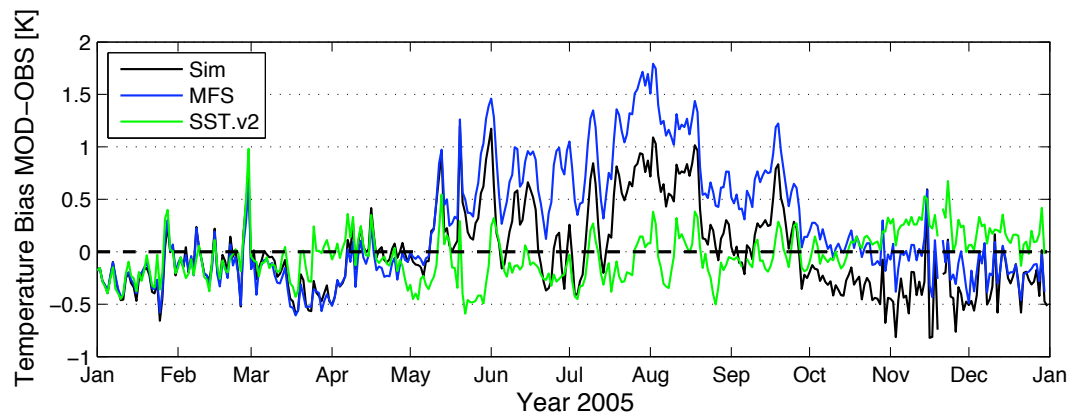


Figure 4.3: Daily surface-averaged misfits for the test year 2005. The black line represents the control experiment, without data assimilation, while the blue line include SST nudging realized using the standard MFS nudging approach with a constant restoring coefficient ( $dQ/dT = -40 \text{ W/m}^2/\text{°K}$ ). The green line represents experiment SST.v2, on which the SST misfits have been decomposed into large-scale and small-scale ones. The latter is the only assimilated component, using the OceanVar scheme, while the former errors have been reduced by implementing an alternative air-sea physics parametrization based on the work of Pettenuzzo et al. [in press].

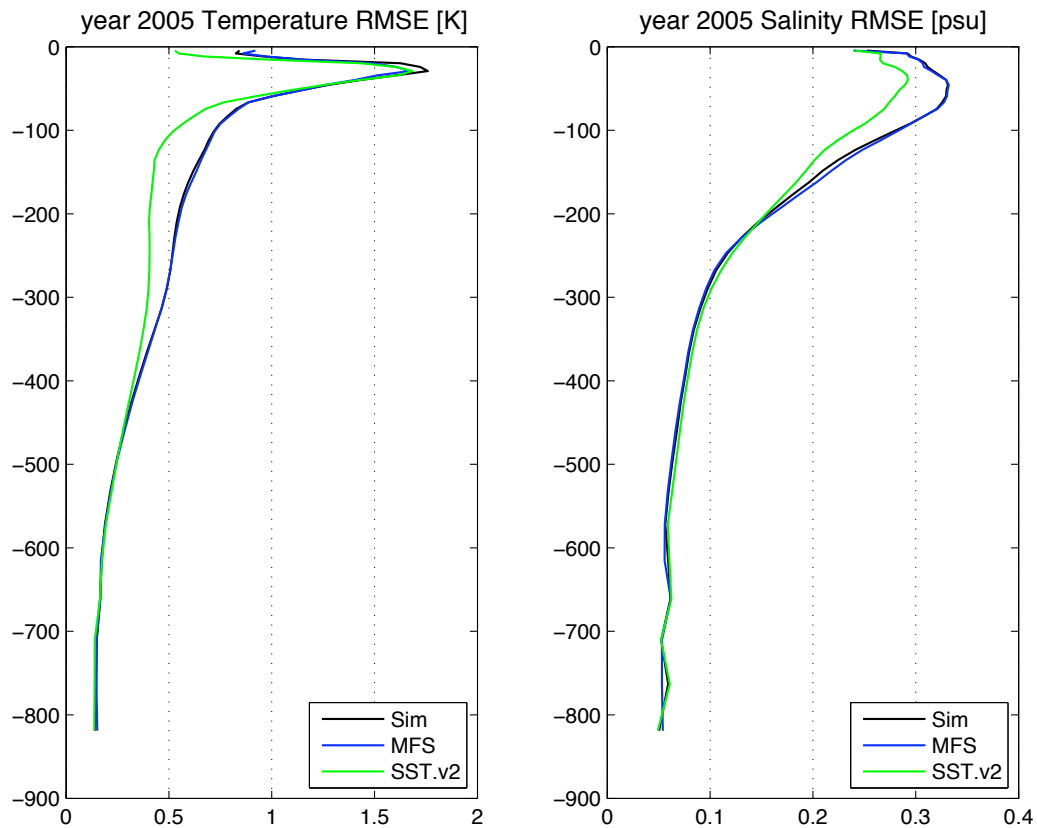


Figure 4.4: Temperature and salinity RMSE profiles averaged over the year 2005 for experiments Sim (black line), MFS (blue line) and SST.v2 (green line). The temperature field is shown on the left panel, while the right one represents the salinity.

technique is not able to produce any improvements in the subsurface temperature. The salinity field is also positively affected in SST.v2 experiment, and its RMS errors are smaller than those computed for experiments Sim and MFS up to 200 metres.

## 4.6 Summary and Conclusion

The study describes the development and implementation of a new oceanographic SST data assimilation method applied with the OceanVar scheme of [Dobricic and Pinardi, 2008] in the Mediterranean Forecasting System.

At present, the SST is assimilated in MFS by means of a nudging which corrects the total surface heat flux according to a corrective term proportional to the observed SST misfit with a proportionality factor corresponding to a restoring time of 2.5 days. However, we proved that the nudging approach fails to improve SST representation during the summer months of the year 2005, which has been chosen as the test period for our study (see Figure 4.2 and 4.3; blue line). Moreover, the nudging approach cannot effectively correct the subsurface thermodynamical structure of the ocean, as the correction is applied and limited to the very first model layer. For this reason, we specifically adapted the OceanVar scheme, which has been widely tested and used in MFS to assimilate Sea Level Anomaly (SLA) as observed by satellite and temperature and salinity profiles from XBT and ARGO floats, in order to insert satellite derived SST information into the MFS ocean general circulation model. In this way we could enhance the model SST representation (see Figure 4.2) comparing with both simulation and analysis carried out using the standard setting SST nudging.

The innovative aspect of the data assimilation scheme proposed in this work, however, lies in the scale decomposition approach for the SST error field. The initial assumption that we made is that the causes which affect the representation of the sea surface temperature in an ocean general circulation model are basically two: the first is a large-scale factor, connected to the only partial precision of the computation of net sur-

## 4.7 Appendix 1: SST nudging and wind-dependent restoring coefficient

---

face fluxes using classical bulk formulation; the second, with a characteristic small-scale structure, is instead due to some dynamical features of the ocean circulation which are not properly captured by the model itself (Figure 4.1). Given this assumption, it follows that the two different components must be treated separately, especially for the different correlations of the errors that they involve at the surface with those observed in the entire water column. In experiment SST.v2, these two aspects have been considered by implementing a new air-sea physics [Pettenuzzo et al., in press], which is able to reduce the biases in the fluxes computation, and extending to the subsurface the correction computed by OceanVar only relative to the small-scale SST observed error component. This combined approach showed good results both in terms of SST representation (Figure 4.3) and in the comparison with in-situ salinity and temperature profiles (Figure 4.4).

## 4.7 Appendix 1: SST nudging and wind-dependent restoring coefficient

In MFS, the SST is assimilated by means of an addition term, which is added each time step to the prescribed surface total heat flux  $Q_{T0}$ , according to:

$$Q_T = Q_{T0} + \frac{\partial Q_T}{\partial T_S}(T_S - OISST) \quad (4.5)$$

where  $T_S$  is the model surface temperature,  $OISST$  is the optimally interpolated satellite observed Sea Surface Temperature and  $\partial Q_T / \partial T_S = -40 W/m^2/^\circ K$  is the relaxation coefficient. This formulation assures that  $Q_T = Q_{T0}$  for model temperatures equal to observations. Since the relaxation term can be computed as:

$$\frac{\partial Q_T}{\partial T_S} = \rho_0 C_P \frac{h}{\tau_T} \quad (4.6)$$

it follows that with a mean sea density  $\rho_0 = 1025 Kg/m^3$ , an ocean specific heat  $C_P = 4000 J/m^3/^\circ K$  and a model first layer  $h$  of 3 m, the associated restoring time  $\tau_T$  is

equal to about 2.5 days. This methodology is based on Haney, 1971, a pioneering work that was the first to formulate a surface thermal boundary condition to be used in ocean climate models. He based his formulation on physical considerations by assuming that the ocean is in contact with an atmospheric equilibrium state (i.e., an atmosphere with near-infinite heat capacity). Under this assumption, the net heat flux across the air-sea interface  $Q_T$  was written as a truncated Taylor series expansion about a state where there is no temperature contrast between the two media:

$$Q_T(T_S) = Q_T(T_A) + \left( \frac{\partial Q_T}{\partial T_S} \right)_{T_A} (T_S - T_A) \quad (4.7)$$

where  $T_A$  represents the temperature of the atmospheric equilibrium state. In this way, Haney obtained a simple net heat flux parametrization of the form:

$$Q_T = R^*(T_A^* - T_S) \quad (4.8)$$

where  $R^* = - \left( \frac{\partial Q_T}{\partial T_S} \right)_{T_A}$  is a measure of the actual coupling between the ocean and the overlying atmosphere and  $T_A^* = T_A + Q_T(T_A)/R^*$  is the apparent atmospheric equilibrium temperature to which the model sea surface temperature is restored. Furthermore, other authors (i.e., Pierce [1996], Chu et al. [1998], Killworth et al. [2000]) applied Haney's formulation and assumed that it pertains even when used for relaxing toward observations and thus replacing the apparent temperature in equation (4.8) with some observed SST data sets.

However, assuming the restoring coefficient to be constant is in disagreement with the original parametrization derived by Haney himself. We can prove this statement, by simply expressing  $R^*$  starting from the parametrization of the surface heat fluxes in MFS.

The net heat flux at the surface is given by the sum of its four terms:

$$Q_T = Q_S + Q_L + Q_E + Q_H \quad (4.9)$$

## 4.7 Appendix 1: SST nudging and wind-dependent restoring coefficient

---

with  $Q_S$  and  $Q_L$  being the shortwave and longwave radiation fluxes respectively,  $Q_E$  the latent heat of evaporation and  $Q_H$  the sensible heat flux. Following Haney's formulation,  $R^*$  can be written as:

$$R^* = - \left( \frac{\partial Q_T}{\partial T_S} \right)_{T_A} = - \left( \frac{\partial Q_S}{\partial T_S} \right)_{T_A} - \left( \frac{\partial Q_L}{\partial T_S} \right)_{T_A} - \left( \frac{\partial Q_E}{\partial T_S} \right)_{T_A} - \left( \frac{\partial Q_H}{\partial T_S} \right)_{T_A} \quad (4.10)$$

For the shortwave radiation flux computation, MFS uses the Reed [1977] formula, with a clear sky irradiance modified according to Rosati and Miyakoda [1988] that does not depend on the SST. Thus the first term of the right hand side of eq. (4.10) is equal to 0.

The net longwave radiation heat flux is computed according to the Bignami et al. [1995] formulation, which was strictly derived from regression to fluxes in the Western Mediterranean. Its only component that depends on the sea surface temperature is the upward one (black-body law), therefore:

$$\left( \frac{\partial Q_L}{\partial T_S} \right)_{T_A} = -4\varepsilon\sigma T_A^3 \quad (4.11)$$

In MFS, the latent  $Q_E$  and sensible  $Q_H$  heat fluxes are given by the standard empirical formulas:

$$Q_H = -\rho_A C_P C_H \|\vec{V}\| (T_S - T_A) \quad (4.12)$$

$$Q_E = -\rho_A L_E C_E \|\vec{V}\| (q_S - q_A) = L_E E \quad (4.13)$$

where  $\|\vec{V}\|$  is the 10-metre wind speed,  $\rho_A$  is the density of the moist air,  $C_P$  is the specific heat capacity,  $C_E$  and  $C_H$  are wind-dependent turbulent exchange coefficients for temperature and humidity [Kondo, 1975],  $q_A$  is the specific humidity of air and  $q_S$  is the specific humidity saturated at temperature  $T_S$ . The latent heat of vaporization  $L_E$

is calculated as function of the sea surface temperature according to the formula [Gill, 1982]:

$$L_E(T_S) = 2.501 \times 10^6 - 2.3 \times 10^3 T_S \quad (4.14)$$

Following the equations (4.12), (4.13) and (4.14), we end up with the expressions:

$$\left( \frac{\partial Q_E}{\partial T_S} \right)_{T_A} = -\rho_A C_E \|\vec{V}\| L_E(T_A) \left( \frac{\partial q_S}{\partial T_S} \right)_{T_A} \quad (4.15)$$

$$\left( \frac{\partial Q_H}{\partial T_S} \right)_{T_A} = -\rho_A C_P C_H \|\vec{V}\| \quad (4.16)$$

Combining equations (4.10), (4.11), (4.16) and (4.15) we obtain the final form for  $R^*$ :

$$R^* = - \left( \frac{\partial Q_T}{\partial T_S} \right) = 4\varepsilon\sigma T_A^3 + \rho_A \|\vec{V}\| \left[ C_E L_E(T_A) \left( \frac{\partial q_S}{\partial T_S} \right)_{T_A} + C_P C_H \right] \quad (4.17)$$

where it is evident the dependence of the restoring coefficient on the wind regimes. In the Mediterranean Sea the wind field variability is mainly dominated by the recurrence of offshore blowing of strong continental winds (e.g. Mistral, Bora and Ethesians) alternated with weak wind periods. Low-wind regimes are mainly present in summer and are characterized by land-sea breeze.

Bearing in mind those fundamental considerations, Artale et al. [2002] proposed a simplified wind-dependent restoring time formulation that was able to take into account these two main types of wind regimes and especially the related adjustments of the atmospheric boundary layer over the ocean. In low-wind regimes the thermodynamic properties of the atmospheric boundary layer adjust to the underlying SST to minimize fluxes and then reach a local air-sea interface equilibrium. In contrast, in the case of strong air advection, especially from continental areas, this equilibrium is not reached. In this case the fluxes are much greater and are dominated by the latent heat of evaporation.

## 4.7 Appendix 1: SST nudging and wind-dependent restoring coefficient

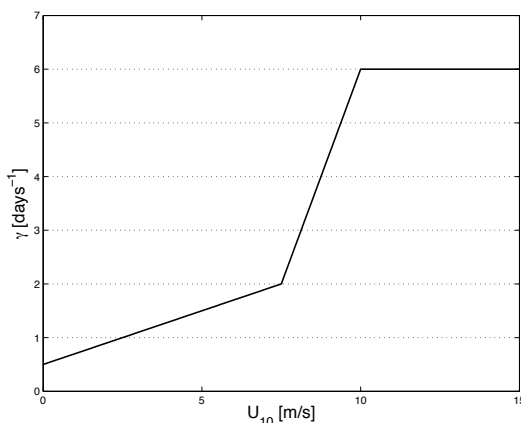


Figure 4.5: Plot of the restoring coefficient  $\gamma$  (computed according to equation (4.18)) as a function of 10-metre wind intensity.

The Artale et al. [2002] formulation is based on the definition of a dimensionless function  $\gamma = c/\tau_T$  (with  $c = 86400 s$  is a dimensional factor) that depends on the wind intensity as follows:

$$\begin{cases} \gamma = 0.2 \|\vec{V}\| + 0.5 & \text{for } \|\vec{V}\| \leq 7.5 m/s \\ \gamma = 0.2 \|\vec{V}\| + 0.5 & \text{for } 7.5 < \|\vec{V}\| \leq 10.0 m/s \\ \gamma = 6.0 & \text{for } \|\vec{V}\| > 10.0 m/s \end{cases} \quad (4.18)$$

that is,  $\gamma$  is an almost step-like function of the wind (see figure 4.5) increasing slowly for winds up to  $7.5 m/s$  and then, after a rapid transition, reaching a saturation value for  $\|\vec{V}\| > 10 m/s$ . Introducing  $\tau_T = c/\gamma$  in equation (4.6), the resulting correcting flux given by equation (4.5) will directly depend on the wind regime. The restoring timescale  $\tau_T$  varies between 2 days (for  $\|\vec{V}\| = 0.0 m/s$ ) and 4 hours (for  $\|\vec{V}\| \geq 10 m/s$ ), thus always bigger than the constant factor applied in the standard technique of MFS.

This alternative parametrization has also been tested in MFS and the results are reported in Figure 4.6. The daily surface averaged bias (model-observations) of the experiment with the wind-dependent restoring time (red line; W-DEP) is smaller than that computed for the experiment where the fluxes are corrected using a constant factor (blue line) in the entire period considered.

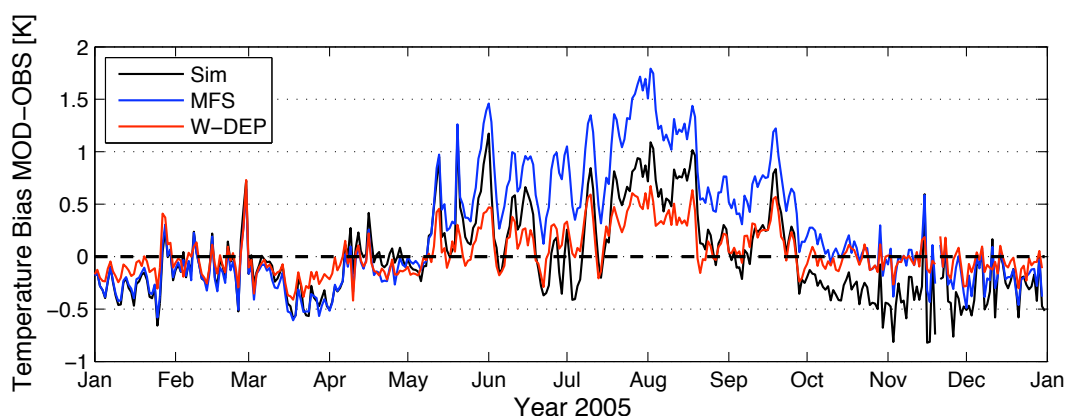


Figure 4.6: Daily surface-averaged misfits for the test year 2005. The black line represents the control experiment, without data assimilation, while blue and red lines include SST nudging realized according to equation (4.5) by using a constant ( $dQ/dT = -40 W/m^2/^\circ K$ ) and a wind-dependent ( $\tau_T = c/\gamma$ ; with  $\gamma$  computed as in (4.18)) restoring coefficient respectively.

Unfortunately, the relaxation approach described in this section, despite its beneficial impacts on avoiding temperature drifting in the integrations, presents the well-known problem of providing incorrect, and sometime unrealistic, total surface fluxes. Moreover, since the flux correction terms computed using the wind-dependent formulation (equation (4.18)) are higher than the ones calculated with the constant restoring factor, the effects in this sense are strengthened. Figure 4.7 shows the surface total heat fluxes for a snapshot taken at 10:00 of 31 January 2005. In panel (A) the fluxes computed in simulation mode (experiment Sim) are presented. The pattern and the amplitude are very reasonable showing a north-south positive gradient and the characteristic cooling structures related to the effects of the three major continental winds: the Bora (Adriatic Sea), Mistral (Gulf of Lion) and Ethesian (Aegean Sea) [Pettenuzzo et al., in press]. This pattern is maintained in experiment MFS by using a constant relaxation factor (panel (B)), and the only impact of the SST nudging is a slight increase in the intensity of the air-sea fluxes. In experiment W-DEP, however, several small-scale structures with an ocean-atmosphere exchanged heat amount that can sometimes reach  $1000 W m^2$  are present (panel (C)). These features are due to high model-observation SST differences, which may be reinforced by the presence of local strong wind intensities (which entails a high restoring coefficient), which however are not due to errors in the computation of

#### 4.7 Appendix 1: SST nudging and wind-dependent restoring coefficient

fluxes, but rather to the model's lack of capacity to reproduce some particular dynamical features of the ocean circulation.

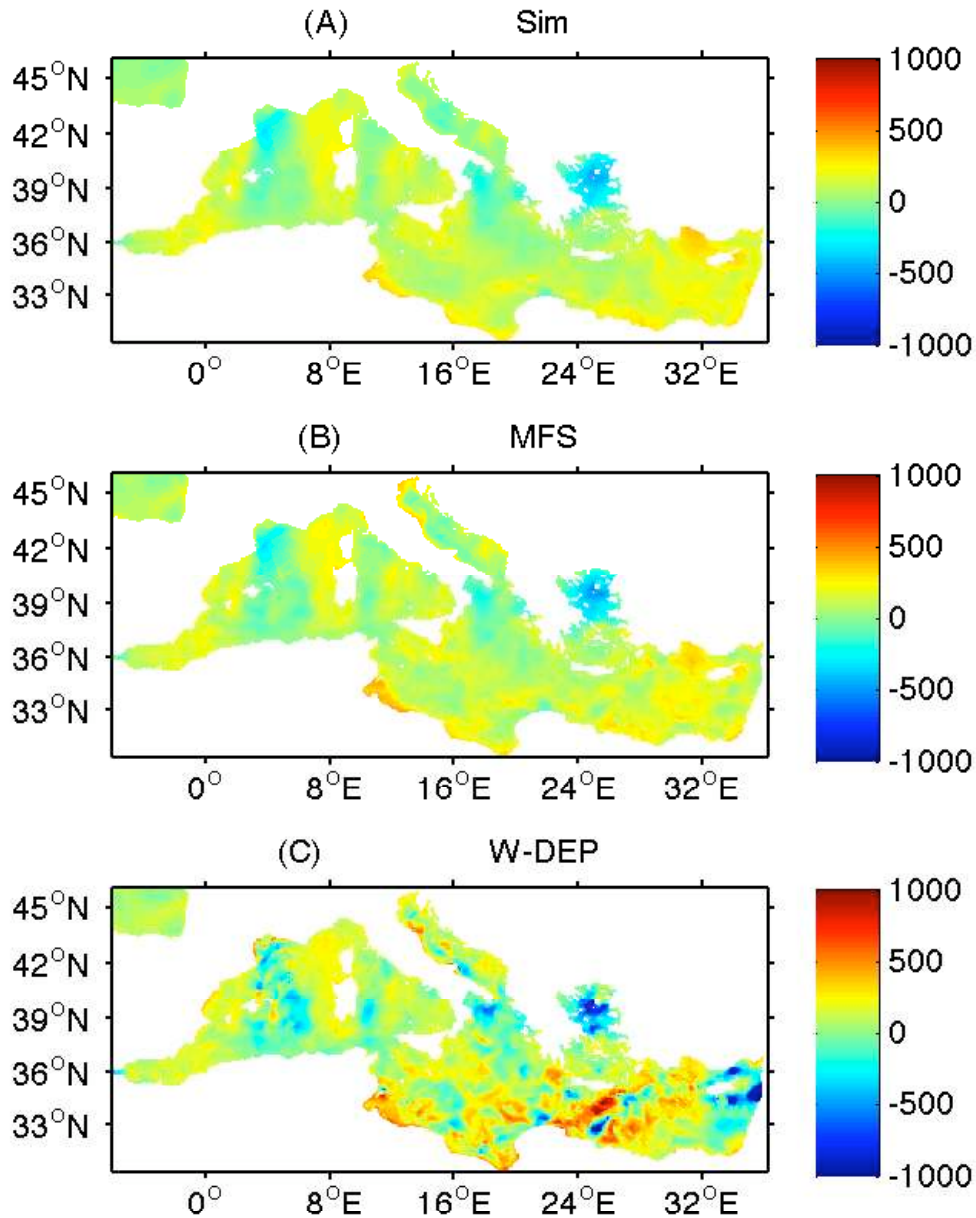


Figure 4.7: Surface total heat flux maps 10:00 snapshots for the day 30 January 2005: Panel (A) shows the fluxes computed in experiment Sim where no fluxes corrections occur; Panel (B) is relative to the standard setting of MFS (experiment MFS) for SST nudging with a constant restoring coefficient  $\partial Q/\partial T = -40 \text{ W/m}^2/\text{K}$  corresponding to a restoring time of about 2.5 days; Panel (C) shows the fluxes computed in experiment W-DEP with a correction term wind-dependent calculated starting from equation (4.18).



# Chapter 5

## Summary and Conclusions

This study describes the development of a combined approach aimed at improving SST simulations and analysis by an Ocean General Circulation Model plus the OceanVar assimilation system, and their implementation in the Mediterranean Forecasting System [Pinardi et al., 2003].

As we have pointed out, there are two main factors that limit the accuracy of the SST representation skill by the OGCM. The first can be connected to errors in the formulation of air-sea surface fluxes and the second is related to the inability of the model itself to reproduce several dynamical features of the ocean circulation.

In this thesis we discussed the different spatial-scale structures of the SST misfits introduced by those two causes and their correlation with the subsurface, the former being characterized by a large-scale influence limited to the very first layer while the latter by a small-scale one that largely extends to the deeper part of the water column. For this reason, our combined approach deals with these error sources separately, reducing the large-scale component by using an enhanced air-sea physics parametrization and assimilating satellite-derived SST observations with the purpose of eliminating the small-scale error part.

In Chapter 2, the development of the new air-sea physics was presented. Given the peculiar semi-enclosed nature of the Mediterranean Basin, and the consequent constraint

on the total heat flux that should be compensated at the steady state by the measured heat inflow at Gibraltar, we could prove using the ECMWF ERA-40 reanalysis [Uppala et al., 2005] that the MFS standard setting boundary condition fails to close the budget. Moreover, we showed that the individual components of the ERA-40 surface heat balance are incompatible with some in-situ local observations. The new physics that we propose is composed of two parts: the modification of the bulk formulae for the computation of the radiative part of the heat balance and a correction methodology, based on the work of Large and Yeager [2008], for the basic forcing fields realized by comparison with observational data sets. These corrections, averaged over the basin, entail an increase of the shortwave radiation and of the wind speed by  $21 \text{ W/m}^2$  and 25% respectively. The specific humidity and the sea surface temperature, which presented an underestimation, have also been corrected, by about  $1 \text{ g/m}^3$  and  $1 \text{ }^\circ\text{C}$ . The precipitation is also augmented by a factor of 2 off some northern coasts, but slightly reduced along the southern and eastern margins.

Using the ‘Corrected ERA-40 data set’ and the new formulation, we were able to close both heat and water budgets in the Mediterranean and, moreover, an analysis of the interannual variability observed in the corrected fluxes showed the fundamental contribution of the latent and sensible heat fluxes to this achievement. In this sense, we proved that the wind anomalies, which occur during winter and crucially affect the turbulent fluxes, are responsible for half the negative budget of the basin. Furthermore, in Chapter 2 the teleconnection between the corrected total heat flux and the NAO index is explored. The correlation between the two time series has been found to be significantly high (0.68), but only after applying a 5-year running mean filter to both fields. We may thus argue that only the long time scale modulation in the net heat flux can be associated with the teleconnection. Ultimately, this aspect along with the relevance that we demonstrated of a few severe wind regime events on the final budget allowed us to underline the importance of a long time series of fluxes so as to truly understand their low frequency variability and realize such a budget study.

## Summary and Conclusions

---

The impact of the novel air sea physics parametrization on the MFS numerical model [Oddo et al., 2009] is described in Chapter 3, and the evaluation of the effects have been realized by comparison with satellite-observed Sea Surface temperature and in-situ temperature and salinity profiles. Different experiments have been carried out aimed at showing the contribution of the single component of the new physics to the model output.

The major difference in terms of model SST reproduction is given by the reduced radiation, which transforms a previously observed warm bias during the warmest months of the year into a cold one. The addition of the bias reduction term for the downward shortwave radiation is thus able to decrease the underestimation of the ECMWF radiative product and, consequently, the cold bias. The effects of the correction to a 10-metre wind speed and specific humidity, in terms of SST, are instead relatively small. The increased corrected winds entail greater turbulent fluxes and, as a consequence, a reduction of the net heat amount provided to the ocean from the atmosphere, but this effect is partially compensated by a smaller evaporation, due to the higher specific humidity. In this case the cold bias is slightly increased, but the yearly averaged value of  $0.29^{\circ}K$  is smaller than that obtained with the MFS standard physics ( $0.32^{\circ}K$ ). The good impact of the proposed corrected boundary condition is also confirmed by the validation with in-situ data. We showed that the positive effects of the parametrization are not limited to the sea surface, but also extend to the first part of the water column. In particular, the improvement in the salinity field up to 150 metres reinforces the correctness of the increased evaporation as a direct consequence of the corrected fluxes obtained.

However, we found that the effects of the proposed new physics are strongly model dependent. In order to prove this, the new parametrization was also implemented in the first version of the operational MFS numerical model [Tonani et al., 2008]. The differences with the one implemented by Oddo et al. concern the vertical discretization, the parametrization of the water flux and of the tracer advection and, most importantly, the connection of the Mediterranean Sea with the North Atlantic Ocean, which now

includes open boundary conditions and a nesting with the MERCATOR global model.

A twin experiment was realized starting from the same initial conditions, but the resulting model SSTs start to differ by about  $0.5^{\circ}\text{C}$  after the first three months of the integration. This behaviour must be necessarily addressed to the different parametrizations mentioned above.

The second aspect of our proposed combined approach – the data assimilation – is considered in Chapter 4. At the present time, MFS assimilates the SST observations by means of a nudging scheme, which corrects at each time step the model prescribed total heat flux by adding a correction term proportional to the observed SST misfit. However, we proved that this methodology fails to improve the SST representation during the summer month of the test year 2005 and that it cannot effectively correct the subsurface thermodynamical structure of the ocean. In this chapter, we propose a new oceanographic SST data assimilation scheme based on OceanVar [Dobricic and Pinardi, 2008], which is able to enhance the MFS SST model representation. The innovative feature of our proposed scheme is the scale decomposition of SST errors. The large-scale component of the observed misfit is filtered out using a spatial mean filter and the small-scale component is the only assimilated part. In this way, it would ultimately be possible to carry out an experiment embodying the main object of this thesis; that is, an integration with a model where both the new physics described in the previous chapters and the new SST data assimilation scheme are implemented.

This combined approach can effectively improve the SST representation, providing a yearly averaged bias of  $0.18^{\circ}\text{K}$  compared with the  $0.32^{\circ}\text{K}$  obtained in the simulation with the MFS standard setting boundary condition. Moreover, the corrections derived from the small-scale error component, which have been extended to the subsurface, also enhance the temperature and salinity fields in the deeper part of the water column.

The contents of this doctoral thesis has been submitted to well-renowned scientific journals, and some of them subjected to peer-review and thereafter published:

## Summary and Conclusions

---

- Pettenuzzo D., W. G. Large and N. Pinardi: Surface heat and freshwater fluxes into the Mediterranean Sea for the period 1985-2001. Flux News Issue 5, January 2008
- Oddo, P., M. Adani, N. Pinardi, C. Fratianni, M. Tonani, and D. Pettenuzzo: A nested Atlantic-Mediterranean Sea general circulation model for operational forecasting, *Ocean Sci.*, 5, 461-473, 2009.
- Pettenuzzo, D., W. G. Large, and N. Pinardi: On the corrections of ERA-40 surface flux products consistent with the Mediterranean heat and water budgets and the connection between basin surface total heat flux and NAO, *J. Geophys. Res.*, doi:10.1029/2009JC005631, in press.
- Pettenuzzo, D., N. Pinardi, M. Tonani, P. Oddo and W. G. Large: Impact studies of a novel air-sea physics parametrization in the MFS numerical models, in preparation.

Moreover, the results have been disseminated at international scientific conferences, such as:

- Pettenuzzo D., W. G. Large and N. Pinardi: Correction to the ERA-40 surface flux products consistent with the Mediterranean heat and water budgets, EGU General Assembly 2009, Air-Sea Physics Parametrizations, Vienna, Austria, 2009. Poster presentation.
- Pettenuzzo D., S. Dobricic and N. Pinardi: Air-sea physics model errors and assimilation of SST: a combined approach, EGU General Assembly 2009, Operational Oceanography, Vienna, Austria, 2009. Oral presentation.
- Pettenuzzo D., N. Pinardi, S. Dobricic and W. G. Large: Air-Sea physics parametrizations and assimilation of sea surface satellite temperatures for the Mediterranean Forecasting System (MFS), 9th EMS / 9th ECAM Meeting, Air-Sea Physics, Toulouse, France, 2009. Oral Presentation.

- Pettenuzzo D., S. Dobricic, N. Pinardi, P. Oddo, M. Tonani, M. Pastore and C. Fraianni: New methods of assimilation of SST and their impacts on model forecasting. 2010 Ocean Science Meeting, Quantifying the SST Error Budget, Portland, Oregon. Poster presentation.
- Pettenuzzo D., S. Dobricic, P. Oddo and N. Pinardi: Enhanced air-sea physics parametrization and assimilation of SST: a combined approach. EGU General Assembly 2010. Accepted.

# Acknowledgments

The OI-SST products used in this paper were jointly produced by ENEA Department of Environment, Global Change and Sustainable Development and Gruppo Oceanografia da Satellite (GOS) of the CNR - ISAC (Istituto di Scienze dell' Atmosfera e del Clima) as part of the EU project MFSTEP (EVK3-CT-2002-00075).

The National Center for Atmospheric Research is sponsored by the National Science Foundation.

The in situ AGIP data were kindly supplied by ENI-AGIP division, Milan.

ARGO temperature and salinity data were collected and made freely available by the International Argo Project and the national programs that contribute to it. (<http://www.argo.ucsd.edu>, <http://argo.jcommops.org> ). Argo is a pilot program of the Global Ocean Observing System.



# Bibliography

- V. Artale, D. Iudicone, R. Santoleri, V. Rupolo, S. Marullo, and F. D'Ortenzio. The role of surface fluxes in ogcm using satellite sst. validation and sensitivity to forcing frequency of the mediterranean thermohaline circulation. *Journal of Geophysical Research*, 107:3120+, 2002.
- J. P. Bethoux. Budgets of the mediterranean sea; their dependence on the local climate and on the characteristics of the atlantic waters. *Oceanologica Acta*, 2(2):157–163, 1979.
- J. P. Bethoux and B. Gentili. The mediterranean sea, a test area for marine and climatic interaction. *Ocean processes in climate dynamics*, 46:239–254, 1994.
- F. Bignami, S. Marullo, R. Santoleri, and M. E. Schiano. Longwave radiation budget on the mediterranean sea. *Journal of Geophysical Research*, 100:2501–2514, 1995.
- M. Boukthir and B. Barnier. Seasonal and inter-annual variations in the surface fresh-water flux in the mediterranean sea from the ecmwf re-analysis project. *Journal of Marine Systems*, 24(3-4):343–354, March 2000. ISSN 09247963. doi: 10.1016/S0924-7963(99)00094-9. URL [http://dx.doi.org/10.1016/S0924-7963\(99\)00094-9](http://dx.doi.org/10.1016/S0924-7963(99)00094-9).
- K. Bryan and M. D. Cox. A numerical investigation of the oceanic general circulation. *Tellus*, (19):54–80, 1967.

- S. Castellari, N. Pinardi, and K. Leaman. A model study of air-sea interactions in the mediterranean sea. *Journal of Marine Systems*, 14:89–114, 1998.
- T. M. Chin, R. F. Milliff, and W. G. Large. Basin-scale, high-wavenumber sea surface wind fields from a multiresolution analysis of scatterometer data. *Journal of Atmospheric and Oceanic Technology*, 15(3):741–763, June 1998.
- P. C. Chu, Y. Chen, and S. Lu. On haney-type surface thermal boundary conditions for ocean circulation models. *Journal of Physical Oceanography*, 28:890–901, 1998.
- E. Demirov, N. Pinardi, C. Fratianni, M. Tonani, L. Giacomelli, and P. De Mey. Assimilation scheme in the mediterranean forecasting system: operational implementation. *Annales Geophysicae*, 21:189–204, 2003.
- K. L. Denman and M. Miyake. Upper layer modification at ocean station papa: Observations and simulation. *Journal of Physical Oceanography*, 3(2):185–196, April 1973.
- S. Dobricic, N. Pinardi, M. Adani, A. Bonazzi, C. Fratianni, and M. Tonani. Mediterranean forecasting system: an improved assimilation scheme for sea-level anomaly and its validation. *Quarterly Journal of the Royal Meteorological Society*, 131:3627–3642, 2005.
- Srdjan Dobricic and Nadia Pinardi. An oceanographic three-dimensional variational data assimilation scheme. *Ocean Modelling*, 22:89–105, 2008.
- C. J. Donlon. Proceedings of the second godae high resolution sea surface temperature pilot project workshop. *available from the GHRSSST-PP International Project Office*, May 2002b.
- C. J. Donlon. The godae high resolution sea surface temperature pilot project development and implementation plan (gdip). *GHRSSST-PP International Project*, 2003.

## BIBLIOGRAPHY

---

- M. Drevillon, R. Bourdallé-Badie, C. Derval, Y. Drillet, J. M. Lellouche, E. Rémy, B. Tranchant, M. Benkiran, E. Greiner, S. Guinehut, N. Verbrugge, G. Garric, C. E. Testut, M. Laborie, L. Nouel, P. Bahurel, C. Bricaud, L. Crosnier, E. Dombrosky, E. Durand, N. Ferry, F. Hernandez, O. Le Galloudec, F. Messal, and L. Parent. The godae/mercator-ocean global ocean forecasting system: results, applications and prospects. *Journal of Operational Oceanography*, pages 51–57, 2008. ISSN 1.
- A. Estubier and M. Lévy. Quel schéma numérique pour le transport d’organismes biologiques par la circulation océanique. *Note Techniques du Pôle de modélisation, Institut Pierre-Simon Laplace*, 2000. ISSN 81.
- R. H. Evans and G. Podesta. Second report to the sea surface temperature science working group. *Rosenstiel School of Marine and Atmospheric Science, Univ. of Miami*, 1996.
- C. W. Fairall, E. F. Bradley, J. E. Hare, A. A. Grachev, and J. B. Edson. Bulk parameterization of air-sea fluxes: Updates and verification for the coare algorithm. *Journal of Climate*, pages 571–591, 2003. ISSN 16.
- B. M. Fekete, C. J. Vörösmarty, and W. Grabs. Global, composite runoff fields based on observed river discharge and simulated water balances. *Technical Report 22, Global Runoff Data Center, Koblenz, Germany*, 1999.
- C. Garrett, R. Outerbridge, and K. Thompson. Interannual variability in mediterranean heat and buoyancy fluxes. *Journal of Climate*, 6(5):900–910, 1992.
- M. Ghil and P. Malanotte-Rizzoli. Data assimilation in meteorology and oceanography. *Advances in Geophysics*, 33:141–266, 1991.
- A. E. Gill. Atmosphere-ocean dynamics. *Academic Press*, pages 664+, 1982.
- C. Gilman and C. Garrett. Heat flux parameterizations for the mediterranean sea: The

- role of atmospheric aerosol and constraints from the water budget. *Journal of Geophysical Research*, (99):5119–5134, 1994.
- S. Griffies, A. Biastoch, C. Boning, F. Bryan, G. Danabasoglu, E. Chassignet, M. England, R. Gerdes, H. Haak, R. Hallberg, W. Hezeleger, J. Jungclaus, W. Large, G. Madex, B. Samuels, M. Sheinert, C. Severijns, H. Simmons, A. Treguier, M. Winton, S. Yeager, and J. Yin. Coordinated ocean-ice reference experiments (cores). *Ocean MOdell*, 11:59–74, 2008.
- J. Grist and S. Josey. Inverse analysis adjustments of the soc air-sea flux climatology using ocean heat transport constraints. *Journal of Climate*, pages 3275–3295, 2003. ISSN 16.
- R. L. Haney. Surface thermal boundary condition for ocean circulation models. *Journal of Physical Oceanography*, 1(4):241–248, October 1971.
- J. T. Houghton, L. G. Meiro Filho, B. A. Callander, N. Harris, A. Kattenburg, and K. Maskell. Climate change 1995—the science of climate change. *Changes in Sea Level*, pages 359–405, 1996.
- J. W. Hurrell, Y. Kushnir, and M. Visbeck. The north atlantic oscillation. *Science*, 2001.
- H. J. Isemer, J. Willebrand, and L. Hasse. Fine adjustment of large scale air-sea energy flux parameterizations by direct estimates of ocean heat transport. *Journal of Climate*, pages 1173–1184, 1989. ISSN 2.
- S. A. Josey, E. C. Kent, and P. K. Taylor. The southampton oceanography centre (soc) ocean - atmosphere heat, momentum and freshwater flux atlas. Technical report, 1998.
- A. B. Kara, H. E. Hurlburt, and A. J. Wallcraft. Stability-dependent exchange coefficients for air-sea fluxes. *Journal of Atmospheric and Oceanic Technology*, pages 1080–1094, 2005. ISSN 22.

## BIBLIOGRAPHY

---

- E. C. Kent, P. K. Taylor, B. S. Truscott, and J. A. Hopkins. The accuracy of voluntary observing ship's meteorological observations. *J. Atmos. Oceanic Technol*, pages 591–608, 1993. ISSN 10.
- J. T. Kiehl and K. E. Trenberth. Earth's annual global mean energy budget. *Bull. Amer. Met. Soc.*, 78:197–208, 1997.
- Peter D. Killworth, David A. Smeed, and George A. J. Nurser. The effects on ocean models of relaxation toward observations at the surface. *Journal of Physical Oceanography*, 30(1):160–174, January 2000.
- J. Kondo. Air-sea bulk transfer coefficients in diabatic condition. *Boundary-Layer Meteorology*, 9:91–112, 1975.
- V. H. Kourafalou and K. Barbopoulos. High resolution simulations on the north aegean sea seasonal circulation. *Annals of Geophysics*, 21:251–265, 2003.
- W. G. Large and S. G. Yeager. The global climatology of an interannually varying air-sea flux data set. *Climate Dynamics*, August 2008.
- P. Y. Le Traon, F. Nadal, and N. Ducet. An improved mapping method of multisatellite altimeter data. *Journal of Atmospheric and Oceanic Technology*, 15:522–533, 2003.
- P. F. J. Lermusiaux and A. R. Robinson. Data assimilation via error subspace statistical estimation. part i: Theory and schemes. *Mon. Wea. Rev.*, pages 1385–1407, 1999. ISSN 127.
- S. Levitus. Nodc world ocean atlas 1998 data. *report: NOAA-CIRES Climate Diagnostic Center Boulder, Colorado*, 1998.
- P. R. Lowe. An approximating polynomial for the computation of saturation vapor pressure. *Journal of Applied Meteorology*, 16(1):100–103, 1977.

- A. Macdonald, J. Candela, and H. L. Bryden. An estimate of the net heat transport through the strait of gibraltar. seasonal and interannual variability of the western mediterranean sea. *American Geophysical Union*, 46:13–32, 1994.
- G. Madec. Nemo ocean engine. *Note du Pole de modelisation, Institut Pierre-Simon Laplace (IPSL), France*, 27:1288–1619, 2008.
- G. Madec, P. Delecluse, M. Imbard, and C. Levy. ), opa version 8. ocean general circulation model reference manual. *Rapp. Int., LODYC, France*, pages 200+, 1997.
- G. Madec, P. Delecluse, M. Imbard, and C. Levy. Opa8.1 ocean general circulation model reference manual. *Note du Pole de modelisazion, Institut Pierre-Simon Laplace (IPSL), France*, 11, 1998.
- S. Manabe and K. Bryan. Climate calculations with a combined ocean-atmosphere model. *Journal of the Atmospheric Sciences*, 26:786–789, 1969.
- G. M. R. Manzella, F. Reseghetti, G. Coppini, M. Borghini, A. Cruzado, C. Galli, I. Gertman, T. Gervais, D. Hayes, C. Millot, A. Murashkovsky, E. Ozsoy, C. Tziavos, Z. Velasquez, and G. Zodiatis. The improvements of the ships of opportunity program in mfstep. *Ocean Sciences*, 3:245–258, 2007.
- A. Mariotti and M. V. Struglia. The hydrological cycle in the mediterranean region and implications for the water budget of the mediterranean sea. *Journal of Climate*, 15 (13):1674–1690, 2002.
- S. Marullo, B. B. Nardelli, M. Guarracino, and R. Santoleri. Observing the mediterranean sea from space: 21 yeàrs of phatfinder-avhrr sea surface temperature (1985 to 2005): re-analysis and validation. *Ocean Science*, (3):299–310, 2007.
- P. Oddo, M. Adani, N. Pinardi, C. Fratianni, M. Tonani, and D. Pettenuzzo. A nested atlantic-mediterranean sea general circulation model for operational forecasting. *Ocean Science*, (5):461–473, 2009.

## BIBLIOGRAPHY

---

- R. E. Payne. Albedo of the sea surface. *Journal of the Atmospheric Sciences*, 29(5): 959–970, July 1972.
- D. Pettenuzzo, W. G. Large, and N. Pinardi. On the corrections of era-40 surface flux products consistent with the mediterranean heat and water budgets and the connection between basin surface total heat flux and nao. *Journal of Geophysical Research*, in press.
- David W. Pierce. Reducing phase and amplitude errors in restoring boundary conditions. *Journal of Physical Oceanography*, 26:1552–1560, 1996.
- N. Pinardi, I. Allen, E. Demirov, P. De Mey, G. Korres, A. Lascaratos, P. Y. Le Traon, C. Maillard, G. Manzella, and C. Tziavos. The mediterranean ocean forecasting system: first phase of implementation (1998-2001). *Annales Geophysicae*, (21):3–20, 2003.
- P. M. Poulain, R. Barbanti, J. Font, A. Cruzado, C. Millot, I. Gertman, A. Griffa, A. Molcard, V. Rupolo, S. Le Bras, and Petit de la Villeon. Medargo: a drifting profiler program in the mediterranean sea. *Ocean Science*, 3:379–395, 2007.
- C. A. Poulson and J. J. Simpson. Irradiance measurements in the upper ocean. *Journal of Physical Oceanography*, 7:952–956, 1977.
- F. Raicich. On fresh water balance of the adriatic sea. *Journal of Marine Systems*, 9: 305–319, 1996.
- R. K. Reed. On estimating insolation over the ocean. *Journal of Physical Oceanography*, 7:482–485, 1977.
- M. Rixen, J. M. Beckers, S. Levitus, J. Antonov, T. Boyer, C. Maillard, M. Fichaut, E. Balopoulos, S. Iona, H. Dooley, M. J. Garcia, B. Manca, A. Giorgetti, G. Manzella, N. Mikhailov, N. Pinardi, and M. Zavatarelli. The western mediterranean deep water: A proxy for climate change. *Geophysical Research Letters*, 32, June 2005.

- A. R. Robinson, A. Hecht, N. Pinardi, J. Bishop, W. G. Leslie, Rosentroub, Mariano, and S. Brenner. Small synoptic/mesoscale eddies and energetic variability of the eastern levantine basin. *Nature*, 327:131–134, 1987.
- A. Rosati and K. Miyakoda. A general circulation model for upper ocean simulation. *Journal of Physical Oceanography*, 18:1601–1626, 1988.
- G. Roullet and G. Madec. Salt conservation, free surface and varying volume: a new formulation for ocean gcms. *Journal of Geophysical Research*, 105:23927–23942, 2000.
- D. Stammer, K. Ueyoshi, W. G. Large, S. Josey, and C. Wunsch. Estimating air-sea fluxes of heat, freshwater and momentum through global ocean data assimilation. *Journal of Geophysical Research*, pages 1–16, 2004. ISSN 109.
- J. D. Stark and C. J. Donlon. An assessment of the use of edspiration / ghrsst-pp data in met office foam and ostia systems. Technical report, MERSEA, 2006.
- Y. Tang and R. Kleeman. A new strategy for assimilating sst for enso predictions. *Geophysics Research Letter*, pages 1841+, 2002. ISSN 29.
- Y. Tang, R. Kleeman, and A. Moore. Sst assimilation experiments in a tropical pacific ocean model. , *Journal of Physical Oceanography*, 34:623–642, 2004.
- D. Tolmazin. Changing coastal oceanography of the black sea. ii: Mediterranean effluent. *Progress in oceanography*, 15:277–316, 1985.
- M. Tonani, N. Pinardi, S. Dobricic, I. Pujol, and C. Fratianni. A high-resolution free-surface model of the mediterranean sea. *Ocean Science*, (4):1–14, 2008.
- E. Tragou. Role of aerosols on the mediterranean solar radiation. *Journal of Geophysical Research*, 108, 2003.
- S. M. Uppala, P. W. Kallberg, A. J. Simmons, U. Andrae, Da, M. Fiorino, J. K. Gibson, J. Haseler, A. Hernandez, G. A. Kelly, X. Li, K. Onogi, S. Saarinen, N. Sokka,

## BIBLIOGRAPHY

---

- R. P. Allan, E. Andersson, K. Arpe, M. A. Balmaseda, A. C. M. Beljaars, Vande L. Berg, J. Bidlot, N. Bormann, S. Caires, F. Chevallier<sup>1</sup>, A. Dethof, M. Dragosavac, M. Fisher, M. Fuentes, S. Hagemann, E. Holm, B. J. Hoskins, L. Isaksen, P. A. E. M. Janssen, R. Jenne, McNally, J. F. Mahfouf, J. J. Morcrette, N. A. Rayner, R. W. Saunders, P. Simon, A. Sterl<sup>8</sup>, K. E. Trenberth, A. Untch, D. Vasiljevic, P. Viterbo, and J. Woollen. The era-40 re-analysis. *Quarterly Journal of the Royal Meteorological Society*, 131:2961–3012, October 2005.
- B. Van Leer. Towards the ultimate conservative difference scheme, v. a second order sequel to godunov’s method. *Journal of Computational Physics*, 32:101–136, 1979.
- S. D. Woodruff, R. J. Slutz, R. L. Jenne, and P. M. Steurer. A comprehensive ocean-atmosphere data set. *Bulletin of the American Meteorological Society*, 68(10):1239–1250, October 1987.
- P. Xie and P. A. Arkin. Analyses of global monthly precipitation using gauge observations, satellite estimates, and numerical model predictions. *Journal of Climate*, 9(4): 840–858, April 1996.
- L. Yu and R. A. Weller. Objectively analyzed air-sea fluxes for the global ice-free oceans (1981-2005). *Bulletin of the American Meteorological Society*, pages 527–539, 2007. ISSN 88.
- Y. Zhang, W. B. Rossow, A. A. Lacis, V. Oinas, and M. I. Mishchenko. Calculation of radiative fluxes from the surface to top of atmosphere based on isccp and other global data sets: Refinements of the radiative transfer model and the input data. *Journal of Geophysical Research*, 109, 2004.